2015 / Volume 53 / Number 2
ISSN 1641-4640

Folia NEUROPATHOLOGICA

www.folianeuro.termedia.pl

Official Journal of Mossakowski Medical Research Centre Polish Academy of Sciences
and
Polish Association of Neuropathologists

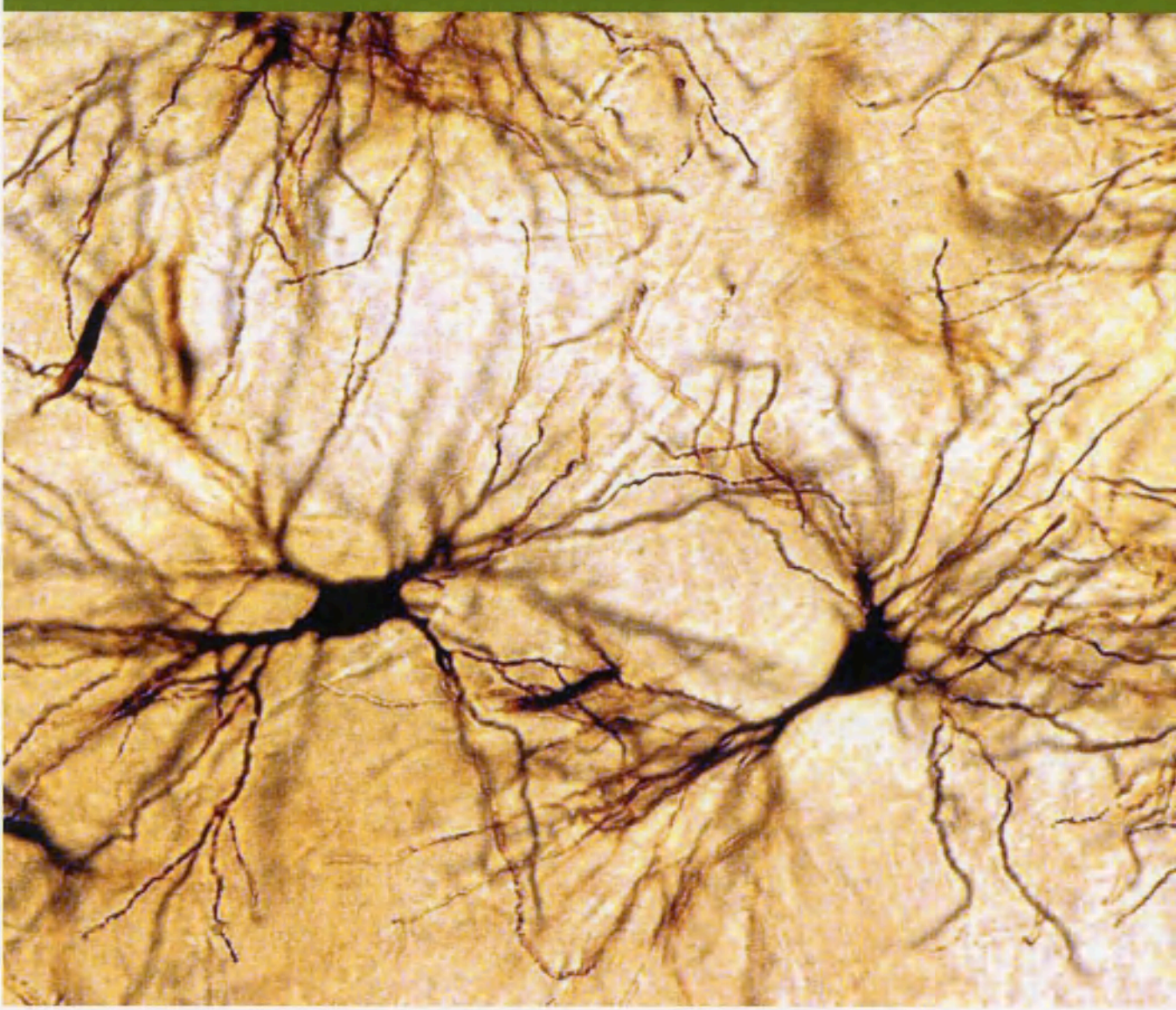

ISSN 1641-4640

Folia Neuropathologica

TERMEDIA Publishing House

Folia
Neuropathologica
former *Neuropatologia Polska*

Official Journal of Mossakowski Medical Research Centre Polish Academy of Sciences and Polish Association of Neuropathologists

The journal is partly financially supported
by the Ministry of Science and Higher Education

termedia

Termedia Publishing House
Kleeberga 2, 61-615 Poznań, Poland
phone/fax: +48 61 822 77 81
e-mail: termedia@termedia.pl
www.termedia.pl
www.folianeuro.termedia.pl

Warsaw office
phone/fax: +48 22 827 75 14
e-mail: biuro.warszawa@termedia.pl

president of the management board
editor-in-chief of the Publishing House, director
Janusz Michalak
e-mail: j.michalak@termedia.pl

director of the Publishing House
Andrzej Kordas
e-mail: a.kordas@termedia.pl

Marketing and Advertising Department
Renata Dolata
phone: +48 61 822 77 81 ext. 508
e-mail: r.dolata@termedia.pl

Distribution Subscription Department
Jolanta Jankowiak
phone: +48 61 656 22 00
e-mail: prenumerata@termedia.pl

Impact Factor for Folia Neuropathologica equals 1.667
MNiSW score for Folia Neuropathologica equals 15.00
Index Copernicus score (2011) for Folia Neuropathologica equals 18.13
Position in Index Copernicus ranking systems available at http://www.indexcopernicus.pl

Abstracted and indexed in Index Medicus/MEDLINE, Neuroscience Citation Index, SciSearch, Research Alert, Chemical Abstracts, EMBASE/Excerpta Medica, Polish Medical Bibiography, Index Copernicus

The journal is financially supported by the Ministry of Sciences and Higher Education.

Print run: 450 copies

Folia
Neuropathologica
2015; 53/2: 89-172

Contents

Review paper

Folia Neuropathologica

Neurogenesis and neuroprotection in postischemic brain neurodegeneration with Alzheimer phenotype: is there a role for curcumin?

Ryszard Pluta[1], Anna Bogucka-Kocka[2], Marzena Ułamek-Kozioł[1], Wanda Furmaga-Jabłońska[3], Sławomir Januszewski[1], Judyta Brzozowska[4], Mirosław Jabłoński[5], Janusz Kocki[6]

[1]Laboratory of Ischemic and Neurodegenerative Brain Research, Mossakowski Medical Research Centre, Polish Academy of Sciences, Warsaw, [2]Department of Pharmaceutical Botany, Medical University of Lublin, [3]Department of Neonate and Infant Pathology, Medical University of Lublin, [4]Department of Clinical Psychology, Medical University of Lublin, [5]Department of Rehabilitation and Orthopaedics, Medical University of Lublin, [6]Department of Clinical Genetics, Medical University of Lublin, Lublin, Poland

Folia Neuropathol 2015; 53 (2): 89-99 DOI: 10.5114/fn.2015.52405

Abstract

For thousands of years, humankind has used plants for therapeutics. Nowadays, there is a renewed public interest in naturally occurring treatments with minimal toxicity and diets related to health. Alterations in hippocampal neurogenesis have been recognized as an integral part of brain ischemia. Neuronal stem/progenitor cells in the hippocampus are positively and negatively regulated by intrinsic and extrinsic agents. One positive regulator of neurogenesis in the hippocampus is curcumin in the diet. This review provides an assessment of the current state of the field in hippocampal neurogenesis and neuroprotection studies in brain ischemia and focuses on the role of curcumin in the diet. Data suggest that dietary intake of curcumin enhances neurogenesis. Recent studies performed in ischemic models have suggested that curcumin also has neuroprotective features. One potential mechanism to explain several of the general health benefits associated with curcumin is that it may prevent ageing-associated changes in cellular proteins that lead to protein insolubility and aggregation after ischemia such as β-amyloid peptide and tau protein. Here, we also review the evidence from ischemic models that curcumin improves cognition and health span by overexpression of life supporting genes and preventing or delaying the onset of neurodegenerative changes. Available data provide evidence that curcumin induces neurogenesis and neuroprotection and may provide a novel therapeutic agent for both regenerative medicine and for the treatment of neurodegenerative diseases such as postischemic brain neurodegeneration with Alzheimer phenotype.

Key words: *brain ischemia, neurodegeneration, dementia, neurogenesis, neuroprotection, curcumin.*

Communicating author:
Prof. Ryszard Pluta, MD, PhD, Laboratory of Ischemic and Neurodegenerative Brain Research, Mossakowski Medical Research Centre, Polish Academy of Sciences, 5 Pawińskiego St., 02-106 Warsaw, Poland, phone: +48 22 6086-540 or 6086-469, fax: +48 22 668 55 32, e-mail: pluta@imdik.pan.pl

Introduction

Age-related disorders such as Alzheimer's disease and brain ischemia represent a major clinical problem in developed countries [18,28,41] and are a major economic burden for health care systems [15,37]. Dietary, genetic and molecular factors are important determinants in progression and treatment of the above diseases [1,47-51,53]. In developed countries ischemic stroke is a major cause of physical disability, the third leading cause of mortality and the second most common cause of dementia [28,41]. In a population of 1 million people 2.4 thousand individuals will have a stroke each year, of whom less than 50% will be independent 1 year later [28]. Numerous self-governing survivors have lasting physical and/or cognitive deficits and/or behavioral abnormalities which can affect family life and have a significant professional cost. An overarching consequence of ischemic brain injury is both short- and long-term cognitive deficits. These deficits typically occur in attention, memory, learning and higher order executive functions [3,24,29]. Cognitive deficits after ischemia can be attributed to damage to certain vulnerable brain regions including the hippocampus [47] and temporal cortex [42], as well as sub-cortical white matter tracts [44,45]. The hippocampus, which is crucial for declarative memory formation, demonstrates atrophy [43,46,47]. Postischemic dementia is one of the main causes of dependency in survivors. An enormous rise in the occurrence and problem of postischemic dementia is likely to happen because of the drop in mortality following brain ischemia and ageing of populations. Finally, global hippocampal neuronal loss with atrophy, temporal lobe atrophy and white matter changes are hallmarks of postischemic dementia [28,50]. Even when the above factors do not lead to dementia by themselves, their cumulative effect can reach the threshold of changes required to develop dementia. The prevalence of postischemic dementia is likely to increase in the near future because of better survival following brain ischemia and ageing of the population. Recognition of these patients is important because they have higher mortality, are frequently functionally damaged and need treatment. Studies should now focus on delineation of the goal of postischemic cognitive decline without dementia, which could be a preliminary stage of postischemic dementia and is much more frequent in clinical practice. Brain ischemia like Alzheimer's disease is a neuropathological condition accompanied by neuroinflammation and immune system changes [33,46,64,72]. One minute of brain ischemia is estimated to destroy approximately 2 million neurons and 14 million synapses [57].

β-amyloid peptides derived from amyloid precursor protein via β-secretase and γ-secretase cleavage are characteristic for postischemic brain neurodegeneration in animals and humans [52,53,55]. Oxidative stress mediates β-amyloid peptide neurotoxicity, and the latter contributes to neuronal death following brain ischemia [52]. Along with β-amyloid peptide, tau protein changes in neuronal microtubules also contribute to the postischemic neurodegeneration in adult animals [68,70]. Abnormal phosphorylation and aggregation of tau protein lead to postischemic neuronal dysfunction [70]. These data provide a neuropathological basis for dementia development in animals and patients following a postischemic episode. Failed clearance of β-amyloid peptide resulting from impaired autophagy may also contribute to postischemic neurodegeneration [65].

Apolipoprotein A1, E and J can influence the structure, toxicity and accumulation of the β-amyloid peptide in the postischemic brain [52,53,55]. Apolipoproteins may also be involved in β-amyloid peptide metabolism prior to its deposition. Additive effects of apolipoproteins on β-amyloid peptide deposition may play an important role in regulating extracellular β-amyloid peptide accumulation independent of β-amyloid peptide synthesis. The above data indicate that apolipoprotein A1, E and J accumulation after ischemia may represent a secondary injury factor that could exacerbate the healing of ischemic neurons and the outcome [52,53]. Extracellular apolipoprotein deposition was noted mainly following neuronal death. Transient brain ischemia led to changes in the presynaptic protein α-synuclein in the hippocampus [52,53]. Strong α-synuclein staining was observed in the hippocampus CA1 sector with postischemic long-term survival. Abnormal α-synuclein deposition might impair synaptic function, resulting in memory problems and additional postischemic neuronal death. Thus, the induction of amyloid precursor protein, apolipoproteins, presenilins and other Alzheimer's disease-related genes and proteins after ischemia may be the molecular link between Alzheimer's disease pathways and ischemia-reperfusion neurodegeneration [51,53]. As an effect of induction of the above genes there was

noted long-term abnormal co-accumulation of amyloid precursor protein and amyloid precursor protein cleaving enzymes [52]. The concentration of these proteins may lead to amyloid precursor protein proteolysis and β-amyloid peptide formation with final extracellular deposition as plaques [52,55]. Summing up, experimental data on postischemic brains show that Alzheimer's disease-related changes render the brain more susceptible to ischemic damage and in consequence lead to the development of Alzheimer-type dementia [3,24,29].

Old age is associated with enhanced susceptibility to ischemic stroke and poor recovery from postischemic injury, but the cellular mechanisms which trigger these phenomena are only partially understood [30,46,52-54,68,70]. Therefore, studying the complex processes underlying postischemic recovery of structural and cognitive functions in individuals a long time after birth is of considerable clinical importance [54]. Cognitive and morphological analysis of aged brain after ischemia in animals shows that: first, behaviorally they are more severely impaired and they show diminished functional recovery; second, they have a larger amount of apoptotic neurons and a higher degree of cellular disintegration; third, macrophages and astrocytes are activated early and strongly in the postischemic period; fourth, the early, powerful proliferation of glial cells leads to the precipitous development of scar tissue, enlarged by the chronic deposition of neurotoxic C-terminal of amyloid precursor protein; and fifth, the timing of the regenerative genetic response and cellular capability of the brain is altered and mechanisms are dysregulated and reduced, thereby additionally compromising functional recovery [30,44,54]. Whether endogenous neurogenesis is a factor that contributes to spontaneous recovery after ischemia has not yet been established. If the development of new neurons from endogenous stem cells is to become an effective treatment for postischemic neurodegeneration after birth, we need to more completely understand the factors that promote neurogenesis and how those factors change in later life. If neurogenesis from endogenous neuronal stem cells is to be used therapeutically, an individual approach will be required to assess the possible extent of the neurogenic response as well as the possibilities to alter this response for functional improvement or prevention of pathological neurogenesis with formation of improper synaptic junctions. The above alterations of hippocampal neurogenesis constitute a possible therapeutic target after ischemia. This endogenous self-repair mechanism may be further enhanced by extrinsic agents, one of which is curcumin in the diet.

There are a few clinically active therapies available for postischemic neurodegeneration, but no regenerative therapy exists currently. A few clinically active, yet not fully effective, therapies such as acetylsalicylic acid, statins and tissue type plasminogen activator are available for ischemic stroke [17,35,36]. In the wake of this neurodegenerative pathology, with limited medical therapies, alternative treatments are required which can control the progression of postischemic neurodegeneration. All the neurodegenerative diseases have common mechanisms of neuropathogenesis which include genetic alterations, protein and mitochondrial dysfunction, oxidative stress, cytokine changes and neuroinflammation [46,52,53]. Current research has shown that dietary polyphenols target the molecular changes of neurodegeneration with their ability to cross the blood-brain barrier as they control neuronal disease pathways at a molecular level by targeting these common features of neurodegeneration [14]. Polyphenols naturally occur e.g. in vegetables, fruits and red wines, exhibiting neuroprotective properties [4,40]. Dietary polyphenols are also involved in prevention of oxidative damage and human LDL oxidation [21,61]. Our analysis briefly outlines the therapeutic role of polyphenols such as curcumin in preventing the development of postischemic neurodegeneration with Alzheimer phenotype based on the most recent literature. We present the change of curcumin from a long-established spice and food coloring to a natural regulator of life processes.

The importance of hippocampal neurogenesis in postischemic brain neurodegeneration

Ischemic stroke is generally an age-related acute arterial disorder causing loss of neuronal and glial cells, with final development of functional and cognitive deficits. Apart from thrombolysis during the first hours, which can be given only to a small percentage of patients, no effective regenerative treatment to improve functional recovery exists in the postischemic period [17,35,36]. The persistence of neural stem cells and neurogenesis in the brain after birth, first suggested in 1912 [2], is accepted now. This change is based mostly on facts accumulated recently, indi-

cating that neural stem/progenitor cells occupy two main regions, the subventricular zone of the lateral ventricles and the subgranular zone of the dentate gyrus in the hippocampus, where they give rise to neurons after birth [30,38,54,58]. Neurogenesis has been found in these brain areas in all mammalian species, including humans [9,30,38,54,58], and may serve to replace brain cells damaged by insults. Two discrete brain regions presented contain progenitor cells that are capable of differentiating into neuronal or glial cells. Current research shows that neurogenesis can be modified by a variety of factors, including stress, neurohormones, growth factors, neurotransmitters and also stroke pathology [30]. In particular, hippocampal neurogenesis may play a role in modulation associated with neuropathology, such as cognitive disorders [38]. The stimulated neurogenesis at sites of brain damage may represent an attempt by the brain at self-regeneration after ischemia. Present research strongly focuses on the questions whether neurogenesis replaces lost and/or dying cells, and if so, to what extent.

Neural stem/progenitor cells could potentially be used to develop regenerative treatments to bring back the function of the postischemic hippocampus. Two major neural stem/progenitor cell-based tactics are currently being explored in experimental models: first, to deliver neural stem/progenitor cells locally or systemically in the brain where they act as stimulators of neurogenesis; and second, to replace diseased neurons and restructure neuronal network by stimulation of endogenous self-neurogenesis [31].

One of the earliest affected brain structures in brain ischemia is the hippocampus, which is involved in the formation and consolidation of memory [46,53]. The subgranular zone of the hippocampus dentate gyrus constitutes one of the only two neurogenic zones of the mature brain. Neurogenesis there is a process of generating neurons from neuronal progenitor cells. In the subgranular zone, these neurons proliferate and give rise to immature cells which migrate into the granule cell layer, mature, and integrate into the preexisting network by receiving inputs from the entorhinal cortex and extending projections into the hippocampus CA3 area [71].

Since neurogenesis is required for memory and learning, and its activity has shown to be decreased after ischemia in humans and rodents [25,26], it has been suggested that impaired hippocampal neurogenesis might be an integral part of postischemic progression [58]. Particularly, a variety of key factors involved in brain ischemia, among them presenilin 1 and 2, amyloid precursor protein and its products β-amyloid peptides, play either a positive or a negative role in hippocampal neurogenesis [7,27]. Furthermore, several growth factors, such as brain-derived neurotrophic factor (BDNF), fibroblast growth factor and vascular endothelial growth factor, have been reported to be upregulated in the neighborhood of β-amyloid peptide deposits [6,60]. These factors are also known to be potent stimulators of neural stem/progenitor cell activity. On the other hand, neuroinflammation and microglia activity that are associated with β-amyloid peptide store [43], and represent events in the postischemic brain [46], have been demonstrated to reduce neurogenesis [5].

So far, it has not been resolved when and what triggers hippocampal neurogenesis impairment in the postischemic brain. A long-term study attempting to investigate neurogenesis was performed to assess ischemic neurogenic activity [58]. Moreover, numerous aspects of hippocampal neurogenesis, differentiation, and survival of neurons have not been uniformly addressed in the above studies, preventing straightforward comparisons. Nevertheless, animal models will improve our understanding of the hippocampal neurogenesis after ischemia and point out still unresolved issues which demand further investigation.

The role of hippocampal neurogenesis in postischemic brain neurodegeneration

It has been suggested that an increase in hippocampal neurogenesis might serve as a replacement mechanism for neuronal loss, thereby slowing down postischemic progression to dementia [24,58]. However, the native increase in hippocampal neurogenesis might not be sufficient to compensate for the massive ischemic neuronal loss [26,30,58]. Recently, β-amyloid peptide oligomers have been reported to promote the generation of new neurons, but with no effect on cell survival [32]. On the other hand, β-amyloid peptide injection into the hippocampus in adult mice reduced progenitor cell activity [76] and led to the development of dementia in an animal model of brain ischemia [29]. Therefore, many questions regarding postischemic hippocampal neurogenesis remain open, among them the aspect of timing after ischemia. Neurogenesis in the hippocampus is regulated by numerous elements, including neuropathological conditions such as ischemic

episodes and diet [11,30]. Given that dietary factors have been proved to change the time course after ischemic neurodegeneration [66,77], and the same factors have been shown to modulate neurogenesis in the hippocampus [59], it is possible that the effects of diet on postischemic neurodegeneration are mediated by modulation of hippocampal neurogenesis. Additionally, dietary habits are an important component of lifestyle, which is recognized as one of the ischemic risk factors. To our best knowledge, amongst the current reviews concerning postischemic hippocampal neurogenesis [30,54], diet and brain ischemia and diet and postischemic hippocampal neurogenesis, our review is the first to put together neurogenesis in the hippocampus and postischemic brain neurodegeneration through the effects of dietary influence on both phenomena, in this manner providing a unique and new perspective on the state of postischemic hippocampal neurogenesis. Given that these days there are no effective therapies for postischemic brain neurodegeneration, and no regenerative therapy exists [17,35,36], dietary intervention may be an option to help delay disease progression.

Potent neurogenic activity of curcumin in hippocampus

Dietary content is important for the positive influence on neurogenesis and subsequent hippocampus mediated cognitive ability. Dietary polyphenols are known to have a beneficial influence on the brain by protecting neuronal cells against injury. For example, curcumin is a natural phenolic component obtained from the plant *Curcuma longa*, and it has been used in India to treat disorders associated with inflammation and oxidative stress [16]. Curcumin is used as a spice and coloring in foodstuffs with its characteristic yellow color. Due to its yellow color, curcumin is systematically used for coloring e.g. mustard, canned fish and dairy products [13]. Health benefits of curcumin may be limited in view of the fact of its low oral accessibility. On the other hand, due to its lipophilicity curcumin can cross the blood-brain barrier and can reach brain tissue at a functional pharmacological level [13,14,63]. The highest curcumin level in the brain tissue is reached approximately 60 min following intravenous and/or intraperitoneal injection of 100 mg/kg body weight curcumin in animals [13]. As a consequence of curcumin's immediate metabolism, it is not detectable in the brain after 2 h [13]. It should be remarked that curcumin can probably attain a therapeutic level in the brain tissue when it is taken on a regular basis [12]. In the above situation curcumin accumulates intracellularly and/or influences epigenetic regulation of gene expression such as DNA methylation and miRNA expression.

In recent years the focus on curcumin has been shifted to its influence on cognition alterations. Clinical data have shown that regular curcumin supplementation improves cognitive function [12]. Additionally, curcumin administration in various animal models of memory impairment reverses memory deficits [12]. These outcomes may be due to curcumin's effects on oxidative stress, BDNF and extracellular signal-regulated kinase (ERK)/P38 signaling pathways and degradation of PKCδ [12].

It was found that curcumin's anti-inflammatory and antioxidant therapeutic activities reversed β-amyloid peptide-induced cognitive deficits and neuropathological alterations [16]. Recently, it was reported that curcumin supports impaired hippocampal neurogenesis [69,73]. Curcumin has biphasic effects on neural stem/progenitor cells, whereby a low concentration modulates cell proliferation and a high concentration is neurotoxic [69]. This is in agreement with the finding that a high concentration of curcumin induces oxidative stress and triggers apoptosis in cells [39,69]. Previous data indicated that the neural stem/progenitor cells' specific mitogenic action of low concentration curcumin is mediated by the activation of ERK and p38 MAP kinases [39]. All considered, the dose-dependent neurogenic activity of curcumin resembles the hormesis theory of curcumin. The hormesis dose consequence phenomenon is characterized by low dose activation and high dose inhibition. In one study, the administration of curcumin significantly increased the number of new neurons in the hippocampus dentate gyrus by stimulating their proliferation [39]. Enhanced neurogenesis by stimulation of neural stem/progenitor cell proliferation is naturally observed during exercises [30]. Exercises elevate reactive oxygen species formation, and polyphenols including curcumin can promote the nuclear factor-erythroid 2-related factor 2 (Nrf2) antioxidant response [30]. Therefore, altered redox balance in the hippocampus is believed to trigger neural stem/progenitor cell proliferation. In addition, elevated hippocampal BDNF level is considered to be important for enhancing neurogenesis by exercises and/or curcumin [39,69]. Hippocampal BDNF

also seems to be correlated with memory and spatial learning, since a polyphenol-rich diet has been reported to increase intensity of hippocampal neurogenesis under a persistently stressful situation by increasing the hippocampal BDNF amount and CREB expression [16,69]. The above data suggest that the signaling pathways of ERK and BDNF can improve neurogenic activity, which will allow the discovery of a possible therapy that stimulates hippocampal neurogenesis after birth and will be useful for the treatment of postischemic neurodegeneration with Alzheimer phenotype.

Curcumin treatment increases neurite outgrowth and proliferation of neural stem cells in persistently stressed animals and reverses memory deficits in aged rats [63]. According to Tiwari *et al*., [63] the molecular mechanism by which curcumin induces neurogenesis is connected with canonical Wnt/β-catenin pathway initiation and glycogen synthase kinase-3β (GSK-3β) inhibition. They found that curcumin stimulates neural stem cell proliferation and neuronal differentiation and reverses β-amyloid peptide-induced inhibition of hippocampal neurogenesis and memory deficits in an Alzheimer's disease rat model [67] through activation of the canonical Wnt/β-catenin pathway. Curcumin activates Wnt/β-catenin signaling and stimulates adult neurogenesis through interaction with Wnt inhibitor factor (Wif-1), Dickkopf (Dkk-1) and GSK-3β.

Curcumin is an approved stimulator of hippocampal neurogenesis, but its exact role in ischemic hippocampal neurogenesis remains to be determined. In a β-amyloid peptide model of Alzheimer's disease in rat, curcumin suppressed glial activity and enhanced spatial memory [67]. It is probable that by downregulation of glial activity, curcumin protects hippocampal neurogenesis and improves cognitive deficits in neurodegenerative disorders such as postischemic injury [5]. Apart from the above-mentioned prevention of glial activity, curcumin might act by upregulation of serotonin receptor 1A and BDNF, and via activation of extracellular signal-regulated kinases and p38 MAPKs [30,39]. Both pathways are involved in the modification of neuronal plasticity. Moreover, curcumin might influence neurogenesis by affecting genes, including histone acetyltransferases and histone deacetylases, among them sirtuin 1 (SIRT1) (Table I) [8,56].

A recent investigation demonstrated that long-term administration of curcumin stimulated hippocampal neurogenesis and improved cognition in aged rats [12]. The gene responses in the hippocampus and cortex of the aged rats suggest a beneficial role of prolonged treatment by curcumin in modifying the neuronal network that influences synaptic plasticity and cell growth [12]. Curcumin did not affect induction of anxiety, locomotor activity and/or improvement of physical body strength, but affected non-spatial and spatial memory in aged rats [10, 12]. Prolonged treatment with curcumin increases neurogenesis in both the subgranular zone of the dentate gyrus and the hilus of the hippocampus. Data suggest a beneficial role of long-term treatment by curcumin in improving memory and learning by the induction of neurogenesis in the dentate gyrus.

Prolonged treatment with curcumin positively influences the aged rat's gene dysregulation in the hippocampus and cortex, and this phenomenon was larger in the cortex than in the hippocampus [12]. It was noted that the amount of upregulated genes decreased in the hippocampus but it increased in the cortex with time of treatment with curcumin. One important finding of the genetic investigation is that the majority of those differentially expressed genes have implications in brain development and memory and are involved in hippocampal neurogenesis [12]. The NeuroD1 gene, which was overexpressed in the cortex, is downstream of the Wnt pathway and is very important for the neurogenesis and survival of neuronal progenitors [12]. Cortical upregulation of the Fezf2 gene after curcumin treatment was noted, and this gene has been involved in neurogenesis and growth of subcortical projection neuronal cells. Next the Wnt2 gene was overexpressed in the adult hippocampus and has been implicated in neurogenesis, dendrite growth and arborization. Long-term treatment with curcumin upregulated the Tiam1 gene, which is vital for neurite outgrowth and for dendrite spine morphogenesis. It is interesting that curcumin upregulated in the hippocampus genes associated with neurotransmission such as synaptotagmin 9 (Syt9) [12]. The physiological role of Syt9 in synaptic neurotransmission, plasticity and memory is currently not clear. Earlier investigations demonstrated that other synaptotagmin genes such as Syt1 and Syt4 are closely associated with associative and spatial memory. Dong *et al*. [12] found overexpression of neurotransmission genes such as syntaxin 1a (Stx1a) and complexin 3 (Cplx3) in

Table I. Summary of the potential positive health effects of curcumin according to human and animal model studies

No.	Health benefits	References
1.	Antioxidant activity – *Modulation of Nrf2 signaling pathway*	[12,13,16,19,30,34,62,63]
2.	Anti-inflammatory activity – *Inhibition of nuclear factor κB*	[12,13,16,19,34,62]
3.	Neurogenesis improvement	[8,12,30,39,56,63,69]
4.	Neuroprotection	[13,34,62,63,66,73,74,75]
5.	Excitotoxicity protection	[13]
6.	Mitochondrial dysfunction reduction	[13]
7.	Neuronal apoptosis inhibition	[13,66,74,75]
8.	Brain edema protection	[13,20]
9.	Blood-brain barrier protection	[13,75]
10.	β-amyloid peptide plaque reduction	[12,13,34,62]
11.	β-amyloid peptide concentration reduction	[13,19,34,62]
12.	β-amyloid peptide inhibition of extracellular aggregation	[13,34,62,63]
13.	Amyloid precursor protein maturation inhibition and suppression of β-amyloid peptide production	[13,34,62]
14.	β-amyloid peptide clearance increase	[13]
15.	τ-protein phosphorylation inhibition	[19,34,62,63]
16.	Soluble τ-protein reduction	[34]
17.	Soluble τ-protein increase clearance	[34]
18.	Microglia and astrocyte activity inhibition	[5,67]
19.	Overexpression of genes involved in neurotransmission, signal transduction, metabolism and neural development – *Reelin, Nestin, Pax6, Neurogenin, NeuroD1, Nuroregulin, Neuroligin, Stat3, Syt9, Stx1a, Cplx3, Fezf2, NeuroD6, Adcyl1, Kit, Htr2c, LPL, Wnt2, Nnat, Tiam1, Unc5d, Shank3, Htr2a, Cip98, CD74, Snip, Wee1, Cav1, Nlgn2, Sirt1*	[8,12,56,63]
20.	Cognition improvement	[5,12,13,16,19,63,66,67,75]
21.	Anticarcinogenic activity	[13,39,69]

the cortex following curcumin treatment. The above genes influence neurotransmission and are strongly associated with synaptic plasticity and memory. Other synaptic transmission and memory formation genes were upregulated in the hippocampus such as adenylyl cyclase 1 (Adcyl1), LPL and Kit and in the cortex Cip98, Shank3, Snip and Nlgn2. In summary, the above data suggest that the curcumin upregulated genes in the hippocampus and cortex may be a factor responsible for the improvement of cognition activity in aged rats [12]. Dong *et al.* [12] additionally noted overexpression of the CD74 gene in the cortex of aged animals after prolonged treatment with curcumin. The CD74 gene is important in Alzheimer's disease neuropathology and cooperates together with amyloid precursor protein and finally reduces β-amyloid peptide generation. The study of upregulated genes after curcumin administration suggested that these genes are important for neurotransmission, synaptic plasticity, neurogenesis and memory creation.

Potent neuroprotective activity of curcumin

Nowadays curcumin has been intensively studied as a promising therapeutic for postischemic neurodegeneration with Alzheimer phenotype. Evidence indicates that curcumin may act as a neuroprotective substance on postischemic outcome and behavioral deficits in rodents and this neuroprotective effect is presented by antiapoptotic action [66,74,75]. Other studies have shown that curcumin reverses the permeability of the ischemic blood-brain barrier and decreases brain edema [13,20]. Additionally in behavioral studies in rodents curcumin reverses cognitive changes [13]. Curcumin by stimulation of protein kinase C activity decreases NMDA receptor function. Curcumin has been shown to decrease the calcium-dependent induction of caspases [13]. Curcumin inhibits nNOS activity and protects against peroxynitrite-induced neuronal cell death *in vitro*. Additionally, Esatbeyoglu *et al*. [13] showed that curcumin inhibits hydrogen peroxide triggered neurotoxicity in Neuro2-A cells. In summary, curcumin presents anti-amyloid, anti-tau protein hyperphosphorylation, antioxidative and anti-inflammatory actions, and it has been proposed that curcumin might be neuroprotective in brain ischemia neurodegeneration (Table I) [34,62]. As a consequence of curcumin's beneficial health potential, including anti-inflammatory, antioxidative and anti-excitotoxic activities, it may be considered as a promising substance in the treatment of postischemic brain neurodegeneration with Alzheimer phenotype (Table I).

Curcumin lowers amyloid deposits and inhibits tau protein aggregation in a transgenic model of Alzheimer's disease and reduces oxidative injury, neuroinflammatory response, as well as cognitive deficit after infusion of amyloid into the brain [19]. Experimental models show that curcumin reduces neuroinflammation, oxidative stress and the density of β-amyloid peptide plaques and soluble β-amyloid peptide level in the brain tissue both *in vitro* and *in vivo* [12,13]. Curcumin prevents the aggregation of β-amyloid peptide *in vitro* and supports the clearance of β-amyloid peptide aggregates. Curcumin inhibits the maturation of amyloid precursor protein and stops the generation of β-amyloid peptide *in vitro* [13]. Curcumin reduced soluble tau protein and elevated heat shock protein involved in tau protein clearance, showing that even after tangles have been formed, tau protein-dependent behavioral and synaptic deficits could be reversed [34].

Curcumin neuroprotection activity was noted in experimental models of Parkinson's, Huntington's and Alzheimer's disease and multiple sclerosis [63]. Curcumin acts by its antioxidant activity and by inducing the transcription factor Nrf2, a regulator of antioxidant stress [63]. It was shown that curcumin inhibits β-amyloid peptide oligomerization and τ-protein phosphorylation in the brain tissue [63]. On the whole, curcumin research indicates its possible neuroprotective function.

Additionally, some investigations have indicated anticarcinogenic action of curcumin. It has been shown that curcumin exerts its potential anticarcinogenic activities by regulating the tumor suppressor gene p53 and a variety of transcription factors, e.g. Nrf2 and NFκB, by modifying inflammatory signaling and by triggering apoptosis (Table I) [13].

Conclusions

Every mammal has stem cells in different organs, being particularly important in the brain, and nowadays these cells are believed to play a role in cell substitute after birth [23]. The existence of neural stem/progenitor cells in the mammalian mature brain that are capable of forming new neurons continues to push the developments of new approaches to brain repair after ischemia. In particular, the modulation of impaired neurogenesis in the hippocampus is associated with the amelioration of cognitive deficits and better outcomes related to brain ischemia (Table I) [66,75]. Therefore, the latest focus has been concentrated on the development of new natural drugs that can simulate proliferation of ischemic neural stem/progenitor cells after birth. The mechanisms and factors that control the formation of new neurons in the animal and human brain after ischemia are by and large unknown, and finding such factors is likely to lead to new ways of treating brain ischemia [10,58]. This review presents the neurogenic and neuroprotective properties of curcumin and provides a new basis for a possible reparative strategy whereby endogenous neural stem/progenitor cells are recruited by dietary stimulation to address ischemic neuronal loss [1,39]. Curcumin improves the survival rate of newly generated neurons and stimulates impaired neurogenesis after ischemia by elevation of neurotrophic factors [30,39]. However, curcumin triggers the mitogenic property of neural stem/

progenitor cells and stimulates their proliferation by BDNF and MAP kinase activation [30,39]. Collectively, understanding the neurogenic mechanisms after ischemia and curcumin neurogenic activity could provide a neurorestorative strategy that stimulates dysregulated endogenous neural stem/progenitor cell activity and as a result prevents neuropathological changes and neurological deficits after ischemia. There are, however, some encouraging results suggesting that curcumin could be of therapeutic relevance in these kinds of diseases (Table I) [12,13,23,63]. Amid all the optimism surrounding the potential of ischemia-induced neurogenesis, there remain a variety of significant concerns. Postischemic epilepsy is a fairly common morbidity after an ischemic episode [22]. It has been suggested that aberrant neurogenesis triggers the epileptic activity [22]. Clearly any research aimed at enhancing neurogenesis might result in this and other unwanted side effects. In addition, enhanced neurogenesis would stimulate cell growth; it is possible that increased proliferation could result in tumor development [22]. In this situation many issues regarding specificity, mechanism and potential toxicity need to be more carefully studied before clinical trials can occur [13,23]. Undoubtedly, more investigations are needed to explore hippocampal neurogenesis and the effects of curcumin in long-term natural interventions [12], and the fact that curcumin seems to be innocuous in animals and humans could prompt additional studies on the effect of curcumin in the onset and progression of postischemic brain neurodegeneration with Alzheimer phenotype. Our review also points out the limitations of available data and potential directions of research into the role of curcumin in hippocampal neurogenesis and neuroprotection in ischemic brain neurodegeneration with Alzheimer phenotype course.

Acknowledgments

The authors acknowledge support by the Polish National Science Centre (DEC-2013/09/B/NZ7/01345-RP,ABK,MUK,SJ,JK) and by the Mossakowski Medical Research Centre, Polish Academy of Sciences, Poland (T3-RP). The paper was developed using equipment purchased within the Project "The equipment of innovative laboratories doing research on new medicines used in the therapy of civilization and neoplastic diseases" within the Operation Program Development of Eastern Poland 2007–2013, Priority Axis I Modern Economy, Operations I.3 Innovation Promotion (JK).

Disclosure

Authors report no conflict of interest.

References

1. Albarracin SL, Stab B, Casas Z, Sutachan JJ, Samudio I, Gonzalez J, Gonzalo L, Capani F, Morales L, Barreto GE. Effects of natural antioxidants in neurodegenerative diseases. Nutr Neurosci 2012; 15: 1-9.
2. Allen E. The cessation of mitosis in the central nervous system of the albino rat. J Comp Neurol 1912; 22: 547-568.
3. Barra de la Tremblaye P, Plamondon H. Impaired conditioned emotional response and object recognition are concomitant to neuronal damage in the amygdale and perirhinal cortex in middle-aged ischemic rats. Behav Brain Res 2011; 219: 227-233.
4. Basli A, Soulet S, Chaher N, Mérillon JM, Chibane M, Monti JP, Richard T. Wine polyphenols: potential agents in neuroprotection. Oxid Med Cell Longev 2012; Article ID 805762.
5. Biscaro B, Lindvall O, Tesco G, Ekdahl CT, Nitsch RM. Inhibition of microglial activation protects hippocampal neurogenesis and improves cognitive deficits in a transgenic mouse model for Alzheimer's disease. Neurodegener Dis 2012; 9: 187-198.
6. Burbach GJ, Hellweg R, Haas CA, Del Turco D, Deicke U, Abramowski D, Jucker M, Staufenbiel M, Deller T. Induction of brain-derived neurotrophic factor in plaque associated glial cells of aged APP23 transgenic mice. J Neurosci 2004; 24: 2421-2430.
7. Choi SH, Veeraraghavalu K, Lazarov O, Marler S, Ransohoff RM, Ramirez JM, Sisodia SS. Non-cell autonomous effects of presenilin 1 variants on enrichment mediated hippocampal progenitor cell proliferation and differentiation. Neuron 2008; 59: 568-580.
8. Chung S, Yao H, Caito S, Hwang JW, Arunachalam G, Rahman I. Regulation of SIRT1 in cellular functions: Role of polyphenols. Arch Biochem Biophys 2010; 501: 79-90.
9. Curtis MA, Kam M, Nannmark U, Anderson MF, Axell MZ, Wikkelso C, Holtås S, van Roon-Mom WM, Björk-Eriksson T, Nordborg C, Frisén J, Dragunow M, Faull RL, Eriksson PS. Human neuroblasts migrate to the olfactory bulb via a lateral ventricular extension. Science 2007; 315: 1243-1249.
10. Deng W, Aimone JB, Gage FH. New neurons and new memories: how does adult hippocampal neurogenesis affect learning and memory? Nat Rev Neurosci 2010; 11: 339-350.
11. Dias GP, Cavegn N, Nix A, Do Nascimento Bevilaqua MC, Stangl D, Zainuddin MS, Nardi AE, Gardino PF, Thuret S. The role of dietary polyphenols on adult hippocampal neurogenesis: Molecular mechanisms and behavioural effects on depression and anxiety. Oxid Med Cell Longev 2012; 2012: 541971.
12. Dong S, Zeng Q, Mitchell ES, Xiu J, Duan Y, Li Ch, Tiwari JK, Hu Y, Cao X, Zhao Z. Curcumin enhances neurogenesis and cognition in aged rats: Implications for transcriptional interactions related to growth and synaptic plasticity. PLos ONE 2012; 7: e31211.

13. Estabeyoglu T, Huebbe P, Ernst IMA, Chin D, Wagner AE, Rimbach G. Curcumin-From molecule to biological function. Angew Rev Int Ed 2012; 51: 5308-5332.
14. Faria A, Pestana D, Teixeira D, Azevedo J, De Freitas V, Mateus N, Calhau C. Flavonoid transport across RBE4 cells: a blood-brain barrier model. Cell Mol Biol Lett 2010; 15: 234-241.
15. Flynn RWV, MacWalter RSM, Doney ASF. The cost of cerebral ischemia. Neuropharmacology 2008; 55: 250-256.
16. Frautschy SA, Hu W, Kim P, Miller SA, Chu T, Harris-White ME, Cole GM. Phenolic anti-inflammatory antioxidant reversal of Abeta-induced cognitive deficits and neuropathology. Neurobiol Aging 2001; 22: 993-1005.
17. Haile WB, Wu J, Echeverry R, Wu F, An J, Yepes M. Tissue type plasminogen activator has a neuroprotective effect in the ischemic brain mediated by neuronal TNF-α. JCBFM 2012; 32: 57-59.
18. Hung CW, Chen YC, Hsieh WL, Chiou SH, Kao CL. Ageing and neurodegenerative diseases. Ageing Res Rev 2010; 9: S36-S46.
19. Ishrat T, Hoda MN, Khan MB, Yousuf S, Ahmad M, Khan MM, Ahmad A, Islam F. Amelioration of cognitive deficits and neurodegeneration by curcumin in rat model of sporadic dementia of Alzheimer's type (SDAT). Eur Neuropsychopharm 2009; 19: 636-647.
20. Jiang J, Wang W, Sun YJ, Hu M, Li F, Zhu DY. Neuroprotective effect of curcumin on focal cerebral ischemic rats by preventing blood-brain barrier damage. Eur J Pharmacol 2007; 561: 54-62.
21. Jones QR, Warford J, Rupasinghe HPV, Robertson GS. Target-based selection of flavonoids for neurodegenerative disorders. Trends Pharmacol Sci 2012; 33: 602-610.
22. Kernie SG, Parent JM. Forebrain neurogenesis after focal ischemic and traumatic brain injury. Neurobiol Dis 2010; 37: 267-274.
23. Kim SJ, Son TG, Park HR, Park M, Kim M-S, Kim HS, Chung HY, Mattson MP, Lee J. Curcumin stimulates proliferation of embryonic neuronal progenitor cells and neurogenesis in the adult hippocampus. J Biol Chem 2008; 283: 14497-14505.
24. Kiryk A, Pluta R, Figiel I, Mikosz M, Ułamek M, Niewiadomska G, Jabłoński M, Kaczmarek L. Transient brain ischemia due to cardiac arrest causes irreversible long-lasting cognitive injury. Behav Brain Res 2011; 219: 1-7.
25. Knoth R, Singec I, Ditter M, Pantazis G, Capetian P, Meyer RP, Horvat V, Volk B, Kempermann G. Murine features of neurogenesis in the human hippocampus across the lifespan from 0 to 100 years. PLoS One 2010; 5: e8809.
26. Kuhn HG, Dickinson-Anson H, Gage FH. Neurogenesis in the dentate gyrus of the adult rat: Age-related decrease of neuronal progenitor proliferation. J Neurosci 1996; 16: 2027-2033.
27. Lazarov O, Marr RA. Neurogenesis and Alzheimer's disease: At the crossroads. Exp Neurol 2010; 223: 267-281.
28. Leys D, Henon H, Mackowiak-Cordoliani MA, Pasquier F. Post-stroke dementia. Lancet Neurol 2005; 4: 752-759.
29. Li J, Wang YJ, Zhang M, Fang CQ, Zhou HD. Cerebral ischemia aggravates cognitive impairment in a rat model of Alzheimer's disease. Life Sci 2011; 89: 86-92.
30. Lichtenwalner RJ, Parent JM. Adult neurogenesis and the ischemic forebrain. JCBFM 2006; 26: 1-20.
31. Lindvall O, Kokaia Z. Stem cell research in stroke: how far from the clinic? Stroke 2011; 42: 2369-2375.
32. Lopez-Toledano MA, Ali Faghihi M, Patel NS, Wahlestedt C. Adult neurogenesis: A potential tool for early diagnosis in Alzheimer's disease? J Alzheimers Dis 2010; 20: 395-408.
33. Luheshi NM, Kovacs KJ, Lopez-Castejon G, Brough D, Denes A. Interleukin-1α expression precedes IL-1β after ischemic brain injury and is localized to area of focal neuronal loss and penumbral tissues. J Neuroinflamm 2011; 29: 186.
34. Ma QL, Zuo X, Yang F, Ubeda OJ, Gant DJ, Alaverdyan M, Teng E, Hu S, Chen PP, Maiti P, Teter B, Cole GM, Frautschy SA. Curcumin suppresses soluble tau dimers and corrects molecular chaperone, synaptic, and behavioral deficits in aged human tau transgenic mice. J Biol Chem 2013; 288: 4056-4065.
35. Menezea AR, Lavie CJ, Milani RV, Okeefe J. The effects of statins on prevention of stroke and dementia: a review. Psychosomatics 2012; 32: 240-249.
36. Molina CA. Reperfusion therapies for acute ischemic stroke: current pharmacological and mechanical approaches. Stroke 2011; 42: 16-19.
37. Olesen J, Gustavsson A, Svensson M, Wittchen HU, Jonsson B. The economic cost of brain disorders in Europe. Eur J Neurol 2012; 19: 155-162.
38. Paizanis E, Kelai S, Renoir T, Hamon M, Lanfumey L. Life-long hippocampal neurogenesis: Environmental, pharmacological and neurochemical modulations. Neurochem Res 2007; 32: 1762-1771.
39. Park HR, Lee J. Neurogenic contributions made by dietary regulation to hippocampal neurogenesis. Ann N Y Acad Sci 2011; 1229: 23-28.
40. Perez-Jimenez J, Neveu V, Vos F, Scalbert A. Identification of the 100 richest dietary sources of polyphenols: an application of the Phenol-Explorer database. Eur J Clin Nutr 2010; 64: 112-120.
41. Pinkston JB, Alekseeva N, Gonzalez Toledo E. Stroke and dementia. Neurol Res 2009; 31: 824-831.
42. Pluta R. Influence of prostacyclin on early morphological changes in the rabbit brain after complete 20-min ischemia. J Neurol Sci 1985; 70: 305-316.
43. Pluta R. Astroglial expression of the beta-amyloid in ischemia reperfusion brain injury. Ann N Y Acad Sci 2002; 977: 102-108.
44. Pluta R, Ułamek M, Januszewski S. Micro-blood-brain barrier openings and cytotoxic fragments of amyloid precursor protein accumulation in white matter after ischemic brain injury in long-lived rats. Acta Neurochir (Suppl) 2006; 96: 267-271.
45. Pluta R, Januszewski S, Ułamek M. Ischemic blood-brain barrier and amyloid in white matter as etiological factors in leukoaraiosis. Acta Neurochir (Suppl) 2008; 102: 353-356.
46. Pluta R, Ułamek M, Jabłoński M. Alzheimer's mechanisms in ischemic brain degeneration. Anat Rec 2009; 292: 1863-1881.
47. Pluta R, Januszewski S, Jabłoński M, Ułamek M. Factors in creepy delayed neuronal death in hippocampus following brain ischemia-reperfusion injury with long-term survival. Acta Neurochir (Suppl) 2010; 106: 37-41.
48. Pluta R, Ułamek M, Jabłoński M. Consideration of the ischaemic basis and treatment of Alzheimer's disease. Folia Neuropathol 2010; 48: 11-26.
49. Pluta R, Furmaga-Jabłońska W, Jabłoński M. Therapeutic food benefits after ischemic brain edema. Nutrition 2012; 28: 1192-1193.

50. Pluta R, Jabłoński M, Czuczwar SJ. Postischemic dementia with Alzheimer phenotype: selectively vulnerable versus resistant areas of the brain and neurodegeneration versus β-amyloid peptide. Folia Neuropathol 2012; 50: 101-109.
51. Pluta R, Kocki J, Maciejewski R, Ułamek-Kozioł M, Jabłoński M, Bogucka-Kocka A, Czuczwar SJ. Ischemia signaling to Alzheimer-related genes. Folia Neuropathol 2012; 50: 322-329.
52. Pluta R, Furmaga-Jabłońska W, Maciejewski R, Ułamek-Kozioł M, Jabłoński M. Brain ischemia activates β- and γ-secretase cleavage of amyloid precursor protein: Significance in sporadic Alzheimer's disease. Mol Neurobiol 2013; 47: 425-434.
53. Pluta R, Jabłoński M, Ułamek-Kozioł M, Kocki J, Brzozowska J, Januszewski S, Furmaga-Jabłońska W, Bogucka-Kocka A, Maciejewski R, Czuczwar SJ. Sporadic Alzheimer's disease begins as episodes of brain ischemia and ischemically dysregulated Alzheimer's disease genes. Mol Neurobiol 2013; 48: 500-515.
54. Popa-Wagner A, Buga AM, Kokaia Z. Perturbed cellular response to brain injury during aging. Ageing Res Rev 2011; 10: 71-79.
55. Qi J, Wu H, Yang Y, Wand D, Chen Y, Gu Y, Liu T. Cerebral ischemia and Alzheimer's disease: the expression of amyloid-β and apolipoprotein E in human hippocampus. J Alzheimers Dis 2007; 12: 335-341.
56. Reuter S, Gupta SC, Park B, Goel A, Aggarwal BB. Epigenetic changes induced by curcumin and other natural compounds. Genes Nutr 2011; 6: 93-108.
57. Saver JL. Time is brain – quantified. Stroke 2006; 37: 263-266.
58. Sekeljic V, Bataveljic D, Stamenkovic S, Ułamek M, Jabłoński M, Radenovic L, Pluta R, Andjus PR. Cellular markers of neuroinflammation and neurogenesis after ischemic brain injury in the long-term survival rat model. Brain Struct Funct 2012; 217: 411-420.
59. Stangl D, Thuret S. Impact of diet on adult hippocampal neurogenesis. Genes Nutr 2009; 4: 271-282.
60. Tarkowski E, Issa R, Sjogren M, Wallin A, Blennow K, Tarkowski A, Kumar P. Increased intrathecal levels of the angiogenic factors VEGF and TGF-beta in Alzheimer's disease and vascular dementia. Neurobiol Aging 2002; 23: 237-243.
61. Thilakarathna SH, Rupasinghe HPV, Needs APW. Apple peel bioactive rich extracts effectively inhibit in vitro human LDL oxidation. Food Chem 2013; 138: 463-470.
62. Thiyagarajan M, Sharma SS. Neuroprotective effect of curcumin in middle cerebral artery occlusion induced focal cerebral ischemia in rats. Life Sci 2004; 74: 969-985.
63. Tiwari SK, Agrawal S, Seth B, Yadav A, Nair S, Bhatnagar P, Karmakar M, Kumari M, Chauhan LKS, Patel DK, Srivastava V, Singh D, Gupta SK, Tripathi A, Chaturvedi RK, Gupta KCh. Curcumin-loaded nanoparticles potently induce adult neurogenesis and reverse cognitive deficits in Alzheimer's disease model via canonical Wnt/β-catenin pathway. ACSNANO 2014; 8: 76-103.
64. Tuttolomondo A, Di Raimondo D, Di Sciacca R, Pinto A, Licata G. Inflammatory cytokines in acute ischemic stroke. Curr Pharm Design 2008; 14: 3574-3589.
65. Ułamek-Kozioł M, Furmaga-Jabłońska W, Januszewski S, Brzozowska J, Ściślewska M, Jabłoński M, Pluta R. Neuronal autophagy: self-eating or self-cannibalism in Alzheimer's disease. Neurochm Res 2013; 38: 1769-1773.
66. Wang Q, Sun AY, Simonyi A, Jensen M, Shelat PB, Rottinghaus GE, MacDonald RS, Miller DK, Lubahn DE, Weisman GA, Sun GY. Neuroprtective mechanisms of curcumin against cerebral ischemia-induced neuronal apoptosis and behavioral deficits. J Neurosci Res 2005; 82: 138-148.
67. Wang Y, Yin H, Wang L, Shuboy A, Lou J, Han B, Zhang X, Li J. Curcumin as a potential treatment for Alzheimer's disease: A study of the effects of curcumin on hippocampal expression of glial fibrillary acidic protein. Am J Chin Med 2013; 41: 59-70.
68. Wen Y, Yang SH, Liu R, Perez EJ, Brun-Ziukemagel AM, Koulen P, Simpkins JW. Cdk5 is involved in NFT-like tauopathy induced by transient cerebral ischemia in female rats. Biochim Biophys Acta 2007; 1772: 473-483.
69. Xu Y, Ku B, Cui L, Li X, Barish PA, Foster TC, Ogle WO. Curcumin reverses impaired hippocampal neurogenesis and increases serotonin receptor 1A mRNA and brain-derived neurotrophic factor expression in chronically stressed rats. Brain Res 2007; 1162: 9-18.
70. Yang SH, Simpkins JW. Ischemia-reperfusion promotes tau and beta-amyloid pathology and a progressive cognitive impairment. In Pluta R, editor. Ischemia-reperfusion pathways in Alzheimer's disease. Nova Science Publishers, Inc., New York 2007, pp. 113-138.
71. Zainuddin MSA, Thuret S. Nutrition, adult hippocampal neurogenesis and mental health. Br Med Bull 2012; 103: 89-114.
72. Zhang W, Potrovita I, Tarabin V, Herrmann O, Beer V, Weih F, Schneider A, Schwaninger M. Neuronal activation of NF-κB contributes to cell death in cerebral ischemia. JCBFM 2005; 25: 30-40.
73. Zhao C, Deng W, Gage FH. Mechanisms and functional implications of adult neurogenesis. Cell 2008; 132: 645-660.
74. Zhao J, Zhao Y, Zheng W, Lu Y, Feng G, Yu S. Neuroprotective effect of curcumin on transient focal cerebral ischemia in rats. Brain Res 2008; 1229: 224-232.
75. Zhao J, Yu S, Zheng W, Feng G, Luo G, Wang L, Zhao Y. Curcumin improves outcomes and attenuates focal cerebral ischemic injury via antiapoptotic mechanisms in rats. Neurochem Res 2010; 35: 374-379.
76. Zheng M, Liu J, Ruan Z, Tian S, Ma Y, Zhu J, Li G. Intrahippocampal injection of Abeta(1-42) inhibits neurogenesis and down-regulates IFN-gamma and NF-kappaB expression in hippocampus of adult mouse brain. Amyloid 2013; 20: 13-20.
77. Zhu DY, Lau L, Wei JS, Liu SH, Lu YM. Activation of cAMP-response-element-binding protein (CREB) after focal cerebral ischemia stimulates neurogenesis in the adult dentate gyrus. Proc Natl Acad Sci USA 2004; 101: 9453-9457.

Original article

Folia Neuropathologica

Age-related dendritic and spinal alterations of pyramidal cells of the human visual cortex

Ioannis A. Mavroudis[1,2], Marina G. Manani[1], Foivos Petrides[1], Dimitrios Dados[1], Alin Ciobica[3,4], Manuela Padurariu[3,5], Konstantina Petsoglou[6], Samuel N. Njau[6], Vasiliki G. Costa[1,2], Stavros J. Baloyannis[1,2]

[1]Laboratory of Neuropathology, First Department of Neurology, AHEPA Hospital, Aristotelian University of Thessaloniki, Greece, [2]Institute for Alzheimer's Disease Research, Heraklion Langada, Greece, [3]"Alexandru Ioan Cuza" University, Iasi, Romania, [4]Center of Biomedical Research of the Romanian Academy, Iasi Branch, Romania, [5]"Gr. T. Popa" University of Medicine and Pharmacy, Iasi, Romania, [6]Laboratory of Forensic Medicine and Toxicology, Aristotelian University of Thessaloniki, Greece

Folia Neuropathol 2015; 53 (2): 100-110 DOI: 10.5114/fn.2015.52406

Abstract

Introduction: *Normal aging is characterized by deterioration of visual abilities, affecting mainly visual acuity, contrast and wavelength sensitivity. In the present study we attempted to describe the morphological and morphometric alterations of the dendrites and the dendritic spines of the pyramidal cells of the visual cortex during normal aging, in order to approach the visual impairment of aged individuals from a neuropathological point of view.*
Material and methods: *We studied the visual cortex in 20 brains using the Golgi technique.*
Results: *In pyramidal cells, which represent the majority of cortical neurons, age-related pathology can be observed in cell somata as well as, most importantly, in dendrite number and morphology. The apical dendrites of some pyramidal cells are distorted and tortuous. Horizontal dendritic arborization is also severely decreased. These alterations were more prominent in the corticocortical pyramidal neurons of the 5th layer.*
Conclusions: *The morphological and morphometric assessment of the dendrites and the dendritic spines in the visual cortex in normal aging revealed substantial alterations of the dendritic arborization and marked loss of the dendritic spines, which may be related to visual impairment even in normal aging.*

Key words: *visual cortex, ageing, pyramidal cells, 3D neuronal reconstruction, Golgi method.*

Introduction

Normal aging is characterized by deterioration of visual abilities, affecting mainly visual acuity, contrast and wavelength sensitivity [14,28,38,47,50,63]. Anatomical and morphological studies concluded that retinal abnormalities and changes of the subcortical areas do not efficiently explain the perceptual deficits [1,27,50], and recent neuroimaging studies suggest that age-related dedifferentiation may apply at a neural level besides photoreceptors [1].

Several conflicting lines of evidence exist so far concerning the possible causative mechanism for such impairment. Hua *et al*. (2006) described signif-

Communicating author:
Ioannis A. Mavroudis, Laboratory of Neuropathology and Electron Microscopy, 1st Department of Neurology, School of Medicine, Aristotelian University, Thessaloniki 54006, Greece, phone: +302310993301, fax: +302310994712, e-mail: iamav79@hotmail.com

icant functional degradation of the primary visual cortex in aged animals, which could be regarded as direct evidence for the loss of function in visual cortical cells [19].

Although a decrease in brain size has been reported with increasing age [11], there is some evidence that gray matter tissue loss is minimal in patients without degenerative abnormalities [12]. Brody (1955) and Samorajski (1976) in their early studies mentioned a significant neuronal loss during normal ageing [7,49], whereas Pakkenberg and Gundersen (1997) in a more recent study suggested a small loss of neurons with age [42]. The latter findings are in agreement with studies of Vincent *et al*. (1989), Peters and Sethares (1993) and Tiggers *et al*. (1990), who concluded that there is no significant loss of neurons during ageing.

According to light microscopy, no significant changes in length and complexity of the dendritic arbor were found to correlate with age-related functional alterations [5,10,36,55] in layer I of rhesus monkeys. However, electron microscopy revealed fewer dendritic and spine profiles per unit area, thickening of the glia limiting membrane and a concomitant decrease in the numerical density of synapses with age [44]. Furthermore, Xu *et al*. (2007) in a Golgi study in rats, revealed age-related changes in dendritic branching and spinal density of the pyramidal cells of the visual cortex [65].

In order to further examine the possible age-related alterations in the human visual cortex, we focused on the pyramidal cells of layer 5 of the human visual cortex. Two main classes of pyramidal neurons have been described in layer 5, each of them playing a unique role in visual information processing. The first one refers to corticocortical pyramidal neurons. Corticocortical pyramidal neurons have short apical dendrites which never reach higher than layers 2/3, small to medium sized cell bodies and a few basal dendrites. Corticocortical neurons participate in direct feedback circuits [8].

The second type of pyramidal neurons refers to corticotectal neurons, which have large cell somata, a long apical dendrite forming a large terminal tuft in layer 1, and their basal dendrites form a dense and symmetrical dendritic field [8].

These cells bear fast-conducting axons that branch to enervate multiple subcortical targets and intracortical collaterals that may end several millimeters away from the soma [15,26,54]. In the primary visual cortex (V1), the great majority of corticotectal neurons are members of this distinctive subpopulation of pyramidal neurons [25,47,58]. Corticotectal neurons of V1 terminate in superficial, retinal recipient layers of the superior colliculus in a roughly topographic manner [16,17].

Thus there are two morphologically distinct projection systems in layer 5, one projecting to cortical and the other one to subcortical targets, suggesting that these two systems transmit different information from the visual cortex.

In previous studies we have shown significant dendritic and spinal changes in the visual cortex during normal ageing [33] and in Alzheimer's disease [32]. In the present study we attempted to describe the morphological and morphometric alterations of the dendrites and the dendritic spines of the pyramidal cells of the visual cortex during normal aging, in order to approach the visual impairment of aged individuals from a neuropathological point of view.

Material and methods

Subjects

Tissue samples from 20 brains were provided by the Laboratory of Forensic Medicine and Toxicology. Tissue blocks were removed post-mortem and immediately immersed in 10% buffered formalin solution. All the brains had been examined using routine histopathology methods and no macroscopic or microscopic signs of underling pathology were observed. The brains were divided into two groups, the first of them consisting of ten individuals aged 40-55 years and the second consisting of the remaining ten aged 75-86 years.

Tissue preparation

Tissue samples of the primary visual cortex were excised from the left hemisphere, stained with a modified Golgi method and cut in a slicing microtome in thick sections at the range of 150 μm.

Cell selection criteria

Neurons examined consequently for quantitative alterations met the criteria set forth by Jacobs *et al*. (1997) that request uniform staining of neuronal processes, absence of precipitated debris, good contrast between cells and background, and relatively uniform tissue thickness [22].

Neuronal tracing and variables analyzed

For each one of 20 brains, 30 pyramidal cells of the fifth layer were selected.

For each selected cell a video recording was taken, using an Amscope 10 Mpx microscope digital camera on an Axiostar Plus Zeiss light microscope, analyzed and converted into multiple image sequences of 200 serial digital images applying the Image J application. They were then imported in the Neuromantic application as image stacks in order to be used for semi-automatic three dimensional neuronal reconstructions. Neuronal tracing was carried out by 5 different individuals in order to avoid experimental bias.

Branch orders were evaluated in an adapted centrifugal fashion as follows: dendrites arising from the cell body were considered as first-order segments until they bifurcated symmetrically into second-order segments; dendritic branches arising from the first-order segments were considered as second-order segments until they bifurcated symmetrically into third-order segments, and so on.

Variables analyzed were the total dendritic length, the total number of dendritic segments and bifurcations, the dendritic tree asymmetry, as well as the length and the number of dendritic segments per order. Furthermore, the tracings were analyzed quantitatively using the Image J program according to Sholl's method of concentric circles [53]. Concentric cycles were drawn, at intervals of 15 μm centered on the cell bodies, and dendritic intersections within each cycle were counted.

For the estimation of qualitative and quantitative changes of the dendrites we used magnifications of 400×.

Spine counts were carried out on the dendrites of layer V pyramidal neurons, on the basis of 300 photomicrographs. Visible spines were counted on three segments of the dendritic field. The first segment, 20-30 μm in length, was located on a basal dendrite; the second segment, 20-30 μm in length, was located on a horizontal branch of the apical dendrite; and the third one, 40-50 μm, was located along the apical dendrite. For each of the segments described above, 20 serial digital pictures were taken and used in the Neuromantic application for the three dimensional representation of the segments including the dendritic spines.

Adjacent samples of the visual cortex were used for Nissl staining for estimation of the borders of cortical layers and the depth of the selected neurons in the visual cortex.

For the statistical analysis, Student's *t* test was performed. Significance was taken as $p < 0.05$.

Results

Golgi-stained tissue did not exhibit irregular varicose enlargements or constriction of dendrites, which were described as autolytic changes by Williams *et al*. (1978) [64].

Qualitative and quantitative observations

Qualitative features

Two types of pyramidal cells were observed (Fig. 1). The first one refers to corticocortical neurons, having small to medium sized cell somata and an apical dendrite which terminates in layers 2/3, and the second one refers to corticotectal pyramidal cells, having large cell somata and an apical dendrite which ends in layer I. Both types of pyramidal neurons carry the standard morphology described by previous studies.

Application of silver impregnation technique revealed significant restriction of the dendritic arborization in aged individuals. Irregular swellings in the soma, as well as in the proximal portions of the apical dendrite and the axon, were observed.

Quantitative changes

The number of tertiary and quaternary branches of the basal dendrites was severely decreased mainly in small pyramidal cells of the older group (Fig. 2A and B). The total number of horizontal dendritic branches was also significantly lower in the above-mentioned group (Fig. 2C).

The total dendritic length was significantly lower in the aged group, being most prominent in the distal branches of small corticocortical pyramidal cells (Fig. 2D). Total number of bifurcations per neuron and the number of terminal branches were also decreased in the pyramidal cells of aged brains, exhibiting statistical significance in small cells but not in the large ones (Fig. 2A and B).

Sholl analysis revealed significant restriction of the dendritic field in the distal intersections, both in

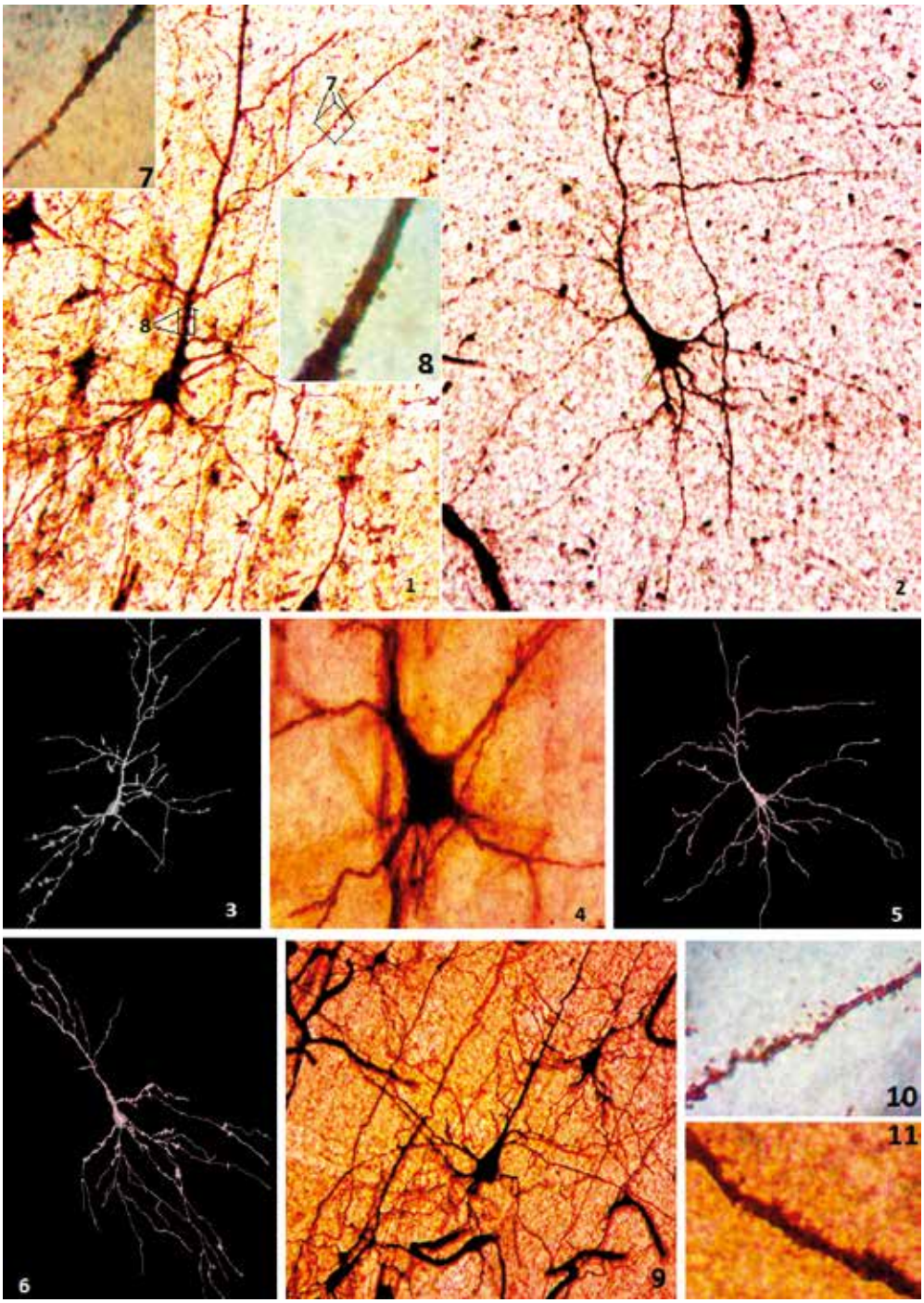

Fig. 1. Corticotectal [1] and corticocortical [2] pyramidal neurons from the older brains (Golgi method, magnification 100×) and their reconstructions [3] and [5]. Cell soma of a corticotectal pyramidal neuron from an older brain [4] exhibiting significant loss of basal dendritic branches and dendritic spines (Golgi method, magnification 400×). Reconstruction from a corticocortical neuron from a younger brain [6]. Higher magnification of an oblique dendritic segment of the neuron in Figure 1.1 [7] and higher magnification of a part of the apical dendrite of the same neuron [8] (Golgi method, magnification 1000×). Corticocortical pyramidal neuron from the visual cortex of an older brain [9], higher magnification of a basal [10] and an apical dendritic segment [11] of younger brains exhibiting higher spinal density than the older ones.

large cells and in small to medium sized pyramidal cells (Fig. 2E and F).

The average length per branching order was severely decreased in the 3rd and 4th ordered branches of the small pyramidal cells of the older group, while the respective differences in the large pyramidal cells exhibited statistical significance only in the 4th and higher ordered branches (Fig. 3A and B). The same holds true for the dendritic branches per order (Fig. 3C and D).

No significant differences were detected in the dendritic tree asymmetry of small and large pyrami-

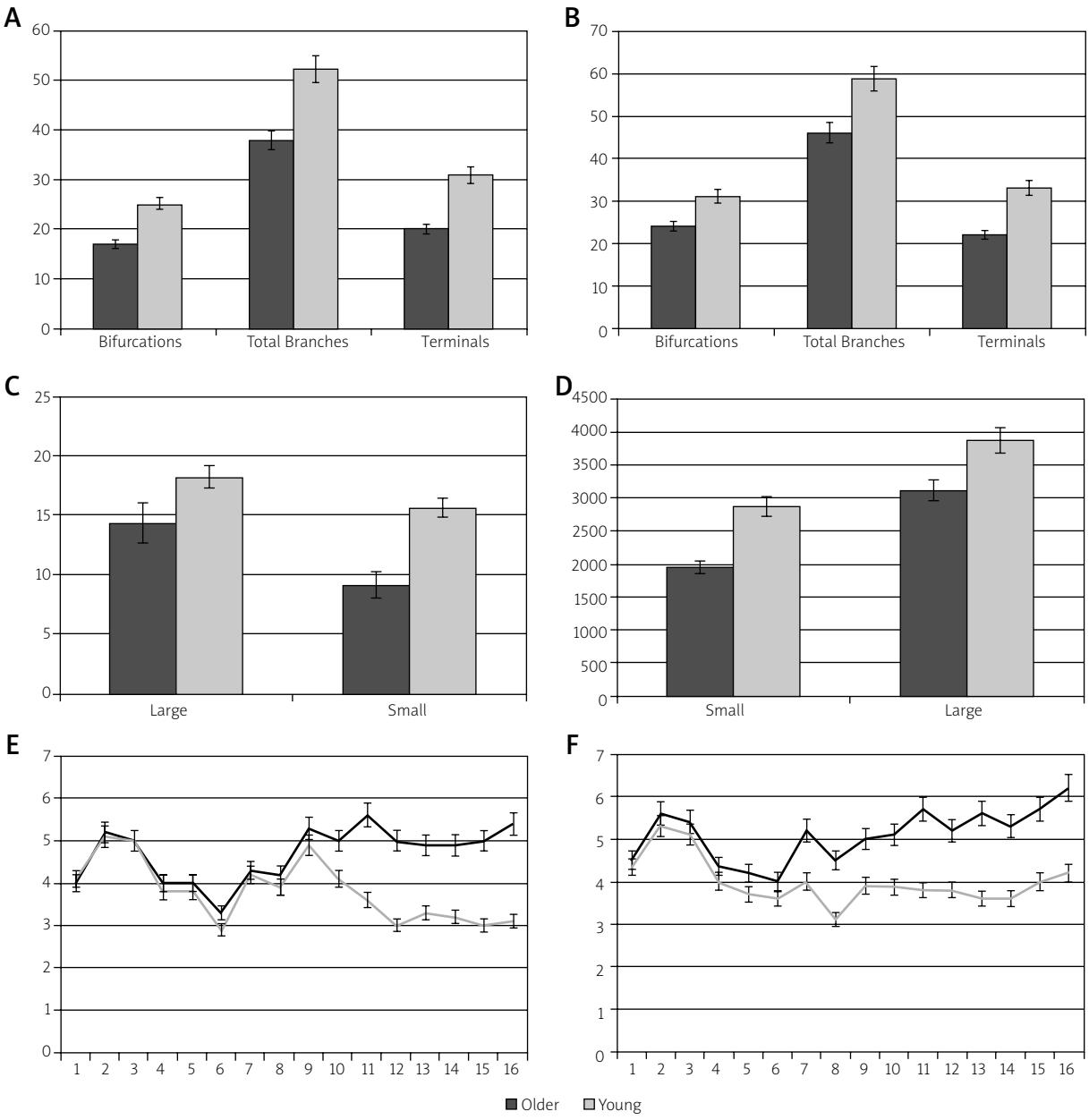

Fig. 2. Comparison of complexity of the dendritic arborizations of small (corticotectal) **(A)** and large (corticocortical) **(B)** pyramidal cells from younger and older individuals. Total number of horizontal branches of large and small pyramidal cell from younger and older individuals **(C)**. Total dendritic length of small and large pyramidal cells from the visual cortex of younger and older individuals **(D)**. Sholl analysis from small **(E)** and large **(F)** pyramidal cells from younger and older individuals.

dal cells in both groups of the study; however, the daughter ratio was significantly lower in the older group (Fig. 3E and F). The average branching order was also lower in the older group (Fig. 4A).

Dendritic spines

At every age, the spine density for the thick dendrites was higher than that of the thinner dendrites.

Spinal density was calculated to be markedly decreased in both pyramidal cell types of the older group (Fig. 4B and C).

Pyramidal cell type differences

Small corticocortical pyramidal cells were more profoundly affected by age, while most of the age-related changes of the morphometric variables

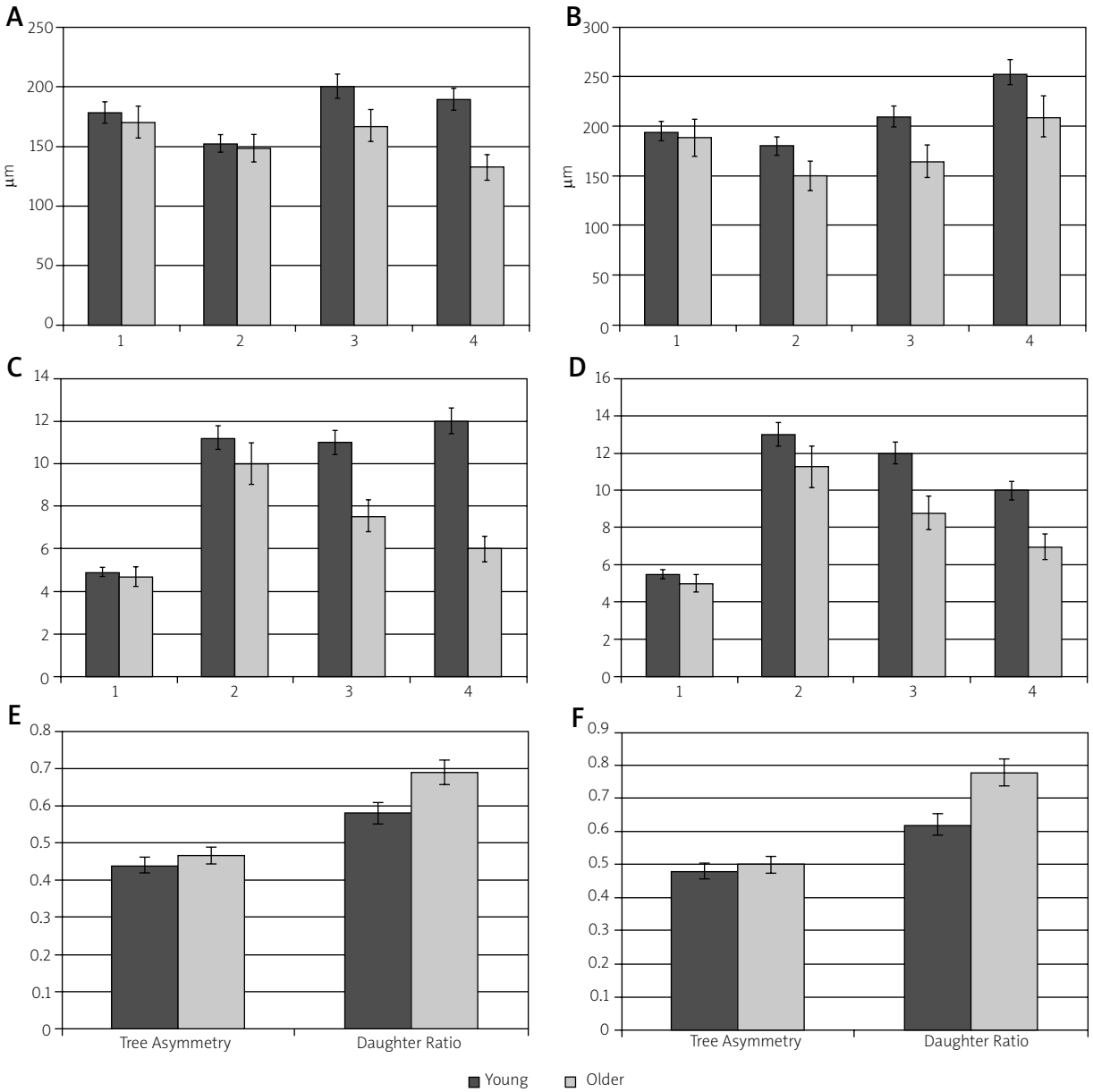

Fig. 3. Dendritic length per order and branches per order from small **(A, C)** and large **(B, D)** pyramidal cells from the visual cortex of younger and older individuals. Tree asymmetry and daughter ratio from small **(E)** and large **(F)** pyramidal cells from younger and older individuals.

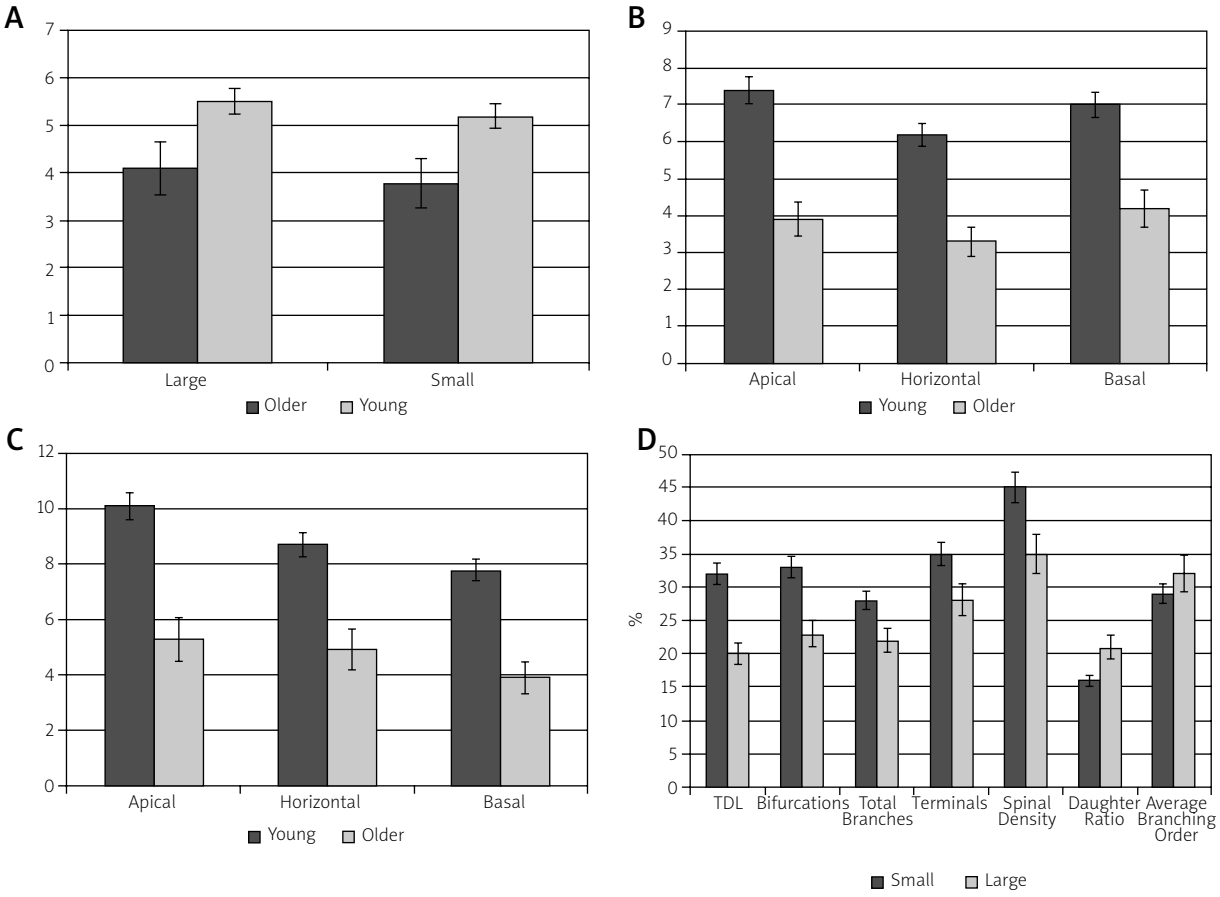

Fig. 4. Average branching orders **(A)**, spinal density from small **(B)** and large **(C)** pyramidal cells. Comparison of age-related alterations of small and large pyramidal cells of the visual cortex **(D)**.

studied are more evident in them, as can be seen in Fig. 4D.

Discussion

Methodological considerations

Golgi staining is a capricious and unpredictable method; however, it has been used for more than 100 years for the study of neuronal morphology and continues to provide a unique view of the neuronal cell soma, dendrites and dendritic spines [33].

The Neuromantic program which was used for the three dimensional neuronal reconstruction is a free application, verified and established for the semi-automatic reconstruction of neurons for single images or image stacks. Furthermore, it can be run by multiple computers simultaneously in more than one computer, allowing as many reconstructions as required in parallel [36].

The three-dimensional neuronal reconstruction allows a better and more accurate depiction of the neuron, its dendrites and dendritic spines. Therefore it can provide the researcher information about neuronal functionality and allows statistical comparison between experimental neuronal populations as well as functional simulation of traced neurons [60].

Light microscopy inherently underestimates branch and spine numbers, and therefore dendritic and spinal differences may actually be greater than observed [18,22]. However, the results are still acceptable as the same methods have been used in both groups of the study.

Age-related changes

Several aspects of age-related visual impairment have been reported during the past decades in studies concerning both humans and other mam-

mals. Some of them refer to visual acuity, impairment of binocular summation, motion direction detection and spatial frequency contrast sensitivity [14,29,40,47,51,57,63].

Many studies have demonstrated age-related regression in the dendritic arbors and spines of pyramidal neurons located in the prefrontal, superior temporal and precentral cortices in humans [29,37,43] and in nonhuman primates [46].

Significant age-related loss of dendrites and dendritic spines was first described in human brain by Scheibel and coworkers, including both shorter and fewer dendritic branches [52].

The effects of aging on dendritic complexity and spinal density of cortical pyramidal neurons in the human brain have also been examined by Anderson and Rutledge (1996), who quantified spine numbers on the basal dendrites of supragranular pyramidal cells in the posterior temporal gyrus and noted a significant decline between 21 and 71 years of age [2]. Moreover, Jacobs and coworkers examined the total dendritic spine number on basal dendrites of supragranular pyramidal cells in prefrontal area 10 and the occipital area in 26 neurologically normal individuals 14-106 years old and reported a 46% decrease in spine numbers and spine density from the younger to the older group [22].

In the present study spinal density was significantly lower in the apical and basal dendrites of the pyramidal neurons of the aged group. These results are congruent with the study of Page *et al*. (2002), who demonstrated a decrease of 28-37% in the basal and apical dendrites of aged animals compared to young ones [41].

Total dendritic length, dendritic length per branching order and total number of terminal branches were also significantly lower in the pyramidal cells of the older group. Animal studies have also found regressive dendritic changes during normal aging in prefrontal area 46 [13] and in the visual cortex [51].

As Sholl analysis revealed, distal segments are mainly affected by age.

Significant age-related decreases in segment numbers were observed at the second branch order for apical dendrites and at the tertiary and quaternary order for basal dendrites. Similar changes have been demonstrated in age-related animal studies in other cortical areas and in area 17 [13,41]. The outermost branches of the dendritic tree are the most plastic ones and contribute significantly to synaptic integration locally and along the entire neuron. The most peripheral dendritic spines are thought to be particularly effective in adjusting potential [23]. Thus the excitability of an entire dendrite may be disproportionately regulated by changes in distal dendrites and dendritic branches.

Although mechanisms underlying age-related changes have not yet been clearly defined, a number of biochemical and genetic alterations have been described during normal aging. Aging is characterized by downregulation of specific genes, such as genes expressing calcium channel subunits, GABA receptor subunits and genes involved in synaptic plasticity and playing a role in DNA repair mechanisms and antioxidant defense [3,21,24,39,62].

Electron microscope studies demonstrated a correlation between oxidative stress and neuronal morphological alterations [4].

Furthermore, a reduction of MAP-2 protein expression and brain-derived neurotrophic factor abnormalities has also been revealed by recent studies, offering a possible etiological background for the age-related changes [9].

Although aged cerebral cortex still display a certain degree of neuronal plasticity, the selective loss of distal dendritic branches and age-related alterations of dendritic spines point to a reduced tolerance of the aged visual cortex towards vascular and biochemical changes.

Cell-specific alterations

Small pyramidal cells of layer V are mainly affected by age, while large pyramidal cells retain higher dendritic and spinal density. The statistical test performed for the comparison of the morphometric changes between the two subpopulations of pyramidal cells confirmed this hypothesis.

The main differences between the subgroups are related to the size of the cell soma, the functionality and their afferent and efferent connections.

Medium sized to large pyramidal cells have thick axons ramifying with collaterals projecting to the superior colliculus [20]. Small to medium sized pyramidal cells are also located at the depth of layer 5, possess basal dendrites that branch in layer 5 and layer 6 as well, and an apical dendrite never reaches the molecular layer. Their axons send recurrent axons to layer 3A [30], to layers 5 and 6, and form efferents to cortical area V2. The different patterns

of connections might play a role in the differences detected in two subpopulations of pyramidal cells detected in the present study.

These findings are consistent with those of a previous study on area 46, where small corticocortical pyramidal neurons seem to be mainly affected by age in comparison to large projection neurons [13].

Conclusions

In conclusion, the present study points to the fact that brain aging is accompanied by rather subtle morphological and molecular changes at the level of single neuronal populations and different types of pyramidal cells of the human visual cortex are differently affected. The loss of dendrites and dendritic spines leads to a substantial decrease of the synaptic contacts of the cells of the visual cortex with the neurons of other cortical and subcortical areas implicated in the modulation of the visual information.

These alterations seen in the thick sections of the silver-impregnated preparations, attributed to the degeneration of the dendritic spines, may explain the impaired central visual function during normal aging.

Disclosure

Authors report no conflict of interest.

References

1. Ahmad A, Spear PD. Effects of aging on the size, density, and number of rhesus monkey lateral geniculate neurons. J Comp Neurol 1993; 334: 631-643.
2. Anderson B, Rutledge V. Age and hemisphere effects on dendritic structure. Brain 1996; 119: 1983-1990.
3. Anderton B. Ageing of the brain. Mech Ageing Dev 2002; 123: 811-817.
4. Baloyannis SJ, Costa V, Mauroudis I, Psaroulis D, Manolides SL, Manolides LS. Dendritic and spinal pathology in the acoustic cortex in Alzheimer's disease: morphological and morphometric estimation by Golgi technique and electron microscopy. Acta Otolaryngol 2007; 127: 351-354.
5. Baracat B, Marquie JC. Age differences in sensitivity, response bias, and reaction time on a visual discrimination task. Exp Aging Res 1992; 18: 59-66.
6. Becker LE, Armstrong DL, Chan F, Wood MM. Dendritic development in human occipital cortical neurons. Brain Res 1984; 315: 117-124.
7. Brody H. Organisation of the cerebral cortex III. A study of aging in the human cerebral cortex. J Comp Neurol 1955; 102: 511-556.
8. Callaway EM. Local circuits in primary visual cortex of the macaque monkey. Annu Rev Neurosci 1998; 21: 47-74.
9. Chauhan N, Siegel G. Age-dependent organotypic expression of microtubule-associated proteins (MAP1, MAP2, and MAP5) in rat brain. Neurochem Res 1997; 22: 713-719.
10. de Brabander JM, Kramers RJ, Uylings HB. Layer-specific dendritic regression of pyramidal cells with ageing in the human prefrontal cortex. Eur J Neurosci 1998; 10: 1261-1269.
11. Dekaban AS. Mental retardation and neurologic involvement with congenital retinal blindness. Dev Med Child Neurol 1972; 14: 436-444.
12. Double K, Halliday G, Kril J, Harasty J, Cullen K, Brooks W, Creasey H, Broe G. Topography of brain atrophy during normal aging and Alzheimer's disease. Neurobiol Aging 1996; 17: 513-521.
13. Duan H, Wearne SL, Rocher AB, Macedo A, Morrison JH, Hof PR. Age-related dendritic and spine changes in corticocortically projecting neurons in macaque monkeys. Cereb Cortex 2003; 13: 950-961.
14. Elliott D, Whitaker D, MacVeigh D. Neuralcontribution to spatiotemporal contrast sensitivity decline in healthy ageing eyes. Vision Res 1990; 30: 541-547.
15. Hallman LE, Schofield BR, Lin CS. Dendritic morphology and axon collaterals of corticotectal, corticopontine, and callosal neurons in layer 5 of primary visual cortex of the hooded rat. J Comp Neurol 1988; 272: 149-160.
16. Harting JK, Updyke BV, Van Lieshout DP. Corticotectal projections in the cat: anterograde transport studies of twenty-five cortical areas. J Comp Neurol 1992; 324: 379-414.
17. Holländer H, Schönitzer K. Corticotectal terminals in the superior colliculus of the rabbit: a light- and electron microscopic analysis using horseradish peroxidase (HRP)-tetramethylbenzidene (TMB). J Comp Neurol 1983; 219: 81-87.
18. Horner CH, Arbuthnott E. Methods of estimation of spine density – are spines evenly distributed throughout the dendritic field? J Anat 1991; 177: 179-184.
19. Hua T, Li X, He L, Zhou Y, Wang Y, Leventhal AG. Functional degradation of visual cortical cells in old cats. Neurobiol Aging 2006; 27: 155-162.
20. Hübener M, Schwarz C, Bolz J. Morphological types of projection neurons in layer 5 of cat visual cortex. J Comp Neurol 1990; 301: 655-674.
21. Iyo T, Yamasaki T. The detection of age-related decrease of dopamine, D1, D2 and serotonin 5-HT2 receptors in living human brain. Prog Neuro-Psycopharmacol Biol Psychiatry 1993; 17: 415-421.
22. Jacobs B, Driscoll L, Schall M. Life-span dendritic and spine changes in areas 10 and 18 of human cortex: a quantitative Golgi study. J Comp Neurol 1997; 386: 661-680.
23. Jaslove SW. The integrative properties of spiny distal dendrites. Neuroscience 1992; 47: 495-519.
24. Kaasinen V, Vilkman H, Hietala J, Någren K, Helenius H, Olsson H, Farde L, Rinne JO. Age-related dopamine D2/D3 receptor loss in extrastriatal regions of the human brain. Neurobiol Aging 2000; 21: 683-688.
25. Kasper EM, Larkman AU, Lubke J, Blakemore C. Pyramidal neurons in layer 5 of the rat visual cortex. I. Correlation among cell morphology, intrinsic electrophysiological properties, and axon targets. J Comp Neurol 1994; 339: 459-474.

26. Keizer K, Kuypers HG, Ronday HK. Branching cortical neurons in cat which project to the colliculi and to the pons: a retrograde fluorescent double-labeling study. Exp Brain Res 1987; 67: 1-15.
27. Kim CB, Tom BW, Spear PD. Effects of aging on the densities, numbers, and sizes of retinal ganglion cells in rhesus monkey. Neurobiol Aging 1996; 17: 431-438.
28. Kline DW, Schieber F, Abusamra LC, Coyne AC. Age, the eye, and the visual channels: contrast sensitivity and response speed. J Gerontol 1983; 38: 211-216.
29. Logan JM, Sanders AL, Snyder AZ, Morris JC, Buckner RL. Under-recruitment and nonselective recruitment: dissociable neural mechanisms associated with aging. Neuron 2002; 33: 827-840.
30. Lund JS, Boothe RG. Interlaminar connections and pyramidal neuron organization in the visual cortex, area 17, of the macaque monkey. J Comp Neurol 1975; 159: 305-334.
31. Mavroudis IA, Fotiou DF, Adipepe LF, Manani MG, Njau SD, Psaroulis D, Costa VG, Baloyannis SJ. Morphological changes of the human Purkinje cells and deposition of neuritic plaques and neurofibrillary tangles on the cerebellar cortex of Alzheimer's disease. Am J Alzheimers Dis Other Demen 2010; 25: 585-591.
32. Mavroudis IA, Fotiou DF, Manani MG, Njaou SN, Frangou D, Costa VG, Baloyannis SJ. Dendritic pathology and spinal loss in the visual cortex in Alzheimer's disease: a Golgi study in pathology. Int J Neurosci 2011; 121: 347-354.
33. Mavroudis I, Petrides F, Manani M, Theocharides C, Ciobica A, Padurariu M, Kiourexidou M, Njau S, Costa V, Baloyannis S. Dendritic and spinal alterations of the spiny stellate cells of the human visual cortex during normal aging. Folia Neuropathol 2012; 50: 261-269.
34. McIlwain JT. Topographic relationships in projection from striate cortex to superior colliculus of the cat. J Neurophysiol 1973; 36: 690-701.
35. Mrzljak L, Uylings HBM, Kostović I, van Eden CG. Prenatal development of neurons in the human prefrontal cortex. II. A quantitative Golgi study. J Comp Neurol 1992; 316: 485-496.
36. Myatt DR, Nasuto SJ. Three-Dimensional Reconstruction of Neurons with Neuromantic. AISB Quarterly 2008; 125: 1-2.
37. Nakamura S, Akiguchi I, Kameyama M, Mizuno N. Age-related changes of pyramidal cell basal dendrites in layers III and V of human motor cortex: a quantitative Golgi study. Acta Neuropathol 1985; 65: 281-284.
38. Nomura H, Ando F, Niino N, Shimokata H, Miyake Y. Age-related change in contrast sensitivity among Japanese adults. Jpn J Ophthalmol 2003; 47: 299-303.
39. Ota M, Yasuno F, Ito H, Seki C, Kozaki S, Asada T, Suhara T. Age-related decline of dopamine synthesis in the living human brain measured by positron emission tomography with L-[β-11C]DOPA. Life Sci 2006; 79: 730-736.
40. Owsley C, Sekuler R, Boldt C. Aging and low-contrast vision: face perception. Investig Ophthalmol Vis Sci 1981; 21: 362-365.
41. Page TL, Einstein M, Duan H, He Y, Flores T, Rolshud D, Erwin JM, Wearne SL, Morrison JH, Hof PR. Morphological alterations in neurons forming corticocortical projections in the neocortex of aged Patas monkeys. Neurosci Lett 2002; 317: 37-41.
42. Pakkenberg B, Gundersen HJG. Neocortical neuron number in humans: effects of sex and age. J Comp Neurol 1997; 384: 312-320.
43. Park DC, Polk TA, Park R, Minear M, Savage A, Smith M R. Aging reduces neural specialization in ventral visual cortex. PNAS 2004; 101: 13091-13095.
44. Peters A. Aging in monkey cerebral cortex. In: Cerebral cortex, Vol. 9, Normal and altered states of function. Peters A, Jones EG (eds.). Plenum Press, New York 1991, pp. 485-510.
45. Peters A, Sethares C. Aging and the Meynert cells in rhesus monkey primary visual cortex. Anat Rec 1993; 236: 721-729.
46. Peters A, Sethares C, Moss MB. The effects of aging on layer 1 in area 46 of prefrontal cortex in rhesus monkey. Cereb Cortex 1998; 8: 671-684.
47. Ross JE, Clarke DD, Bron AJ. Effect of age on contrast sensitivity function: uniocular and binocular findings. Br J Ophthalmol 1985; 69: 51-56.
48. Rumberger A, Schmidt M, Lohmann H, Hoffman K-P. Correlation of electrophysiology, morphology, and functions in corticotectal and corticopretectal projection neurons in rat visual cortex. Exp Brain Res 1998; 119: 375-390.
49. Samorajski T. How the human brain responds to aging. J Am Geriat Soc 1976; 24: 4-11.
50. Satorre J, Cano J, Reinoso-Suarez F. Stability of the neuronal population of the dorsal lateral geniculate nucleus (LGNd) of aged rats. Brain Res 1985; 339: 375-377.
51. Schefrin BE, Tregear SJ, Harvey Jr LO, Werner JS. Senescent changes in scotopic contrast sensitivity. Vision Res 1999; 39: 3728-3736.
52. Scheibel ME, Lindsay RD, Tomiyasu U, Scheibel AB. Progressive dendritic changes in aging human cortex. Exp Neurol 1975; 47: 392-403.
53. Sholl DA. Dendritic organization in the neurons of the visual and motor cortices of the cat. J Anat 1953; 87: 387-406.
54. Swadlow HA. Influence of VPM afferents on putative inhibitory interneurons in S1 of the awake rabbit: evidence from cross-correlation, microstimulation, and latencies to peripheral sensory stimulation. J Neurophysiol 1995; 73: 1584-1599.
55. Takashima S, Chan F, Becker LE, Armstrong DL. Morphology of the developing visual cortex of the human infant: a quantitative and qualitative Golgi study. J Neuropathol Exp Neurol 1980; 39: 487-501.
56. Tigges J, Herndon JG, Peters A. Neuronal population of area 4 during the life span of the rhesus monkey. Neurobiol Aging 1990; 11: 201-208.
57. Tran DB, Silverman SE, Zimmerman K, Feldon SE. Age-related deterioration of motion perception and detection. Graefes Arch Clin Exp Ophthalmol 1998; 236: 269-273.
58. Tsiola A, Hamzei-Sichani F, Peterlin Z, Yuste R. Quantitative morphologic classification of layer 5 neurons from mouse primary visual cortex. J Comp Neurol 2003; 461: 415-428.
59. Uylings HBM, de Brabander JM Neuronal changes in normal human aging and Alzheimer's disease. Brain Cogn 2002; 49: 268-276.
60. Van Pelt J, Van Galen E, Wolters P, Ramakers GJA, Vajda I. Effects of low-frequency stimulation on spontaneous firing dynamics in dissociated cortical cultures on multi-electrode arrays. Proceedings MEA Meeting 2006, BIOPRO edition vol. 3, BIOPRO Baden-Wurttemberg Gmbh, Stuttgart 2006, pp. 19-21.

61. Vincent SL, Peters A, Tigges J. Effects of aging on the neurons within area 17 of rhesus monkey cerebral cortex. Anat Rec 1989; 223: 329-341.
62. Wang, Y, Chan GLY, Holden J E, Dobko T, Mak E, Schulzer M, Huser JM, Snow BJ et al. Age-Dependent Decline of Dopamine D1 Receptors in Human Brain: A PET Study. Synapse 1998; 30: 56-61.
63. Weale RA. Senile changes in visual acuity. Trans Ophthalmol Soc UK 1975; 95: 36-38.
64. Williams RS, Ferrante RJ, Caviness VS Jr. The Golgi rapid method in clinical neuropathology: morphological consequences of suboptimal fixation. J Neuropathol Exp Neurol 1978; 37: 13-33.
65. Xu YH, Wang H, Chen Q, Zhou YF. Age and Sex-related changes of the visual cortex of the rat. Zool Res 2007; 28: 297-302.

Original article

Folia Neuropathologica

IgG4-related inflammatory orbital pseudotumors – a retrospective case series

Krzysztof Oles[1], Wojciech Szczepanski[2], Jacek Skladzien[1], Krzysztof Okon[2], Joanna Leszczynska[1], Emilia Bojanowska[1], Magdalena Bialas[2], Agnieszka Wrobel[3], Joanna Mika[4]

[1]Department of Otolaryngology, Head and Neck Surgery of the Jagiellonian University, Krakow, [2]Department of Pathomorphology, Medical College Jagiellonian University, Krakow, [3]Department of Otolaryngology, Medical College Jagiellonian University, Krakow, [4]Department of Pain Pharmacology, Institute of Pharmacology, Krakow, Poland

Folia Neuropathol 2015; 53 (2): 111-120 DOI: 10.5114/fn.2015.52407

Abstract

Orbital diseases may be divided into congenital defects of the orbit, infectious and inflammatory diseases, orbital tumors (including malignant and benign tumors) and injuries. Idiopathic inflammatory syndromes are often encountered within the orbit and are usually classified as orbital pseudotumors. The etiology of pseudotumors of the vision organ is unknown. Infectious agents, autoimmune disorders and improper healing are taken into consideration in the pathogenesis of this disorder. Thanks to detailed studies conducted in recent years, a new disease syndrome was identified in 2001. It is known as IgG4-related disease, and its differentiation is based on the analysis of IgG4 levels in the affected tissues. Orbital locations of the disease were first reported in Japan as late as at the end of 2009. This finding triggered the European studies on this subject. To date, no such studies have been conducted in Poland. The starting study population consisted of 167 patients with isolated infiltrative tumor diseases within the orbital region treated at the Department of Otolaryngology, Head and Neck Surgery of the Medical College Jagiellonian University in Krakow. Detailed analysis and diagnostic screening for IgG4-related disease was performed in a total of 17 patients diagnosed with orbital pseudotumor.

Key words: *orbital diseases, pseudotumors, IgG4-related disease, idiopathic inflammation of the orbit.*

Introduction

Orbital diseases may be divided into congenital defects of the orbit, infectious and inflammatory diseases, injuries and tumors, including malignant and benign tumors. The diseases may either originate at orbital structures, or be due to continuous spread of the pathological process from adjacent tissues, or constitute distant metastases as well as symptoms of a systemic disease. The variety of tumors observed within the orbit is due to its complex development and structure [21].

Idiopathic inflammatory syndromes are often encountered within the orbit and are usually classified as orbital pseudotumors. Usually, inflammatory orbital pseudotumors are represented as non-granulomatous inflammatory processes in the orbit or the eyeball, with unknown local or systemic etiology. In most cases, the diagnosis is made on the basis of

Communicating author:
Krzysztof Oles, Department of Otolaryngology, Head and Neck Surgery, Jagiellonian University, Krakow, Poland,
e-mail: olokrista@op.pl

the interview, clinical presentation, response to steroid treatment and the results of laboratory investigations and biopsies. The clinical presentation of pseudotumors is very diverse and may resemble numerous other diseases, such as lymphoma, sarcoidosis, fibromatosis, or systemic connective tissue disorders [22]. Pseudotumors should exclude inflammations due to Wegener's granulomatosis, persistent foreign bodies, sclerosing hemangiomas, complications of injuries and inflammation of paranasal sinuses. Pseudotumors are the most common orbital disorder in adults after Graves' orbitopathy; their incidence is estimated at 4.7-6.3% of all orbital diseases [27]. Bilateral location of pseudotumors in adult patients may suggest the presence of a generalized disease such as generalized vasculitis or generalized lymphoid hyperplasia. Patients suffering from pseudotumors often complain of acute pain located within the orbit, limited mobility of the eyeball, eyeball protrusion and impaired acuity of vision. Conjunctival hyperemia, eyelid swelling and redness and excessive lacrimation are also common. Pseudotumors may affect various orbital structures, such as muscles, adipose tissue or lacrimal glands. The etiology of pseudotumors of the vision organ is unknown. Infectious agents, autoimmune disorders and improper healing are taken into consideration in the pathogenesis of this disorder. Macroscopically, orbital pseudotumors are most commonly solid, well-differentiated masses of yellow/gray or pink/gray color. Inflammatory pseudotumors are commonly multifocal and may cause inflammation of extraorbital muscles, lacrimal tracts, Tenon's capsule and cerebral meninges surrounding the optic nerve and the adjacent tissues [35].

Thanks to detailed studies conducted in recent years, a new disease syndrome was identified in 2001. It is known as IgG4-related disease, and its differentiation is based on the analysis of IgG4 levels in the affected tissues [39]. Orbital locations of the disease were first reported in Japan as late as at the end of 2009. This finding triggered the European studies on this subject. To date, no such studies have been conducted in Poland. It has been established that IgG4-related orbital disease is a recently defined inflammatory process that is characterized by 1) inflammatory infiltration of IgG4-producing plasma cells; 2) tendency to form tumorous lesions at different sites; 3) increased serum IgG4 levels, although this is not a required condition [22]. IgG4-related disease is considered to be a generalized process involving a wide spectrum of various diseases that may affect distant organs. Particular progress was made recently due to in-depth clinical and pathological studies of diseases suspected of being dependent on increased levels of IgG4-positive plasma cells [27]. This type of lesion has been observed in a variety of organs, such as pancreas, hepatobiliary duct, salivary glands, orbits, lymph nodes, retroperitoneal space, kidneys, lungs, skin, and aorta. It is difficult to estimate the incidence rate of IgG4-related diseases due to the relatively low awareness of the possibility of this disease among physicians. The most reliable data originating from Japan estimate the incidence rate of IgG4-related disease to be 0.28-1.08 cases per 100 000 individuals [30].

Clinical experiments on primary, isolated orbital tumors show that they remain difficult to diagnose and treat for physicians of different specialties; we decided to address this issue in light of the recent establishment of IgG4-related disease as a new nosocomial entity. Orbital IgG4-related disease is a recently reported issue that may prove important for elucidation of the etiology of idiopathic, lymphoplasmacytic or fibrotic disorders of various organs, including the orbits. The goal of this study is to facilitate the diagnostic procedures in the treatment of patients with non-neoplastic, primary, isolated tumors, excluding eyeball tumors, metastatic tumors and tumors infiltrating from adjacent tissues, including from the nose and paranasal sinuses. Detailed assessments were performed in a group of patients diagnosed with orbital pseudotumors in the clinical material of the Otorhinolaryngological Clinic of the Jagiellonian University Medical College over the last 11 years. The usefulness of immunohistochemical diagnostics in correct diagnosis of IgG4-related orbital disease was studied.

Material and methods

The study was undertaken to facilitate the diagnostics and treatment of patients with non-neoplastic, primary, isolated tumors, excluding eyeball tumors, metastatic tumors and tumors infiltrating from adjacent tissues, including from the nose and paranasal sinuses. Detailed, retrospective assessments were performed in a group of patients with isolated orbital diseases in the clinical material of the Otorhinolaryngological Clinic of the Jagiellonian

University Medical College in the years 2002-2012. All the experiments reported in this manuscript were conducted in accordance with the local ethics committee of Medical College Jagiellonian University, Krakow, Poland. The usefulness of immunohistochemical diagnostics in correct diagnosis of IgG4-related orbital disease was studied. The study was conducted in a group of patients qualified for radical procedures or biopsies (often without initial histopathological diagnosis). Patients with a history of previous surgery, radiation therapy and corticosteroid treatment in relation to the vision organ were excluded from the study. All specimens archived at the Chair of Pathomorphology of the Jagiellonian University Medical College in Krakow were subjected to histopathological examination. At the first stage, 17 cases of orbital pseudotumors were selected from histological specimens subjected to routine HE stain.

Immunohistochemical assays were carried out in a standard manner [31,32]. The assessment of eosinophils and neutrophils was carried out by means of HE staining, while quantitation of plasma cells was achieved by using murine monoclonal anti-CD138 antibodies (DakoCytomation, Denmark, 1 : 100, 30 min, citrate buffer). IgG levels were determined using rabbit polyclonal antibodies (DakoCytomation, Denmark, 1 : 800, 30 min proteinase K unmasking), while IgG4 levels were determined using rabbit monoclonal antibodies (Aabcam, 1 : 300, 30 min, citrate buffer). Visualization of the antigen-antibody complex was achieved using the Ultra Vision LP Value Detection System (LabVision Corp.) with 3,3'-diaminobenzidine (DAB) tetrahydrochloride (DAKO Corp.) chromogen kit. Cell nuclei were contrasted using Mayer's hematoxylin for 1 minute and then covered by cover glasses in Cytoseal XYL (Thermo SCIENTIFIC). Microscopic specimens were assessed using Olympus CX41 and Nikon Eclipse 50i microscopes.

In each case, guidelines [32] were followed by searching for three sites with the highest number of $IgG4^+$ plasma cells and assessing the number of these cells at these sites at 40x magnification. Next, total plasma cell counts and IgG-producing plasma cell counts were assessed in identical areas in samples assayed for IgG and CD138. Routinely stained specimens were assessed for fibrosis, other infiltrations within the lesion (infiltrations of acidophils and neutrophils as well as lymphoplasmacytic infiltration with or without formation of follicles) and vascular lesions manifested as wall thickening and lumen narrowing. All these lesions were assessed by semiquantitative methods (1+: small lesions; 2+: medium lesions; 3+: advanced lesions). Immunohistochemical assays using anti-IgG, anti-IgG4 and anti-CD138 antibodies were used to estimate the $IgG4^+/CD138^+$ and $IgG4^+/IgG^+$ ratios.

Results

Of the group of isolated orbital tumors, consisting of 167 patients, patients diagnosed with malignant tumors on the basis of postoperational histopathological assessment were excluded. A total of 116 remaining patients were included in the selected study group on the basis of postoperational histopathological assessment. Histopathological diagnoses included pseudotumor, vascular malformations, cavernous angioma, arterial angioma, dermoid cyst with inflammatory infiltration, mixed tumor of the lacrimal gland, inverted papilloma, neurinoma, neurofibroma, meningioma, and adipoma. Detailed analysis and diagnostic screening for IgG4-related disease was performed in a total of 17 patients diagnosed with orbital pseudotumor. The mean age at diagnosis was 49.65 years. The analysis of tumor locations in patients diagnosed with orbital pseudotumor revealed anteroequatorial location in 7 cases and retroequatorial location in 10 patients. Pseudotumors were located within the right orbit in 7 patients and within the left orbit in 9 patient. In one patient, pseudotumors were located in both orbits. A similar incidence of the tumor was observed in both genders (Fig. 1A); no significant differences were observed in relation to the affected orbit side (Fig. 1B).

A detailed analysis of histopathological lesions (Table I) in patients diagnosed with orbital pseudotumors revealed changes in the $IgG4^+/CD138^+$ and $IgG4^+/IgG^+$ ratios in patients subjected to immunohistochemical diagnostic screening for IgG4-related disease. Extensive vascular lesions with wall thickening and lumen narrowing were observed in all patients; the $IgG4^+/CD138^+$ ratio was higher than 10% in all cases. The mean $IgG4^+/CD138^+$ ratio was 32.4% (Fig. 2A). The results were obtained by calculating the $IgG4^+/IgG^+$ ratio, usually exceeding 40%, and more than 80% in 3 patients. The mean $IgG4^+/IgG^+$ ratio was 53.5% (Fig. 2B). Most histopathological

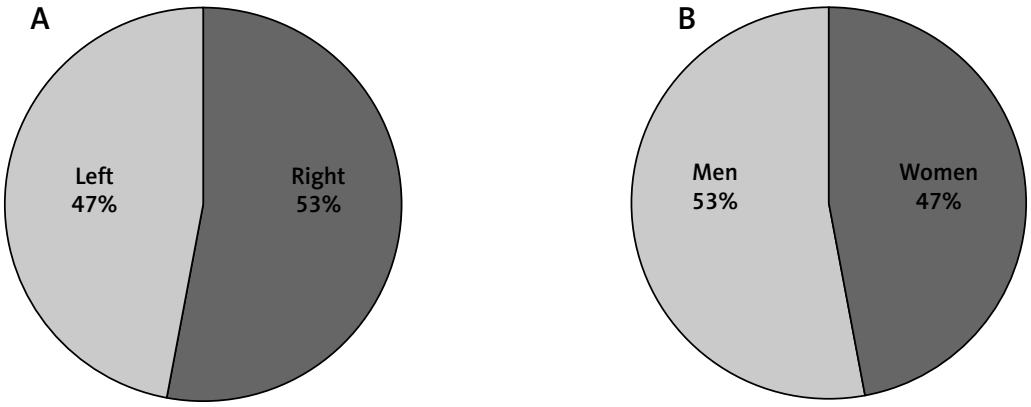

Fig. 1. A) Comparison of incidence of pseudotumors within the right or left orbit. **B)** Comparison of incidence of pseudotumors in females and males.

Table I. Detailed analysis of age, gender and tumor location in patients with histopathological diagnosis of orbital pseudotumor subjected to immunohistochemical screening for IgG4-related disease

Pseudotumor – IgG4⁺-related				
n	Sex	Age	IgG4⁺/CD138⁺	IgG4⁺/IgG⁺
1	F	41	> 20%	> 40%
2	F	44	> 40%	> 60%
3	F	67	> 20%	> 50%
4	M	52	> 30%	> 50%
5	M	17	> 20%	> 40%
6	M	18	> 20%	> 50%
7	M	54	> 40%	> 60%
8	F	75	> 10%	> 40%
9	M	41	> 80%	> 80%
10	F	40	> 50%	> 50%
11	M	62	> 10%	> 40%
12	F	32	> 20%	> 40%
13	F	79	> 10%	> 40%
14	F	50	> 40%	> 60%
15	M	55	> 80%	> 80%
16	M	66	> 20%	> 50%
17	M	51	> 40%	> 80%

F – female, M – male

specimens featured follicles and lacrimal gland tissue. Table I presents the lack of correlation between the IgG4⁺/CD138⁺ and IgG4⁺/IgG⁺ ratios depending on the age and gender of patients.

Table II presents a detailed analysis of histopathological lesions in patients with histopathological diagnosis of orbital pseudotumor subjected to immunohistochemical screening for IgG4-related disease. The following lesions were observed in histopathological examinations of operated patients: extensive fibrosis – mean grade of 2.67 (scale 0-3), numerous plasma cell infiltrations – 2.05 (scale 0-3), eosinophilic infiltrations of grade up to 1.5 (scale 0-3), i.e. as many as 20-25 cells in certain fields under large magnification (40x); in most cases only isolated neutrophils – 0.18 (scale 0-3), vascular lesions (wall thickening and stenosis of tiny vessels of different intensity) in all cases as well as inflammatory thrombotic lesions in 3 cases; the IgG4⁺/CD138⁺ ratio was always more than 10%, 32.3% on average, while the IgG4⁺/IgG⁺ was above 40% in all cases, and more than 80% in 3 patients (ca. 53.5% on average) (Table II). In all cases, fragments of lacrimal gland tissue and follicles were present in all histopathological specimens. Figure 3 presents a typical image of an inflammatory orbital pseudotumor. Profuse lymphoplasmacytic infiltration of fibrous tissue, and CD138⁺ plasma cells are visible. The IgG⁺ reaction seems to be present in a larger number of cells compared to the CD138⁺ reaction. However, it should be noted that IgG may also be produced by some of the B lymphocytes differentiating into plasma cells. What is interesting, nearly all immunohistochemistry-marked plasma cells (CD138⁺) are IgG4-positive.

Discussion

Reports of possible incidence of IgG4-related disease were published in late 2001. The first suspi-

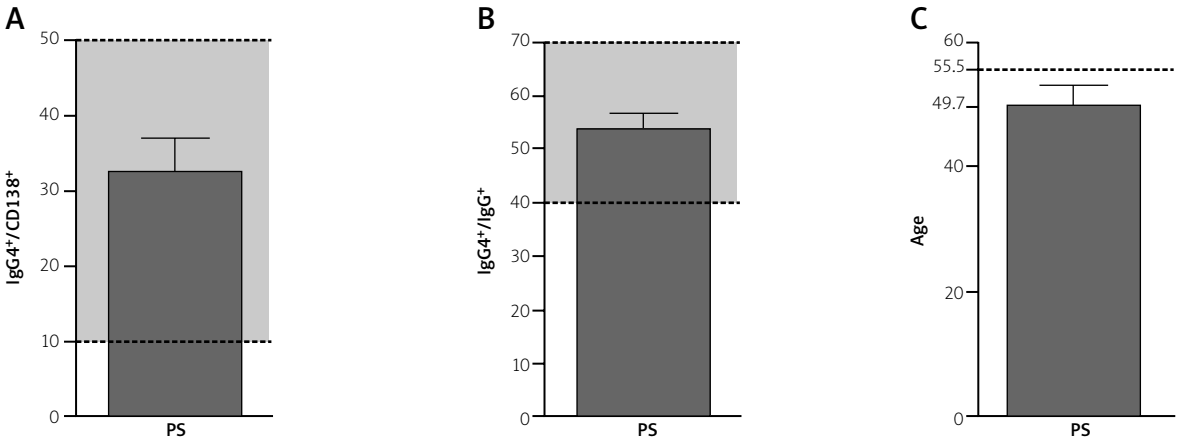

Fig. 2. Comparison of IgG4$^+$/CD138$^+$ ratio **(A)** and IgG4$^+$/IgG$^+$ ratio **(B)** in pseudotumors and average patient age **(C)**. In IgG4$^+$, the IgG4$^+$/CD138$^+$ ratio is 10-50 while the IgG4$^+$/IgG$^+$ ratio is 40-70.

Table II. Detailed analysis of histopathological lesions in patients with histopathological diagnosis of orbital pseudotumor subjected to immunohistochemical screening for IgG4-related disease

Pseudotumor – IGG4$^+$-related diseases						
n	FSS	Cell infiltration			Vascular changes	
		PLAS	NEUT	EOS	TVL	TBVW
1	+++	+++	–	++	++	+
2	+++	++	–	++	+++	++
3	+++	+++	–	+++	++	++
4	+++	+++	–	+++	++	+
5	++	+++	–	+	+	+
6	++	+++	–	+	+	+
7	+++	+++	+/–	++	+++	++
8	+++	+++	–	–	++	+
9	+++++	++	–	+	+++	+++
10	+++	+++/++	–	+++	++	++
11	+++	+++/++	–	+	++	+
12	++	+++/++	–	+	++	+/–
13	++	++	+/–	++	++	
14	+++	+/–	+/–	+/–	++	++
15	++	+++	+/–	+++	+	–
16	++	++	+/–	+	+	+
17	++	++	+/–	+	+	+

Scale: – none, +/– sparse, + low, ++ medium, +++ high, +++++ very high
FSS – fibrosis, PLAS – plasma cells, NEUT – neutrophils, EOS – eosinophils, TVL – thinning of the vascular lumen, TBVW – thickening of blood vessels walls

cions of orbital locations of the disease were reported in Japan as late as at the end of 2009. This finding triggered the European studies on this subject [4]. The basic consensus of the diagnostic criteria for IgG4-related diseases was established in 2010. IgG4-related orbital disease may also be diagnosed by the presence of criteria proposed by Umehara *et al.* [37]. Patients with suspected IgG4-related orbital disease may be assessed and diagnosed according to either of these two sets of diagnostic criteria [37]. In 2010, Zen and Nakanuma demonstrated that IgG4-related disease symptoms may have different anatomical locations despite the same levels of IgG4 in the studied tissues. This conclusion supports the

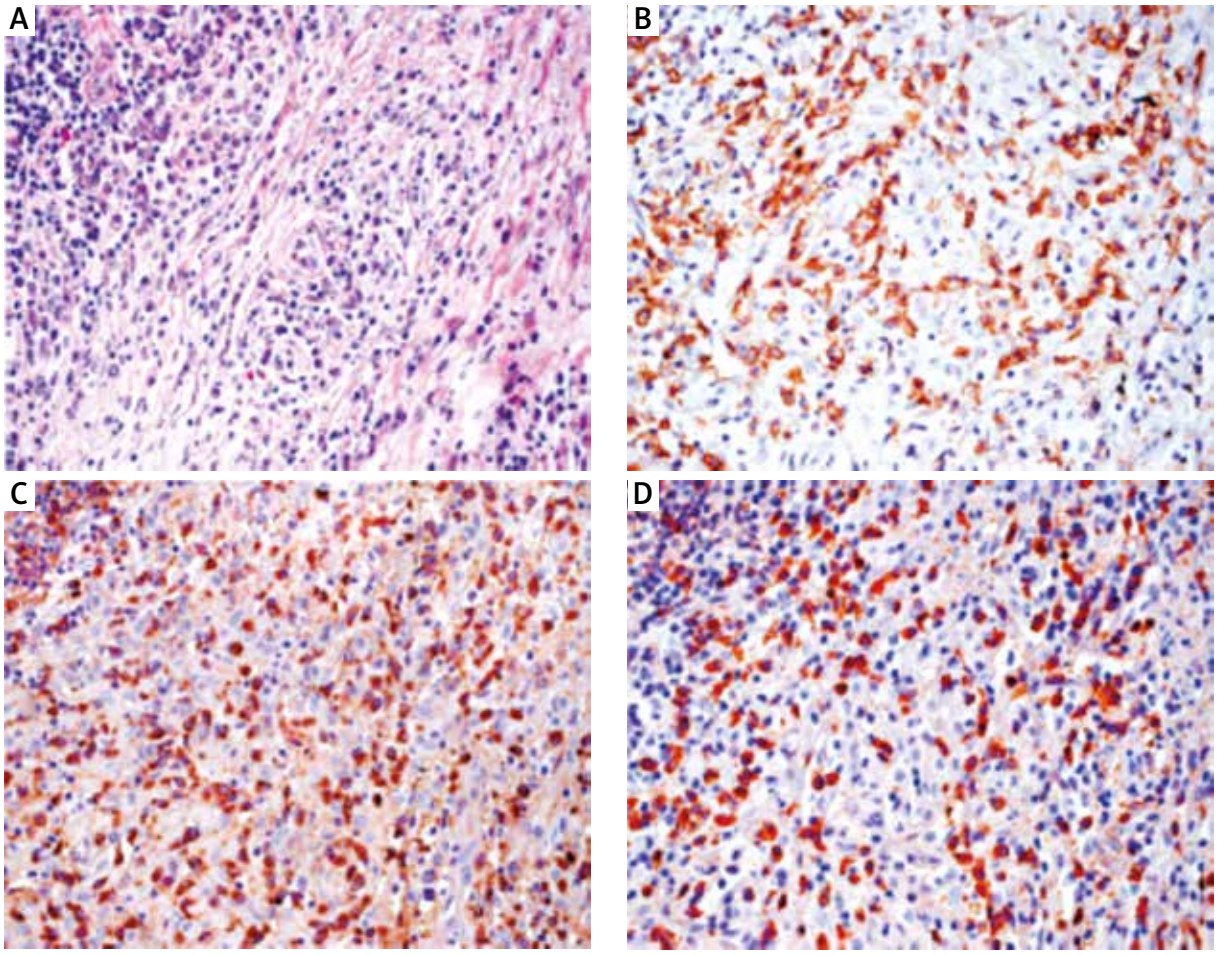

Fig. 3. Inflammatory orbital pseudotumor. **A)** Profuse lymphoplasmacytic infiltration of fibrous tissue. HE. 40x. **B)** Clear positive immunohistochemical reaction to CD138 marking the plasma cells. 40x. **C)** Clear positive immunohistochemical reaction to IgG-positive cells – the reaction appears to be present in a higher number of cells than the reaction to CD138. However, it should be noted that IgG may also be produced by some B lymphocytes differentiating into plasma cells. 40x. **D)** Nearly all immunohistochemistry-marked plasma cells (CD138+) are IgG4-positive. 40x.

IgG4 dependence of the disease [7,8]. IgG4-related orbital disease is a general term for the pathologies in the orbital region. Different orbital locations are possible. Most typically, the disease is diagnosed within the lacrimal gland (IgG4-related dacryoadenitis). This conclusion as drawn by other authors was also confirmed by the results of our study. The disease may also present as an IgG4-related orbital inflammatory pseudotumor or IgG4-related orbital myositis, which was also observed in the patients examined as part of this study.

To date, no such studies have been conducted in Poland. Examinations of such patients were analyzed both retrospectively and prospectively over the last 11 years to assess the possibility of IgG4-related orbital disease. The starting study population consisted of 167 patients with isolated infiltrative tumor diseases within the orbital region treated at the ORL Clinic of the Jagiellonian University Medical College in Krakow. Of all the studied and analyzed patients, a final group was selected to undergo diagnostic examinations for IgG4-related disease. The study group consisted of 17 patients with the diagnosis of pseudotumor lesions. According to the literature, the mean age for the established and probable cases of IgG4-related orbital disease is estimated at 55.5 years [2]. The value was similar in our study, being 49.6 years in the group of pseudotumor patients.

Orbital pseudotumors are idiopathic inflammatory processes occurring within the orbit and involving hypertrophy of fibrovascular tissue with low cellular polymorphism and lymphoplasmacytic infiltrations. Usually, orbital pseudotumors do not extend beyond the borders of the orbit, and their clinical course may be very diverse [21,22,25,40]. A total of 17 patients diagnosed with pseudotumors were selected from the population of non-malignant orbital lesion patients and subjected to diagnostic examinations for IgG4-related disease. The obtained results confirmed IgG4-related orbital disease. A high degree of fibrosis was observed in histopathological specimens, with numerous plasmacytic infiltrations containing numerous eosinophils, up to 25 cells per field. Only isolated neutrophils were observed in about 50% of cases. Vascular lesions (wall thickening and stenosis of tiny vessels of different intensity) were also observed in all cases; inflammatory thrombotic lesions were observed in three cases. Histopathological lesions observed in the study material were very similar to those described by other authors [2]. What is important, in all patients diagnosed with pseudotumors, the $IgG4^+/CD138^+$ ratio in orbital tissues was always more than 10%, and often as much as 40%. The $IgG4^+/IgG^+$ ratio was above 40% in all cases, and more than 80% in 3 patients. In all cases, fragments of lacrimal gland tissue and follicles were present in all histopathological specimens. As demonstrated by an increasing number of papers and confirmed by the results of this study, the tissue $IgG4^+/IgG^+$ ratio is the most important parameter for the diagnosed cases associated with $IgG4^+$ plasma cells, and its value should be higher than 40% [7,8,36,39]. Other criteria, such as obliterated venous pattern without the required inflammatory reaction or storiform fibrosis, are crucial for the diagnosis of IgG4-related disease [3,8,12,29,52,53]. In IgG4-related disease, the total number of IgG4-positive plasma cells must be elevated. It should be underlined that the study material was retrospective and has been analyzed several times.

Venous vessels are obliterated by profuse lymphoplasmacytic infiltration. Lymphocytes and plasma cells are present within both the vessel walls and the lumen. Partial obliteration of veins and inflammatory infiltration of the entire wall are also indicative of IgG4-related disease. Lacrimal gland tissue was predominant in specimens analyzed at the Krakow Clinic. Very high eosinophilic infiltration of up to 20 cells per field of view was a characteristic feature of the specimens. According to worldwide literature, IgG4-related orbital disease is rarely associated with lymphoplasmacytic infiltration and eosinophilic material-containing macrophages [9]. In this aspect of IgG4-related disease, our results are in contrast to these findings. On the other hand, we confirmed the presence of microvascular lesions, reported to occur rarely for IgG4-related disease by other authors [9,26]. The clinical presentation usually excludes definite diagnosis. Most commonly, patients present at the laryngologist's office with increasing orbital pain, impaired mobility of the eyeball and eyeball protrusion. In many cases, conjunctival edema and hyperemia, eyelid plethora and soft tissue edema were observed. Pain of the extraorbital muscle wall suggested a high likelihood of an orbital inflammatory syndrome, particularly myositis. Visual acuity was impaired in cases of optic nerve or posterior sclera involvement. Sometimes, systemic symptoms, such as leukocytosis and fever, might indicate inflammation, which was consistent with observations made by other authors [3,21,22,25,27,40].

Biopsy is not required in all cases, as the clinical and radiological presentation (including CT and MRI scans) may be sufficient to establish the diagnosis and start treatment. Other systemic disorders that accompany IgG4-related disease include autoimmune pancreatitis, retroperitoneal fibrosis, mediastinal fibrosis, sclerosing cholangitis, Sjögren's syndrome, xanthogranuloma, or inflammatory myofibroblastic tumor [4]. The diagnostics of IgG4-related disease involves the use of intravenous gallium-67, which is accumulated at inflammation sites and, as evidenced by numerous studies of IgG4-related diseases, is most commonly gathered within the lung tissue (hila) (77%) and the pancreas (76%). Gallium accumulation is also relatively common in salivary glands (54%), lacrimal glands (54%) and periaortal tissues (23%). Chronic inflammatory conditions that might obscure IgG4-related disease include: salivary tract inflammation, non-malignant oral lesions (e.g. cysts), gastrointestinal diseases (including Crohn's disease and intestinal diverticulitis), synovitis, some malignant tumors (squamous cell carcinoma, adenoid cystic carcinoma), and numerous inflammatory skin diseases.

Each of the examined patients was subjected to CT and/or MRI scans before the scheduled surgery. On this basis, the appropriate treatment method and

surgical approach were determined. Detailed radiological consultation was obtained, providing data to adopt a suitable treatment strategy. The entire management conducted at the Krakow Clinic of Otorhinolaryngology suggests that the group of pseudotumors is of a very diverse character. Pseudotumors may resemble numerous other diseases, such as lymphoma, sarcoidosis, fibromatosis, and systemic connective tissue disorders (e.g. lupus erythematosus and other granulomatous disorders), as was also reported in other studies [18,27,38].

The treatment and the outcomes in patients diagnosed with IgG4-related disease after one or more cycles of corticosteroids were different in female and male patients. IgG4-related orbital disease with the involvement of other organs may be considered a generalized disorder. The orbital location may coexist with an extraorbital location [24]. Most commonly, extraorbital location is associated with the involvement of parotid glands and lymph nodes [5,11,14,15,29,30].

Positron emission tomography is an imaging examination that markedly facilitates the diagnosis of a systemic IgG4-related disease, both in cases distant from the orbit and in clinically silent IgG4-related diseases [19]. Two such patients were identified in the study material, with generalized IgG4-related disease being confirmed by PET scans [9,24,35].

The consensus guidelines for histopathological diagnostics of IgG4-related orbital disease were published at an international symposium in 2011 [7,8]. It was determined that IgG4-related disease is characterized by different degrees of fibrosis and extensive lymphoplasmacytic infiltration of $IgG4^+$ cells [7,8,33]. Lymphoplasmacytic infiltrations are more extensive at early stages of the disease and consist of polyclonal T cells, $IgG4^+$ plasma cells and scattered eosinophils. Subsequent biopsies conducted in a case of IgG4-related inflammation of lacrimal ducts revealed increased fibrosis. The process has been proposed as the natural history of the disease which, when accumulated, in the fibrosis stage [5,10]. However, some diseases may originate from a primary sclerotic process. The histopathological image of IgG4-related orbital disease includes lymphoplasmacytic infiltration of various degree with predominant fibrosis or reactive lymphoid hyperplasia [14,15,26,29,36]. IgG4-related orbital disease may involve infiltrations of lymphoplasma cells, macrophages, as well as eosinophils [14,15]. The clinical material in this study was characterized by significant differences in the histopathological image compared to that presented by other authors. A characteristic trait in the histological presentation of IgG4-related disease is the presence of thromboangiitis obliterans, very rare in orbital IgG4-related disease [16,17,26]. The pathogenesis of the disease may include the immune response to an antigen within the upper segment of the respiratory/alimentary tract. Nosocomial entities currently identified as IgG4-related diseases include numerous disorders of heterogeneous clinical presentations, previously listed as separate and unrelated entities [13]. IgG4-related disease should be suspected on the basis of the presence of one of the accompanying symptoms, such as symmetrical swelling of lacrimal or salivary glands, autoimmune pancreatitis, inflammatory orbital pseudotumor, retroperitoneal fibrosis, lymphadenopathies, or Castleman's disease. The results presented in this study are in agreement with the conclusions of the panel of experts gathered in Boston in 2011 to present the "Consensus statement on the pathology of IgG4-related disease" [7,8]. The comprehensive diagnostic criteria proposed by Umehara *et al*. in 2012 provided a breakthrough in the establishment of IgG4-related orbital disease as a unique nosocomial entity; however, some details require further elucidation. The authors did not report on the size of the large magnification field to be used when counting IgG4-positive cells. IgG4-related orbital disease is a general term for pathologies in the orbital region. Different orbital locations are possible. Most typically, the disease is diagnosed within the lacrimal gland (IgG4-related dacryoadenitis); it may also present as an IgG4-related orbital inflammatory pseudotumor or IgG4-related orbital myositis. Serum IgG4 level is considered to be a less valuable diagnostic marker compared to the tissue IgG4 content and is usually elevated by 40% with biopsy-confirmed IgG4-related disease [28]. Recent results suggest that it is the ratio between serum IgG4 and IgG, rather than the levels themselves, that is important, as the serum levels themselves may be within the normal range. According to recent international studies [19,20] the serum $IgG4^+/IgG^+$ ratio of 5-10% may be a sensitive and specific marker indicative of early and single organ-limited development of an IgG4-related disease. Having analyzed the results of histopathological assays and serum IgG and IgG4 level tests, the researchers observed significantly elevated

serum IgG4 levels in only one case of bilateral orbital pseudotumor. The remaining results were within the normal laboratory range for IgG4 levels while being at the limit of the range in only 2 cases of orbital pseudotumors (single-sided). Despite the fact that the blood levels of IgG and IgG4 were normal, the analysis of the $IgG4^+/IgG^+$ ratio revealed a value of above 8%, indicative of possible development of an IgG4-related disease limited to a single organ, as suggested by Masaki et al. in their article published in 2012. Such results were observed in 3 of the diagnosed patients in whom pseudotumors were shown to be associated with elevated IgG4 levels in orbital tissues.

Idiopathic orbital inflammation poses a significant challenge to therapists and is characterized by a tendency to recur in more than 50% of cases [16,17]. The treatment is empirical in nature, as the pathophysiology of the disease has not been fully explained. Clinical treatment involves administration of corticosteroids. Physicians are often left with symptomatic treatment as the only option, including suppression of inflammation with corticosteroids. Identification of IgG4-related orbital diseases is important as lesions may be very sensitive to targeted biological treatment [13]. Unfortunately, no prospective clinical studies are available with regard to IgG4-related disease, with treatment methods being based on retrospective observations in relatively small patient groups. Before initiating treatment, it is important to establish the histopathological diagnosis and exclude possible malignancy [10]. Rituximab, a monoclonal anti-CD20 antibody, was used against B cells. Rapid reduction in blood IgG4 levels was observed in patients who received the drug [6]. Thus, modulation of B cell function led to a change in interactions between B cells and plasma cells, affording good therapeutic effects. Currently, a chemotherapeutic agent, bortezomib, is also in use.

To sum up, IgG4-related disease is most commonly manifested by a tumorous mass in the affected organ. Correct presurgical screening for IgG4-related disease may allow major orbital procedures to be avoided in some patients. Identification of typical histopathological lesions, particularly infiltrations of IgG4-positive plasma cells, remains the gold standard for establishing a correct diagnosis. Although an increased serum IgG level is neither sufficient nor necessary to diagnose IgG4-related disease, it may be helpful in the diagnostic process.

Disclosure

The authors report no conflict of interest.

References

1. Alinari L, Castellucci P, Elstrom R, Ambrosini V, Stefoni V, Nanni C, Berkowitz A, Tani M, Farsad M, Franchi R, Fanti S, Zinzani PL. 18F-FDG PET in mucosa-associated lymphoid tissue (MALT) lymphoma. Leuk Lymphoma 2006; 47: 2096-2101.
2. Andrew N, Kearney D, Selva D. IgG4-related orbital disease: a meta-analysis and review. Acta Ophthalmol 2012; 11: 1-7.
3. Aznabaev MT, Gabdrakhmanova AF, Gaïsina GF. Comprehensive ultrasound diagnosis of orbital tumors and pseudotumors. Vestn Oftalmol 2006; 122: 7-9.
4. Benlemlih A, Szableski V, Bendahou M, Rivière S, Villain M, Costes V. Eosinophilic angiocentric fibrosis: A form of IgG4-related systemic disease. Ann Pathol 2012; 32: 271-275.
5. Cheuk W. Chronic sclerosing dacryoadenitis: part of the spectrum of IgG4-related sclerosing disease. Am J Surg Pathol 2007; 31: 643-645.
6. Conconi A, Martinelli G, Thieblemont C, Ferreri AJ, Devizzi L, Peccatori F, Ponzoni M, Pedrinis E, Dell'Oro S, Pruneri G, Filipazzi V, Dietrich PY, Gianni AM, Coiffier B, Cavalli F, Zucca E. Clinical activity of rituximab in extranodal marginal zone B-cell lymphoma of MALT type. Blood 2003; 102: 2741-2745.
7. Deshpande V, Zen Y, Chan JK, Yi EE, Sato Y, Yoshino T, Klöppel G, Heathcote JG, Khosroshahi A, Ferry JA, Aalberse RC, Bloch DB, Brugge WR, Bateman AC, Carruthers MN, Chari ST, Cheuk W, Cornell LD, Fernandez-Del Castillo C, Forcione DG, Hamilos DL, Kamisawa T, Kasashima S, Kawa S, Kawano M, Lauwers GY, Masaki Y, Nakanuma Y, Notohara K, Okazaki K, Ryu JK, Saeki T, Sahani DV, Smyrk TC, Stone JR, Takahira M, Webster GJ, Yamamoto M, Zamboni G, Umehara H, Stone JH. Consensus statement on the pathology of IgG4-related disease. Mod Pathol 2012; 25: 1181-1192.
8. Deshpande V. The pathology of IgG4-related disease: critical issues and challenges. Semin Diagn Pathol 2012; 29: 191-196.
9. Deshpande V, Sainani NI, Chung RT, Pratt DS, Mentha G, Rubbia-Brandt L, Lauwers GY. IgG4-associated cholangitis: a comparative histological and immunophenotypic study with primary sclerosing cholangitis on liver biopsy material. Mod Pathol 2009; 22: 1287-1295.
10. Divatia M, Kim SA, Ro JY. IgG4-related sclerosing disease, an emerging entity: a review of a multi-system disease. Yonsei Med J 2012; 53: 15-34.
11. Gayed I, Eskandari MF, McLaughlin P, Pro B, Diba R, Esmaeli B. Value of positron emission tomography in staging ocular adnexal lymphomas and evaluating their response to therapy. Ophthalmic Surg Lasers Imaging 2007; 38: 319-325.
12. Go H, Kim JE, Kim YA, Chung HK, Khwarg SI, Kim CW, Jeon YK. Ocular adnexal IgG4-related disease: comparative analysis with mucosa-associated lymphoid tissue lymphoma and other chronic inflammatory conditions. Histopathology 2012; 60: 296-312.
13. Kamisawa T, Funata N, Hayashi Y, Tsuruta K, Okamoto A, Amemiya K, Egawa N, Nakajima H. Close relationship between

autoimmune pancreatitis and multifocal fibrosclerosis. Gut 2003; 52: 683-687.
14. Khosroshahi A, Stone JH. A clinical overview of IgG4-related systemic disease. Curr Opin Rheumatol 2011; 23: 57-66.
15. Kubota T, Moritani S, Katayama M, Terasaki H. Ocular adnexal IgG4-related lymphoplasmacytic infiltrative disorder. Arch Ophthalmol 2010; 128: 577-584.
16. Kubota T, Moritani S, Yoshino T, Nagai H, Terasaki H. Ocular adnexal marginal zone B cell lymphoma infiltrated by IgG4-positive plasma cells. J Clin Pathol 2010; 63: 1059-1065.
17. Lindfield D, Attfield K, McElvanney A. Systemic immunoglobulin G4 (IgG4) disease and idiopathic orbital inflammation; removing 'idiopathic' from the nomenclature? Eye (Lond) 2012; 26: 623-629.
18. Lindfield D. Rituximab in IgG4-related inflammatory disease of the orbit and ocular adnexae. Eye (Lond) 2012; 26: 1386.
19. Mafee MF, Karimi A, Shah JD, Rapoport M, Ansari SA. Anatomy and pathology of the eye: role of MR imaging and CT. Magn Reson Imaging Clin N Am 2006; 14: 249-270.
20. Masaki Y, Kurose N, Umehara H. IgG4-related disease: a novel lymphoproliferative disorder discovered and established in Japan in the 21st century. J Clin Exp Hematop 2011; 51: 13-20.
21. Masaki Y, Kurose N, Yamamoto M, Takahashi H, Saeki T, Azumi A, Nakada S, Matsui S, Origuchi T, Nishiyama S, Yamada K, Kawano M, Hirabayashi A, Fujikawa K, Sugiura T, Horikoshi M, Umeda N, Minato H, Nakamura T, Iwao H, Nakajima A, Miki M, Sakai T, Sawaki T, Kawanami T, Fujita Y, Tanaka M, Fukushima T, Eguchi K, Sugai S, Umehara H. Cutoff Values of Serum IgG4 and Histopathological IgG4+ Plasma Cells for Diagnosis of Patients with IgG4-Related Disease. Int J Rheumatol 2012; 2012: 580814.
22. Mombaerts I, Goldschmeding R, Schlingemann RO, Koornneef L. What is orbital pseudotumor? Surv Ophthalmol 1996; 41: 66-78.
23. Mombaerts I, Schlingemann RO, Goldschmeding R, Koornneef L. Are systemic corticosteroids useful in the management of orbital pseudotumors? Ophthalmology 1996; 103: 521-528.
24. Nemec SF, Peloschek P, Schmook MT, Krestan CR, Hauff W, Matula C, Czerny C. CT-MR image data fusion for computer-assisted navigated surgery of orbital tumors. Eur J Radiol 2010; 73: 224-229.
25. Pasquali T, Schoenfield L, Spalding SJ, Singh AD. Orbital inflammation in IgG4-related sclerosing disease. Orbit 2011; 30: 258-260.
26. Pemberton JD, Fay A. Idiopathic sclerosing orbital inflammation: a review of demographics, clinical presentation, imaging, pathology, treatment, and outcome. Ophthal Plast Reconstr Surg 2012; 28: 79-83.
27. Plaza JA, Garrity JA, Dogan A, Ananthamurthy A, Witzig TE, Salomão DR. Orbital inflammation with IgG4-positive plasma cells: manifestation of IgG4 systemic disease. Arch Ophthalmol 2011; 129: 421-428.
28. Rootman J, McCarthy M, White V, Harris G, Kennerdell J. Idiopathic sclerosing inflammation of the orbit. A distinct clinicopathologic entity. Ophthalmology 1994; 101: 570-584.
29. Sah RP, Chari ST. Serologic issues in IgG4-related systemic disease and autoimmune pancreatitis. Curr Opin Rheumatol 2011; 23: 108-113.
30. Sato Y, Ohshima K, Ichimura K, Sato M, Yamadori I, Tanaka T, Takata K, Morito T, Kondo E, Yoshino T. Ocular adnexal IgG4-related disease has uniform clinicopathology. Pathol Int 2008; 58: 465-470.
31. Sato Y, Ohshima K, Takata K, Huang X, Cui W, Ohno K, Yoshino T. Ocular adnexal IgG4-producing mucosa-associated lymphoid tissue lymphoma mimicking IgG4-related disease. J Clin Exp Hematop 2012; 52: 51-55.
32. Sato Y, Kojima M, Takata K, Morito T, Asaoku H, Takeuchi T, Mizobuchi K, Fujihara M, Kuraoka K, Nakai T, Ichimura K, Tanaka T, Tamura M, Nishikawa Y, Yoshino T. Systemic IgG4-related lymphadenopathy: a clinical and pathologic comparison to multicentric Castleman's disease. Mod Pathol 2009; 22: 589-599.
33. Shrestha B, Sekiguchi H, Colby TV, Graziano P, Aubry MC, Smyrk TC, Feldman AL, Cornell LD, Ryu JH, Chari ST, Dueck AC, Yi ES. Distinctive pulmonary histopathology with increased IgG4-positive plasma cells in patients with autoimmune pancreatitis: report of 6 and 12 cases with similar histopathology. Am J Surg Pathol 2009; 33: 1450-1462.
34. Smyrk TC. Pathological features of IgG4-related sclerosing disease. Curr Opin Rheumatol 2011; 23: 74-79.
35. Strehl JD, Hartmann A, Agaimy A. Numerous IgG4-positive plasma cells are ubiquitous in diverse localised non-specific chronic inflammatory conditions and need to be distinguished from IgG4-related systemic disorders. J Clin Pathol 2011; 64: 237-243.
36. Suga K, Kawakami Y, Hiyama A, Hori K, Takeuchi M. F-18 FDG PET-CT findings in Mikulicz disease and systemic involvement of IgG4-related lesions. Clin Nucl Med 2009; 34: 164-167.
37. Takahira M, Kawano M, Zen Y, Minato H, Yamada K, Sugiyama K. IgG4-related chronic sclerosing dacryoadenitis. Arch Ophthalmol 2007; 125: 1575-1578.
38. Umehara H, Okazaki K, Masaki Y, Kawano M, Yamamoto M, Saeki T, Matsui S, Yoshino T, Nakamura S, Kawa S, Hamano H, Kamisawa T, Shimosegawa T, Shimatsu A, Nakamura S, Ito T, Notohara K, Sumida T, Tanaka Y, Mimori T, Chiba T, Mishima M, Hibi T, Tsubouchi H, Inui K, Ohara H. Comprehensive diagnostic criteria for IgG4-related disease (IgG4-RD). Mod Rheumatol 2012; 22: 21-30.
39. Weber AL, Romo LV, Sabates NR. Pseudotumor of the orbit. Clinical, pathologic, and radiologic evaluation. Radiol Clin North Am 1999; 37: 151-168.
40. Winn BJ, Rootman J. Sclerosing orbital inflammation and systemic disease. Ophthal Plast Reconstr Surg 2012; 28: 107-118.
41. Zen Y, Onodera M, Inoue D, Kitao A, Matsui O, Nohara T, Namiki M, Kasashima S, Kawashima A, Matsumoto Y, Katayanagi K, Murata T, Ishizawa S, Hosaka N, Kuriki K, Nakanuma Y. Retroperitoneal fibrosis: a clinicopathologic study with respect to immunoglobulin G4. Am J Surg Pathol 2009; 33: 1833-1839.
42. Zen Y, Nakanuma Y. IgG4-related disease: a cross-sectional study of 114 cases. Am J Surg Pathol 2010; 34: 1812-1819.

Original article

Folia Neuropathologica

Analysis of intracranial volume ratios by means of cerebrospinal fluid deployment indicators

Ewa Szczepek[1,2], Leszek Tomasz Czerwosz[3], Krzysztof Nowiński[4], Zbigniew Czernicki[1,2], Jerzy Jurkiewicz[1]

[1]Department of Neurosurgery, Second Faculty of Medicine, Medical University of Warsaw, [2]Department of Neurosurgery, Mossakowski Medical Research Centre, Polish Academy of Sciences, Warsaw, [3]Mossakowski Medical Research Centre, Polish Academy of Sciences, Warsaw, [4]Interdisciplinary Centre for Mathematical and Computational Modelling of the University of Warsaw, Warsaw, Poland

Folia Neuropathol 2015; 53 (2): 121-127 DOI: 10.5114/fn.2015.52408

Abstract

Introduction: *Imaging studies make it possible not only to visualize the general structure of the brain but also to take precise measurements of brain tissue volume and the size of individual lobes and their structure. The aim of this study was to determine the ratio of cerebrospinal fluid (CSF) volume contained in the intracranial ventricular system to the brain tissue volume and the ratio of CSF volume in the subarachnoid space and basal cisterns to the brain tissue volume.*
Material and methods: *The evaluation of volumetric measurements of computed tomographic (CT) images was undertaken on 23 male and female patients (average age 56.9 ± 6.1) diagnosed with normal pressure hydrocephalus (NPH) and 27 male and female patients (average age 70.6 ± 5.2) diagnosed with brain atrophy (BA). In the CT imaging studies, the total brain tissue volume and CSF volume collected in the intracranial fluid cavities were mapped to a colour scale. The VisNow software was used for volumetric evaluation. The groups were compared by means of the non-parametric Kolmogorov-Smirnov test (K-S) for independent samples. Paired data were compared by means of the nonparametric Wilcoxon test.*
Results: *The volumes of brain (brain volume – BV) and cerebrospinal fluid (fluid volume – FV) differ greatly from each other in both groups BA and NPH. The SBR (subarachnoid space and basal cisterns-to-brain ratio) and VBR (ventricle-to-brain ratio) indicators differ significantly and very much within the NPH group as well as within the BA group. In the NPH group a clearly higher value of VBR can be observed in comparison with the BA group. There was a higher value of SBR in the BA than the NPH group.*
Conclusions: *The simultaneous use of two indicators, VBR and SBR, on a study group of 50 patients enabled the total separation of NPH and BA groups. This differentiation can have real diagnostic value. Thus the volumetric assessment of the volume of CSF and brain tissue based on CT of the head can become an important part of the differential diagnosis of hydrocephalus and brain atrophy.*

Key words: *volumetry, hydrocephalus, brain atrophy.*

Introduction

Advances in the diagnostics of central nervous system (CNS) disorders are connected to a large degree with radiological assessment – the analysis of computed tomographic (CT) and magnetic resonance (MRI) images. The largest application is for head examinations, especially the brain. Imaging studies make it possible not only to visualize the general

Communicating author:
Dr Leszek Tomasz Czerwosz, Mossakowski Medical Research Centre, Polish Academy of Sciences, 5 Pawińskiego St., 02-106 Warsaw, Poland, e-mail: czerwosz@imdik.pan.pl

structure of the brain, but also to make precise measurements of brain tissue volume, of the size of individual lobes and their structure (volumetry) [7,15]. The application of specialist software for the analysis of CT and MRI images has made it possible to perform volumetric examinations to obtain non-invasive volume measurements of specific intracranial compartments (i.e., the volume of cerebrospinal fluid [CSF] contained in the subarachnoid space and basal cisterns, in the intracranial ventricular system and the brain tissue volume).

This has been found to be an important clinical application for the non-invasive diagnosis of normal pressure hydrocephalus and various types of brain atrophy. The ageing of society is clearly noticeable in recent years, and the lengthening of life has meant that diseases associated with dementia, the prevalence of which increases with age, currently represent a serious medical and social problem. For this reason, the possibility of early detection of disorders associated with dementia, their diagnosis and differentiation from the symptoms of the development of normal pressure hydrocephalus are of significant importance.

To achieve the intended aim, imaging studies, including CT and MRI volumetric examinations, have made it possible to precisely estimate the volume of the intracranial components of the CNS [16].

From the point of view of differential diagnosis on the basis of CT or MRI studies, we define the intracranial contents as the brain volume and the volume of CSF contained in the intracranial ventricular system and in the subarachnoid space and basal cisterns. According to data from the literature [11], the average brain volume of a healthy person is 1400 cm^3 and the average CSF volume is 140 cm^3.

Difficulty in the diagnosis of normal pressure hydrocephalus (NPH) and differentiating it from brain atrophy (BA) means that normal pressure hydrocephalus is diagnosed in a large percentage of cases that were in fact brain atrophy. It is also possible that brain atrophy is diagnosed in those cases that were in fact hydrocephalus. The commonly applied invasive diagnostic procedure is the infusion test [8], which gives the highest probability of correct diagnosis. This result should always be interpreted together with non-invasive diagnostic procedures, such as neurological examinations, neuropsychological examinations [9], motor and posture parameters [5,6,12], evoked potential, and particularly with CT and/or MRI brain imaging [4].

The Visual Analysis group co-chaired by Dr. Krzysztof Nowiński from the Interdisciplinary Centre for Mathematical and Computational Modelling at the University of Warsaw (ICM) has developed special software, VisNow [14], for the visual analysis of data, in particular for the analysis of a three-dimensional tissue density matrix, which is the result of computed tomography. The software allows not only visualization but also spatial morphometric calculations of tissue density specified in Hounsfield units. Szczepek *et al*. [13] used the VisNow tool for volumetric evaluation of CSF distribution in the intracranial fluid compartments in hydrocephalus and brain atrophy. The real absolute value (in cm^3) of the CSF voxels contained in the subarachnoid space and basal cisterns and in the intracranial ventricular system space was determined. The accuracy of volumetric outcomes has been compared to the planimetry paper of Marszałek *et al*. [9]. Szczepek relied solely on small groups of patients with normal pressure hydrocephalus and with brain atrophy. For both groups the mean value of the volume of CSF in the subarachnoid space and basal cisterns differs at a level of statistical significance from the mean value of CSF volume of normal healthy people. It has also been shown that the ratio of volume of CSF in the ventricles to the volume of CSF in the subarachnoid space and basal cisterns is an important diagnostic indicator for differentiating NPH from brain atrophy.

The aim of this study is to determine the ratio of the intracranial CSF to the brain tissue volume, the volume of CSF contained in the intracranial ventricular system to the brain volume and the volume of CSF in the subarachnoid space and basal cisterns to brain volume.

The aim of the analysis of this study is to answer the question of the clinical relevance of the abovementioned indicators:

– to determine the proportion of the pathologies under study,
– to make it possible to differentiate normal pressure hydrocephalus from brain atrophy with the aid of the abovementioned indicators.

Material and methods

At this neurosurgical clinic, an evaluation of the volumetric measurements of CT images was under-

taken in 23 male and female patients (average age 56.9 ± 6.1) with a diagnosis of normal pressure hydrocephalus and in 27 male and female patients (average age 70.6 ± 5.2) with a diagnosis of brain atrophy. In the CT imaging studies, the total brain tissue volume and the volume of CSF collected in the intracranial fluid compartments were mapped.

The study was undertaken in accordance with the Helsinki Declaration after obtaining the prior agreement of the Bioethical Committee of the Warsaw Medical University. The clinical criteria for the diagnosis of normal pressure hydrocephalus were established based on the following: dilatation of the ventricular system in CT or MRI studies; the Evans indicator with a value > 0.3; the lack of or little evidence of cortical atrophy; Hakim's triad – at least two symptoms; the value of intracranial pressure measured with the aid of a lumbar puncture NL ≥ 10 cmH_2O; resorption resistance R ≥ 11 mmHg/ml/min; and a neuropsychological assessment.

The diagnosis of brain atrophy was established on the basis of the following symptoms: dilatation of the ventricular system in CT or MRI studies of the head; the Evans indicator with a value ≤ 0.3; evidence of cortical and corticobasal atrophy; neurological symptoms; the value of intracranial pressure measured during a lumbar puncture NL < 10 cmH_2O; resorption resistance R < 11 mmHg/ml/min; and a neuropsychological assessment.

The results of the neurological examination were maintained in accordance with the set of tests developed and currently applied in this clinic [9].

Volumetric evaluation using the VisNow software, developed from scratch in ICM for volumetric evaluation, is an impartial, quantitative, statistical method for measuring the voxel characteristics in selected CNS regions. The technical data of the software were published by Szczepek *et al*. in 2015 [13]. A statistical analysis of the voxels was undertaken for the brain tissue volume and the total volume of CSF contained in the intracranial fluid compartments.

In this study, the statistical analysis was based on the volume of the subarachnoid space and basal cisterns, the volume of the intracranial ventricular system and also on the brain tissue volume (BV) in the CT imaging studies of the head (performed at intervals no longer than two months) in patients classified in the group of hydrocephalus and brain atrophy. Total CSF volume (FV) was the sum of the subarachnoid space and basal cisterns and the volume of the intracranial ventricular system.

The following indicators were established:

– VBR (ventricle-to-brain ratio) (expressed as a fraction) – the ratio of the volume of the CSF in the intracranial ventricular system to the brain volume;
– SBR (subarachnoid space and basal cisterns-to-brain ratio) (expressed as a fraction) – the ratio of the volume of CSF in the subarachnoid space and basal cisterns to the brain volume.

The groups were compared by means of the non-parametric Kolmogorov-Smirnov test (K-S) for independent samples. Dependent samples were compared by means of the nonparametric Wilcoxon test.

Results

The results of the statistical analysis (Kolmogorov-Smirnov) for the two groups – normal pressure hydrocephalus (NPH) and brain atrophy (BA) groups – showed that the brain volumes (BV) are different at a statistically significant level in these groups (Table I). The total volumes of CSF (FV) in the intracranial fluid compartments (CSF contained in the subarachnoid space and basal cisterns as well as the intracranial ventricular system) differ in these groups as well. The volumes of BV and FV differ greatly from each other in both groups; there is no need for a statistical test in this case.

A scatter plot of the value of BV and FV together with the mean values of the BA and NPH groups is shown in Figure 1.

A statistical evaluation for the measurements of the mean values of VBR and SBR indicators in patients with normal pressure hydrocephalus and brain atrophy are presented in Table II. Comparisons

Table I. Mean value and standard deviation of the brain volume (BV) and total cerebrospinal fluid (CSF) volume (FV) in the groups of patients with normal pressure hydrocephalus (NPH) and brain atrophy (BA). The NPH and BA groups are compared by means of the Kolmogorov-Smirnov test. Z statistics and exact probability are given

Group	BV (cm^3)	FV (cm^3)
NPH (23)	1258 ± 39	227 ± 17
BA (27)	1130 ± 14	251 ± 24
Comparison of NPH-BA: K-S *Z* value and exact prob.	$Z = 0.28$ $p = 1.8 * 10^{-14}$	$Z = 0.16$ $p = 0.00012$

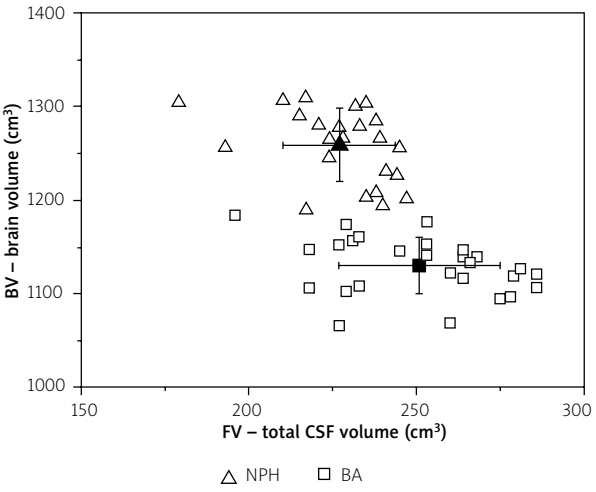

Fig. 1. A scatter plot of individual values of brain volume (BV) and volumes of cerebrospinal fluid (CSF) contained in the subarachnoid space and basal cisterns and also in the intracranial ventricular system (FV) in patients with normal pressure hydrocephalus (NPH) and brain atrophy (BA). The mean volumes with standard deviations of BA and NPH groups are plotted in the same coordinate system.

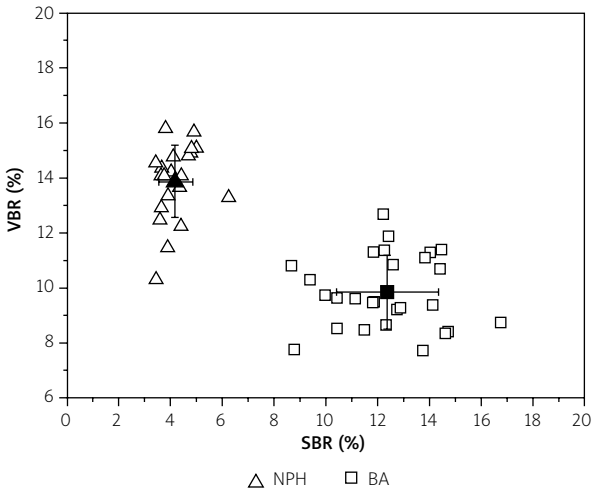

Fig. 2. A scatter plot of individual values of VBR (ventricle-to-brain ratio) and SBR (subarachnoid space and basal cisterns-to-brain ratio) indicators in patients with normal pressure hydrocephalus (NPH) and brain atrophy (BA). The mean volumes with standard deviations of BA and NPH groups are plotted in the same coordinate system.

of two groups are presented for VBR and SBR independently.

The results of the statistical analysis (Wilcoxon test) for dependent variables proved that SBR and VBR indicators differ significantly and very much within the NPH group as well as within the BA group (Table II).

In the patients classified as the normal pressure hydrocephalus group, a clearly higher value of the VBR can be observed in comparison with patients classified as the brain atrophy group. Analysing the SBR indicator, it was found that there was a higher value of SBR in the group of patients with a diagnosis of brain atrophy than in the group of patients with normal pressure hydrocephalus. There is a very low probability of erroneous outcome of statistical tests (less than 10^{-12}).

A scatter plot of individual VBR and SBR indicators together with the mean values of BA and NPH groups is shown in Figure 2. One can observe

Table II. Mean value and standard deviation of the indicators FBR (fluid-to-brain ratio), VBR (ventricle-to-brain ratio) and SBR (subarachnoid space and basal cisterns-to-brain ratio) in the groups of patients with normal pressure hydrocephalus (NPH) and brain atrophy (BA). NPH and BA groups are compared by means of the Kolmogorov-Smirnov test. *Z* statistics and exact probability are given. The Wilcoxon probability was calculated for independent comparisons of VBR and SBR indicators within the BA and NPH groups

Group	VBR (%)	SBR (%)	Comparison of VBR-SBR Wilcoxon probability
NPH (23)	13.9 ± 1.3	4.2 ± 0.7	$p < 2.4 \times 10^{-7}$
BA (27)	9.9 ± 1.3	12.4 ± 2.0	$p < 6.4 \times 10^{-6}$
Comparison of NPH-BA: K-S *Z* value and exact probability	$Z = 0.27$ $p < 4.4 \times 10^{-13}$	$Z = 0.28$ $p < 1.8 \times 10^{-14}$	–

a wide gap between the BA and NPH groups. This observation is consistent with the results of statistical tests.

Discussion

The variety of diagnostic procedures for differentiating normal pressure hydrocephalus and brain atrophy is proof of the difficulty in differentiating the two pathological syndromes. In spite of the fact that invasive procedures carry a risk of development of complications, they are still necessary in the diagnosis of hydrocephalus. For this reason, we attempted to develop a non-invasive differential diagnostic procedure for normal pressure hydrocephalus and brain atrophy. The presented observations are a further attempt to introduce into clinical practice a non-invasive diagnostic procedure – the evaluation of intracranial volumetric indicators of the distribution of the volume of CSF and brain tissue volume.

The volumetric evaluation undertaken in this study using CT imaging studies of the head showed that there were changes in the distribution of the volume of CSF and brain tissue volume in the intracranial compartments of the CNS for both hydrocephalus (NPH) and BA groups of patients. The scope of these changes differed in each particular group.

The new indicators VBR and SBR, identified in the study, made it possible to estimate the value of the volume of CSF in relation to the brain tissue volume in specific intracranial spaces of the CNS in the groups of patients with NPH and BA.

The results obtained in our study are similar to the results obtained by Blatter *et al*. [3]. The authors presented a quantitative evaluation of the volumetric intracranial parameters of volume ratios using MRI imaging studies in a control group. One hundred ninety-four healthy persons, including men and women in the age range from 16 to 65 years old, were divided into five ten-year age groups. The analysis included the total volume of CSF in the intracranial ventricular system and in the subarachnoid space, the total brain volume and the total intracranial volume.

A highly significant change was noticed with age. The authors found that the mean brain volume decreases with age, and the smallest value of brain volume was noted in the 5th decade of life (56-65 years old). The mean volume of CSF increases with age, and the highest value of CSF volume was recorded in the 5th decade of life (56-65 years old).

In the abovementioned study, in the group of healthy persons, the VBR indicator was also identified – the ratio of the volume of CSF in the intracranial ventricular system to the total brain volume. In healthy people in the age range of 56-65 years, the VBR for women was 2.08 ± 1.11 and for men 2.07 ± 0.88. The presented range of the VBR index in the control group in the specified age range should be compared with the VBR results obtained in our publication. It can also be noted that the value of VBR obtained in our study clearly differs from the norms in both of the discussed CNS pathologies. In our study, the VBR coefficient in the BA group (9.9 ± 1.3) is at a lower level than in the volumetric studies of the NPH group (13.9 ± 1.3). An explanation for this could be that in the BA group loss of brain tissue (i.e., brain volume) occurs with increasing age and with the progression of atrophy of the neural pathways. It should be noted that the CSF distribution in the intracranial fluid compartments is different in the group of patients with BA than in the group with NPH. It was observed that a higher value of CSF in the intracranial ventricular system was obtained in the patients with NPH, whereas a higher value of CSF in the subarachnoid space was obtained with patients diagnosed with BA.

The use of volumetric evaluation for tracking the volume changes in the intracranial compartments of the CNS in neurodegenerative disorders is also found in the study by Bigler *et al*. [2]. The authors performed an analysis of the volume parameters in patients with various types of dementia over the age of 65 years (i.e., Alzheimer's disease, vascular dementia). The VBR coefficient was identified. The results of the volumetric parameters presented by the authors in the study in patients with Alzheimer's disease or with vascular dementia are similar to the results of the study obtained in our publication with patients classified to the group of brain atrophy – a reduction in brain volume and an increase in the volume of CSF in the intracranial fluid compartments.

Akdogan *et al*. [1] undertook to use volumetric evaluation to highlight the relationship between TVV (total ventricle volume) and TBV (total brain volume). For their analysis, 40 men (average age 40.9 ± 3.7 years) and 40 women (average age 41.4 ± 3.6 years) were selected. Patients were excluded from

the study if a CT imaging study of the head presented intracranial bleeding or traumatic brain injury. It was found that the ratio TVV/TBV in the group of patients in the first decade was only 1.27%, whereas for the group of patients in the third decade the ratio rose to as much as 3.37%. The results were connected with increasing volume of CSF in the intracranial ventricular system and with decreasing brain volume together with age and the associated ageing process of the brain.

The authors observed that the volume ratio TVV/TBV turned out to be an important indicator for diseases, i.e., hydrocephalus, Alzheimer's, and disorders of a neurodegenerative nature.

In the study of Nestor *et al*. [10], semi-automatic software was presented that enabled the volumetric evaluation of MRI imaging studies for the early detection of dementia disorders. The authors found that the volume of CSF in the intracranial ventricular system can constitute an explanation for Alzheimer's disease or mild cognitive impairments. In the analysed group of patients, the volume of CSF in the brain ventricles was evaluated at an early stage of the illness and after 6 months for control purposes. It was noticed that patients with a diagnosis of Alzheimer's have clearly a larger volume of the ventricles than is the case in the group of patients with mild cognitive impairments. In Nestor's study, the possibility of evaluating the progression of changes of the volume ratios was also mentioned (i.e., a clear increase of the volume in the intracranial ventricular system was noted after 6 months in patients with mild cognitive impairments).

The results obtained in Nestor's study concur with the data from the literature. It should be underlined at this point that all of the abovementioned indicators can be used with success for the evaluation of the development of intracranial pathologies, but they do not give an unambiguous answer whether a specific examined case should be classified as brain atrophy or as hydrocephalus. For differentiating these pathological processes, the best indicator is in our opinion [13] an indicator highlighting the ratio of the volume of CSF in the brain ventricles to the volume of CSF contained in the subarachnoid space and basal cisterns.

It should be emphasized that the simultaneous use of the two indicators VBR and SBR on a study group of 50 patients enabled the total separation of NPH and BA groups. This differentiation can have real diagnostic value. Thus the volumetric assessment of the volume of CSF and brain tissue based on CT of the head can become an important part of the differential diagnosis of hydrocephalus and brain atrophy.

Acknowledgments

The research support was partially provided by the project POIG.02.03.00-00-003/09 "Applications of digital technologies in medicine", which was carried out based on a common project of the Polish Academy of Sciences research institutions – "Biocentrum Ochota – information infrastructure for the strategic areas of biology and medicine".

Disclosure

Authors report no conflict of interest.

References

1. Akdogan I, Kiroglu Y, Onur S, Karabulut N. The volume fraction of brain ventricles to total brain volume: a computed tomography stereological study. Folia Morphologica 2010; 69: 193-200.
2. Bigler ED, Lowry CM, Anderson CV, Johnson SC, Terry J, Steed M. Dementia, quantitative neuroimaging and apolipoprotein E genotype. AJNR Am J Neuroradiol 2000; 21: 1857-1868.
3. Blatter DD, Bigler ED, Gale SD, Johnson SC, Anderson CV, Burnett BM, Parker N, Kurth S, Horn SD. Quantitative volumetric analysis of brain MR: normative database spanning 5 decades of life. AJNR Am J Neuroradiol 1995; 16: 241-251.
4. Czernicki Z, Walecki J, Jurkiewicz J, Grochowski W, Tychmanowicz K. Intracranial volume reserve determination using CT images, numerical analysis and lumbar infusion tests. An experimental study. Acta Neurochir 1992; 115: 43-46.
5. Czerwosz L, Szczepek E. Hydrocephalus. In: Recognition of Posture and Gait Disturbances in Patients with Normal Pressure Hydrocephalus Using a Posturography and Computer Dynography Systems. Czerwosz L, Szczepek E, Sokołowska B, Jurkiewicz J, Czernicki Z. InTech 2012; 12, pp. 189-214.
6. Czerwosz L, Szczepek E, Sokołowska B, Jurkiewicz J, Czernicki Z. Posturography in differential diagnosis of normal pressure hydrocephalus and brain atrophy. Adv Exp Med Biol 2013; 755: 311-324.
7. Duning T, Kloska S, Steinsträter O, Kugel H, Heindel W, Knecht S. Dehydration complicates the assessment of brain atrophy. Neurology 2005; 64: 876-879.
8. Juniewicz H, Kasprowicz M, Czosnyka M, Czosnyka Z, Gizewski S, Dzik M, Pickard JD. Analysis of intracranial pressure during and after the infusion test in patients with communicating hydrocephalus. Physiol Meas 2005; 26: 1039-1048.
9. Marszałek P, Jurkiewicz J, Fersten E, Luczywek E, Czernicki Z, Gielecki J, Bogucki J. Multi-stage method for the diagnosis of low-pressure hydrocephalus. Neurol Neurochir Pol 1997; 31: 527-539.

10. Nestor SM, Rupsingh R, Borrie M, Smith M, Accomazzi V, Wells JL, Fogarty J, Bartha R; Alzheimer's Disease Neuroimaging Initiative. Ventricular enlargement as a possible measure of Alzheimer's disease progression validated using the Alzheimer's disease neuroimaging initiative database. Brain 2008; 131: 2443-2454.
11. Rengachary SS, Ellenbogen RG. Principles of Neurosurgery. Elsevier Mosby, Edinburgh 2005; pp. 99-115.
12. Szczepek E, Czerwosz L, Dąbrowski P, Dudziński K, Jurkiewicz J, Czernicki Z. Posturography and computerized gait analysis in the Computer Dyno Graphy system as non-invasive methods for evaluation of normal pressure hydrocephalus progression. Neurol Neurochir Pol 2008; 42: 139-152.
13. Szczepek E, Czerwosz L, Nowiński K, Jurkiewicz J, Czernicki Z. Evaluation of volumetric changes in differential diagnosis of brain atrophy and active hydrocephalus. Adv Exp Med Biol 2015; 840: 59-67.
14. VisNow visualization software developed at Laboratory of Visual Analysis at Interdisciplinary Center of Mathematical and Computational Modeling (2011). http://visnow.icm.edu.pl. Accessed 18 Apr 2015.
15. Walecki J, Ziemiański A. Magnetic Resonance Imaging and Computed Tomography in clinical practice. Springer PWN, Warsaw 1997; pp. 215-225.
16. Whitwell JL, Crum WR, Watt HC, Fox NC. Normalization of cerebral volumes by use of intracranial volume: implications for longitudinal quantitative MR imaging. AJNR Am J Neuroradiol 2001; 22: 1483-1489.

Original article

Folia Neuropathologica

Effect of oral administration of pig spinal cord hydrolysate on clinical and histopathological symptoms of experimental allergic encephalomyelitis in rats

Kaja Kasarełło[1,2], Roman Gadamski[3], Piotr Piotrowski[3], Katarzyna Kurzepa[4], Barbara Kwiatkowska-Patzer[1], Andrzej W. Lipkowski[1]

[1]Department of Neuropeptides, Mossakowski Medical Research Centre, Polish Academy of Sciences, Warsaw, [2]Department of Experimental and Clinical Physiology, Laboratory of Centre for Preclinical Research, Medical University of Warsaw, [3]Department of Clinical and Experimental Neuropathology, Mossakowski Medical Research Centre, Polish Academy of Sciences, Warsaw, [4]Industrial Chemistry Research Institute, Warsaw, Poland

Folia Neuropathol 2015; 53 (2): 128-138 DOI: 10.5114/fn.2015.52409

Abstract

Oral tolerance is the natural occurring phenomenon of a decreased immune response to previously fed antigens, which prevents induction of a response to dietary antigens. One of the mechanisms is deletion of T lymphocytes reactive to the fed antigen. Knowing that phenomenon, it seems appropriate to engage this mechanism for treatment of autoimmune diseases. Multiple sclerosis (MS) is an autoimmunological disease which causes neurological impairment in humans. Autoreactive T lymphocytes migrate through the open blood-brain barrier into the central nervous system (CNS), where they recognize myelin antigens as foreign, and induce an inflammatory response against the myelin sheath, which causes demyelination and even axonal loss. Experimental allergic encephalomyelitis (EAE), an animal model of MS, resembles the autoimmunological aspect of the disease. We used a broad spectrum of myelin antigens to induce EAE, and also to induce oral tolerance by giving myelin epitopes intragastrically to rats. The aim of our study was to evaluate whether pig spinal cord hydrolysate given intragastrically is able to evoke oral tolerance in rats with an animal model of MS – EAE. In our experiments we fed female Lewis rats with pig spinal cord hydrolysate at doses of 5, 20 and 100 mg per kg of body weight. We observed diminished clinical symptoms of ongoing EAE in rats fed with all doses of pig spinal cord hydrolysate. In the histopathological study, intensity of the inflammatory process in spinal cord was similar in rats not fed with EAE and in rats fed with lower doses of pig spinal cord hydrolysate. In animals fed with the highest dose of pig spinal cord hydrolysate, intensification of the inflammatory response was observed. These results were confirmed by morphometric evaluations. We found that feeding animals with preparations containing myelin antigens can reduce EAE symptoms, which may indicate oral tolerance induction, but the obtained results also underline the importance of dose of the orally given antigens, because of the possibility of enhancement of the inflammatory process in the CNS.

Key words: *multiple sclerosis, EAE, oral tolerance, myelin antigens.*

Communicating author

Barbara Kwiatkowska-Patzer, MD, PhD, Department of Neuropeptides, Mossakowski Medical Reaserch Center, Polish Academy of Sciences, 5 Pawinskiego St., 02-106 Warsaw, Poland, e-mail: bpatzer@imdik.pan.pl

Introduction

Oral tolerance is the phenomenon where a decrease of the immune response to previously fed antigens is observed. This mechanism occurs naturally in our organisms, and is necessary as a means of protection against evoking the immune response to non-pathogenic dietary antigens, and those from natural symbiotic gut bacteria [7,41]. When the short peptide fragments of digested proteins are being absorbed in the intestines, mucosa resident dendritic cells (DC) probe the antigens. There are two mechanisms of oral tolerance induction, depending on the dose of fed antigen. When low doses of antigen are given orally, DC induce differentiation of naive T-cells into regulatory T-cells, producing anti-inflammatory cytokines. This is called active suppression. Feeding with a high dose of antigen results in incomplete costimulation of autoreactive T-cells by DC and consequently anergy or clonal deletion of autoreactive lymphocytes [4,44]. It is now known that both mechanisms occur simultaneously. There is also a "bystander suppression" mechanism involved, when anti-inflammatory cytokines produced by regulatory T lymphocytes suppress neighboring cells [31,40].

Based on knowledge of the mechanism of oral tolerance, it seems to be appropriate to involve this phenomenon to treat autoimmune diseases. Oral administration of antigens, which are known or believed to be immunogenic in a particular disease, should induce oral tolerance, and in consequence "desensitize" the immunological system of the patient to those antigens. Since multiple sclerosis (MS) is an autoimmune disease in which the immune response is directed against myelin antigens, the aim should be to restore immune tolerance for these epitopes [9,35].

Multiple sclerosis is an autoimmunological disease, leading to neurodegeneration, which causes progressive physical impairment in a patient. It is diagnosed in so-called "young adults", people between 20 and 40 years old, but also it affects both older people and children. The etiology of the disease still remains unknown, but there are some hypotheses proposing the involvement of genetic, environmental and infectious agents [28,33]. The unknown etiology is the main reason for the difficulty in developing an effective MS treatment. Unlike the etiology, more is known about mechanisms involved in MS pathogenesis. Incorrectly activated autoreactive T lymphocytes migrate through the open blood-brain barrier into the central nervous system (CNS), and recognize myelin peptides as foreign antigens, which results in induction of an inflammatory response directed against the myelin sheath. Ongoing chronic inflammation can also lead to damage of the axons and neurons [10,35]. Demyelination and axonal loss are the direct cause of the physical impairment in patients. The most common symptoms are connected with vision disorders, paresis and incontinence, but also mental disorders are observed, such as depression, which is related to progressing physical disability [30,33].

Experimental allergic encephalomyelitis (EAE) is the most commonly used MS animal model. It resembles the mechanism involved in the disease pathogenesis. Animals are immunized with a mixture containing myelin antigens to direct the immune response to the myelin sheath in the CNS, and adjuvant to enhance the inflammation (active form of EAE). Animals may also be immunized by passive transfer of autoreactive T-lymphocytes (passive EAE). The most common sources of myelin epitopes in the immunization mixture are single myelin proteins or even fragments of them. Depending on the used epitope, the course and symptoms of induced EAE may differ [2,23,43]. Myelin oligodendrocyte glycoprotein (MOG) 35-55 is considered to be the most encephalogenic myelin epitope, and EAE induced using this epitope is chronic, and characterized by inflammatory infiltrations in the CNS [12,13]. Unlike MOG-induced EAE, the one induced with myelin basic protein (MBP) or its fragments is acute, with no relapses and very rarely observed demyelination. In our experiments we used whole guinea pig spinal cord homogenate as a source of myelin antigens in the immunization mixture. There may be many immunogenic antigens in MS, so using a broad spectrum of myelin epitopes to induce EAE may more closely resemble the disease. In the cerebrospinal fluid (CSF) of the patients, antibodies not only against three main myelin proteins (MBP, MOG, and PLP – proteolipid protein) are found, but also against some other myelin components [14,35]. Experimental allergic encephalomyelitis induced with a mixture containing whole spinal cord homogenate was used in Dark Agouti rats, except for using rat instead of guinea pig spinal cord. The results showed that induced EAE has relapsing-remitting form, and also

inflammatory infiltration and demyelination in the CNS were observed [3].

Most previous studies have concerned evoking oral tolerance to MBP in animals with MBP-induced EAE [6,11,26], but using broad a spectrum of myelin antigens in the preparations given intragastrically to induce oral tolerance seems to be more accurate, since it is not known precisely which myelin antigens are responsible for MS pathogenesis. Hydrolyzed pig spinal cord provides all myelin antigens, which consequently may evoke oral tolerance to all possible immunogenic myelin epitopes.

There are a few common methods of MS treatment so far, but the efficiency is not satisfactory, or the side effects are very severe. General immunosuppression during disease relapse is obtained by the use of glucocorticosteroids [27,34]. Chronic immunomodulation is provided by interferon-β, which unfortunately after some period of use is neutralized by antibodies produced by the patient's body. Also efficacy is not observed in all patients [1]. In recent years there have been some new therapies, which target specific mechanisms involved in MS pathogenesis, for example natalizumab, which inhibits migration of the autoreactive T lymphocytes through the blood-brain barrier into the CNS, but carrying the risk of lethal progressive multifocal leukoencephalopathy (PML) occurrence [5]. Because of the lack of sufficiently effective MS therapy, there is a need to look for new treatment methods. Oral tolerance is very promising as a new MS therapy.

The aim of our study was to evaluate whether feeding of rats with pig spinal cord hydrolysate affects the clinical symptoms and histopathological changes in rats with EAE – an animal model of MS.

Material and methods

Animals

In our experiments we used female Lewis rats, weighing 180-200 g at the beginning of the experiment. Experiments were carried out based on the consent of the Fourth Local Ethics Committee in Warsaw.

Feeding

Experimental animals were fed with a mixture (0.5 ml) containing myelin peptides, with a ball-pointed needle. The source of myelin antigens was the pig spinal cord hydrolysate in doses of 5, 20, 100 mg/kg of body weight. Control animals were fed with a medium dose of pig spinal cord hydrolysate (20 mg/kg). Hydrolysate was prepared by pig spinal cord digestion with pepsin, which resembles the natural process of protein digestion in the gastrointestinal tract. After digestion, a mixture of proteins, peptides, amino acids and lipids was obtained. Such a mixture was then rinsed with water, which allowed extraction of the fraction of amino acids and peptides, which were then rinsed with 70% ethanol. Three fractions were collected: amino acids, low molecular weight peptides and high molecular weight peptides. The fraction of low molecular weight, short peptides was used in our experiments [24]. Rats were fed four times during one week (every second day). Animals were deprived of food for two hours before feeding with preparations.

Experimental allergic encephalomyelitis induction

One week after the last day of feeding, the EAE was induced. Rats under inhaled anesthesia, 0.5-3.5% Narcotan (Leciva a.s.) in oxygen, were injected intradermally into the hind paws with the immunizing mixture (100 µl/paw). The mixture contained 50% guinea pig spinal cord homogenate as a source of myelin antigens mixed in the ratio 1 : 1 with Freund Adjuvant (DIFCO LABORATORIES), and supplemented with 4 mg/1 ml *Mycobacterium tuberculosis* (DIFCO LABORATORIES).

Clinical evaluation

During the experiment animals were weighed every day, and after EAE induction the clinical symptoms were evaluated using a 5-grade scale (1 – limp tail, 2 – hind leg weakness, 3 – paraplegia and incontinence, 4 – quadriplegia, 5 – death). At the 14^{th} day post immunization (14 DPI) rats were subjected to deep anesthesia with the intraperitoneal injection of 0.67 ml/kg ketamine and 0.5 ml/kg xylazine (Vetoquinol Biowet), and perfused transcardially with 4% paraformaldehyde. Lumbar and cervical segments of spinal cords were collected from the spinal canal of the vertebral column for further histopathological analysis.

Body mass index was calculated as the ratio of body mass at 14 DPI and at the day of evoking EAE (0 DPI, taken as 1). Mean clinical score was calculated as the mean of clinical scores between 11 and 14 DPI.

Histopathological studies

Spinal cord fragments were embedded in paraffin, and cut into slices (8 µm). Some of the slices were stained with a 1% water solution of cresyl violet to expose cells. Other slices were labeled with anti-T cells (Anti-CD45R0), anti-GFAP or anti-vimentin antibodies as follows. After blocking of endogenous peroxidase with 3% hydrogen peroxide in dewaxed slices, the background was blocked with 10% albumin. Next, slices were incubated with primary antibodies, washed, and incubated with a secondary antibody coupled with biotin. Streptavidin coupled with peroxidase was afterwards applied, and then chromogen was put on. All primary and secondary antibodies were supplied by DAKO. Subsequently slices were stained with Mayer's hematoxylin. Slices were analyzed using a light microscope.

Morphometric studies

Slices stained with cresyl violet were analyzed. Slices were photographed (3-35AD camera-4, Olympus), and images were scanned from photographic film. Whole spinal cord cross-section area and the area occupied with inflammatory infiltrations were measured using a computer program (GIMP 2.4.5). Percentage of both lumbar and cervical spinal cord segment sections occupied by inflammatory infiltrations was calculated as the ratio of the whole slice area to the area occupied by the inflammatory infiltration.

Statistical analysis

Results are shown as mean ± SD. Statistical analysis was performed using the non-parametric Mann-Whitney statistical test. Results were statistically significant when $p < 0.05$.

Results

Animals fed with all three doses of pig spinal cord hydrolysate (EAE + Hy5, EAE + Hy20, EAE + Hy100) showed a substantial decrease of the clinical score in comparison to non-fed EAE rats (EAE). Figure 1 shows the mean clinical score observed between 11 and 14 DPI. Experimental allergic encephalomyelitis induction decreases the body mass in comparison to not-treated animals (NT) (Fig. 2). Feeding rats with three doses of pig spinal cord hydrolysate (EAE + Hy5, EAE + Hy20, EAE + Hy100) does not reverse the observed body mass drop after EAE induction. Feeding healthy animals with pig spinal cord hydrolysate (Hy) causes no changes in body mass in comparison to non-treated animals (NT).

Slices from collected spinal cord segments from EAE rats underwent histopathological and morphometric evaluation. Cresyl violet staining revealed cross-sectional spinal cord structure differentiated into white and gray matter. Motoneurons were seen in the anterior horns of gray matter (Fig. 3A). After evoking EAE we observed numerous perivascular inflammatory infiltrations in both white and gray matter, and also at the border between the two matters (Fig. 3B). Inflammatory infiltrates showed perivascular location (Fig. 3C). The inflammatory process

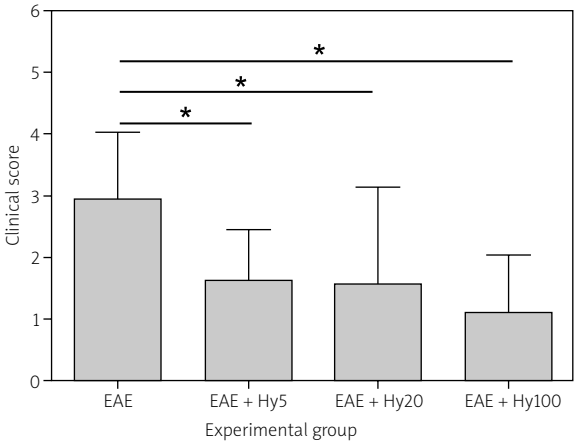

Fig. 1. Mean clinical score between 11 and 14 DPI. n = 5-13; *$p \leq 0.05$.

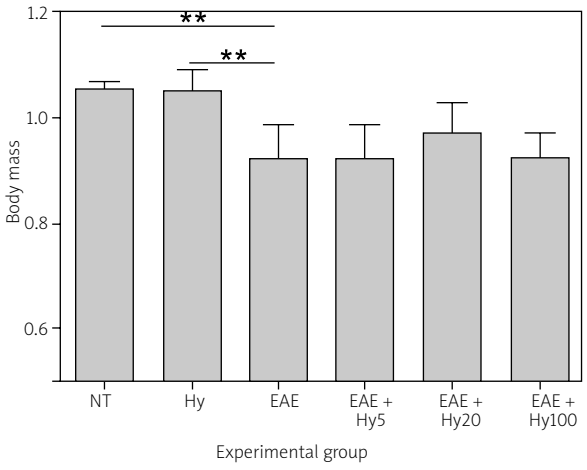

Fig. 2. Body mass at 14 DPI in relation to 0 DPI (taken as 1). n = 5-13; *$p \leq 0.05$; **$p \leq 0.01$.

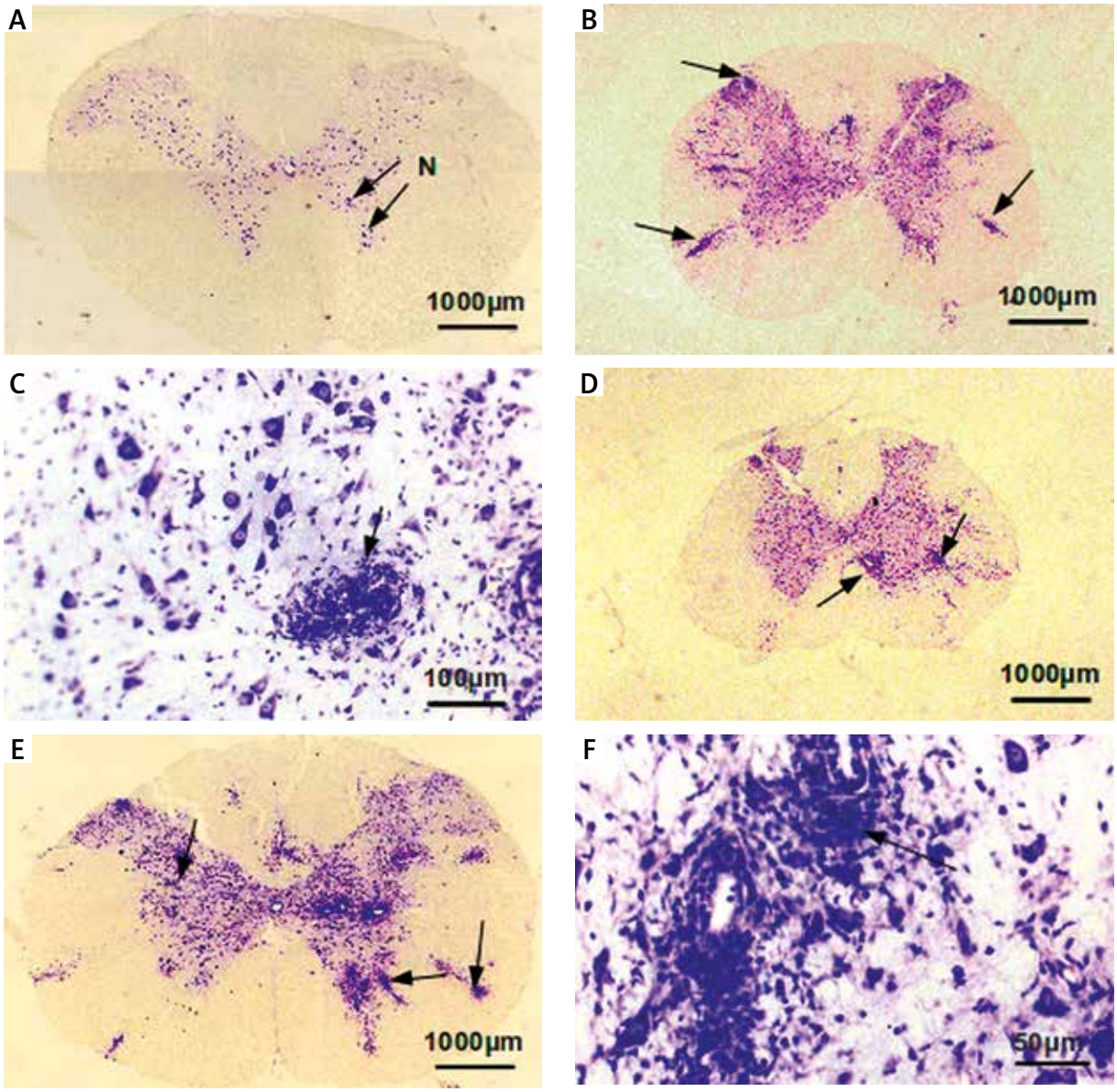

Fig. 3. Morphological changes. Spinal cord cross-section. Cresyl violet staining (KV). **A)** Motoneurons in the anterior horns, non-treated animals. **B, C)** Perivascular inflammatory infiltrations in white and gray matter, non-fed, EAE animals. **D)** Inflammatory infiltrations, EAE animals, fed with hydrolysate in doses 5 and 20 mg/kg. **E, F)** Inflammatory infiltrations, EAE animals, fed with hydrolysate in dose 100 mg/kg. Inflammatory infiltrations marked by arrows. N – motoneuron.

in the animals fed with lower doses of pig spinal cord hydrolysate, 5 and 20 mg/kg, showed similar intensity as in non-fed EAE rats (Fig. 3D). In contrast, in animals fed with the highest dose of pig spinal cord hydrolysate, 100 mg/kg, higher inflammatory activity was observed. There were more perivascular infiltrates present (Fig. 3E), and they were more abundant in inflammatory cells (Fig. 3F).

Anti-T cell labeling showed the presence of T lymphocytes in inflammatory infiltrates. Immunoreaction is visualized as a red tint in the cytoplasm of cells (Fig. 4A) and in neuropil (Fig. 4B).

Anti-GFAP labeling showed reactive astrocytes present in the cross-section of the spinal cord. In non-treated animals there was limited reaction revealing astrocyte processes in white matter (Fig. 5A).

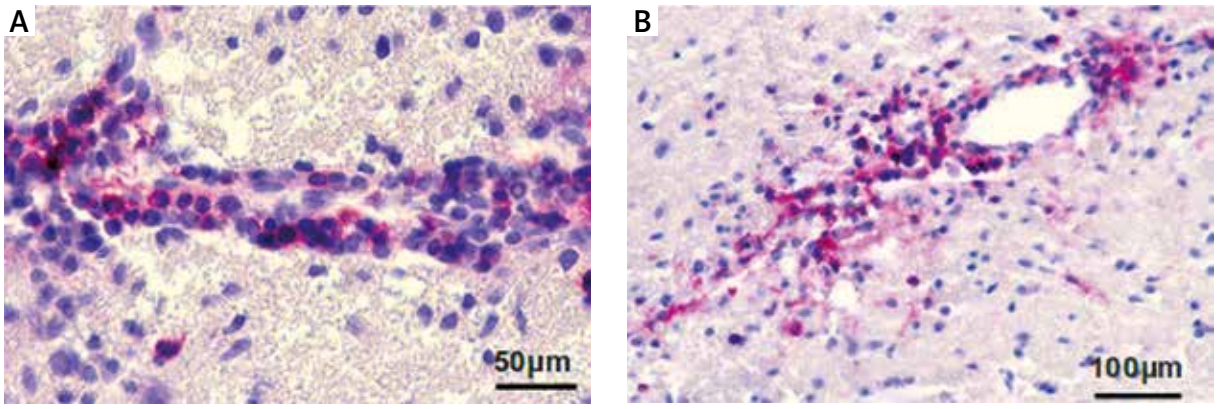

Fig. 4. T lymphocytes in inflammatory infiltrates. Spinal cord cross-section. Anti-T lymphocyte labeling.

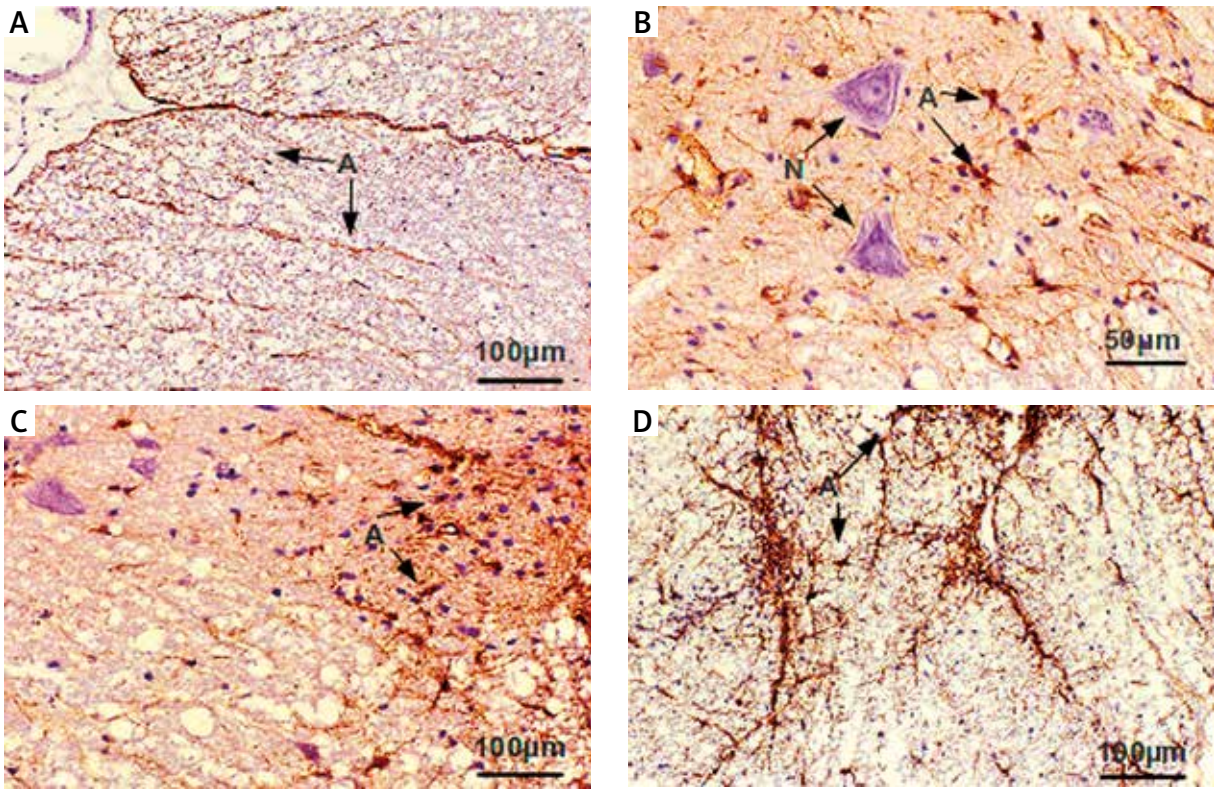

Fig. 5. Astrocytic reaction. Spinal cord cross-section. Anti-GFAP labelling. **A)** Scant astrocytic reaction in the white matter, non-treated animals. **B, C)** Increased number of astrocytes, EAE animals, fed with hydrolysate in doses 5, 20 mg/kg. **D)** Intensive astrocytes immunoreactivity, EAE animals, fed with hydrolysate in dose 100 mg/kg. Astrocytes marked by arrows. N – motoneuron.

A slightly increased number of astrocytes and increase in immunoexpression apparent in astrocyte cytoplasm and processes was observed after EAE induction (Fig. 5B) and in rats fed with both lower doses, 5 and 20 mg/kg, of pig spinal cord hydrolysate (Fig. 5C). Astrocyte immunoreactivity in cross-sections of spinal cords from rats fed with pig spinal cord hydrolysate in a dose of 100 mg/kg was enhanced (Fig. 5D) in comparison to that observed in rats fed with lower doses of hydrolysate.

Anti-vimentin immunoreactivity in the spinal cord sections was similar to GFAP immunoreaction. Limited reaction was observed in sections from non-treated animals (Fig. 6A). Enhanced reac-

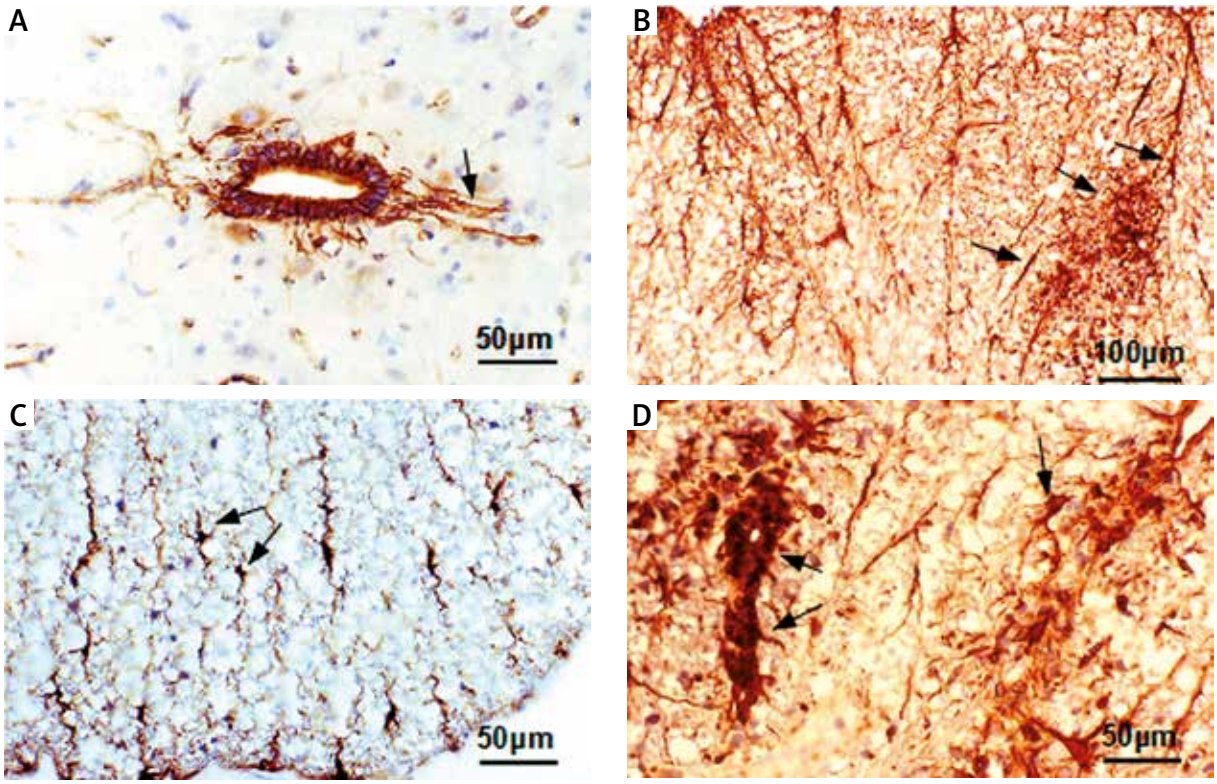

Fig. 6. Astrocytic reaction. Spinal cord cross-section. Anti-Vimentine labelling. **A)** Scant astrocytic reaction, non-treated animals. **B, C)** Enhanced astrocytic reaction, EAE animals, fed with hydrolysate in doses 5, 20 mg/kg. **D)** Enhancement of vimentine expression, EAE animals, fed with hydrolysate in dose 100 mg/kg. Astrocytes marked by arrows.

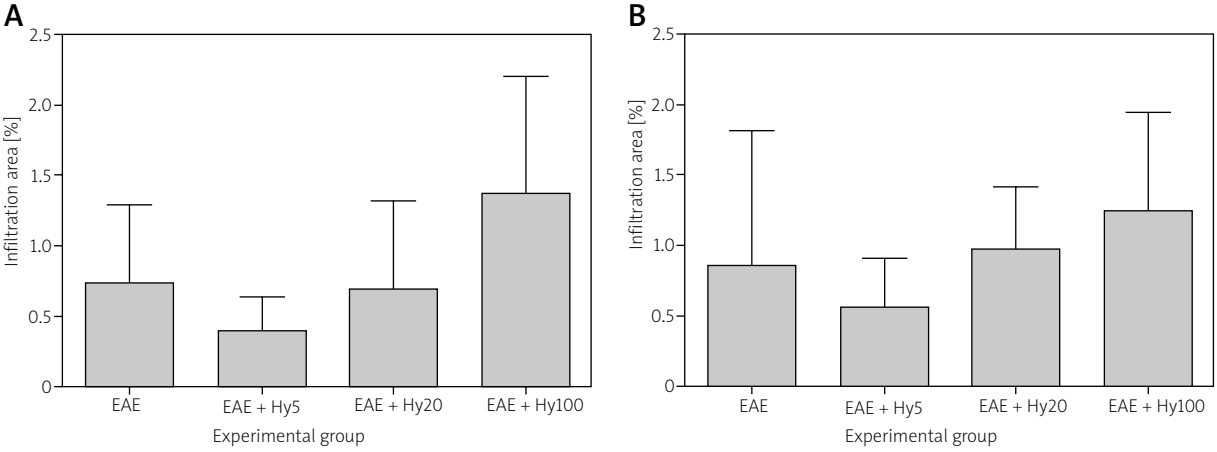

Fig. 7. Percentage of section area occupied by inflammation infiltrations. **A)** Cervical segment of spinal cord. **B)** Lumbar segment of spinal cord. *n* = 5-13.

tion was observed in the sections from animals with induced EAE (Fig. 6B) and in the slices of spinal cord from animals fed with lower doses, 5 and 20 mg/kg, of pig spinal cord hydrolysate (Fig. 6C). As in anti-GFAP labeling, there was enhancement in immunoexpression seen in astrocytes shown in slices obtained from rats fed with 100 mg/kg pig spinal cord hydrolysate (Fig. 6D).

Morphometric analysis confirmed histopathological evaluations indicating similar inflammatory

activity observed in cross-sections of spinal cords from rats fed with 20 mg/kg of pig spinal cord hydrolysate, and the enhancement of inflammatory activity in spinal cords of rats fed with the highest dose, 100 mg/kg of hydrolysate, in comparison to non-fed EAE rats. Figure 7 presents morphometric studies in cervical (Fig. 7A) and lumbar (Fig. 7B) segments of spinal cords. We can observe similar dependencies in both spinal cord segments. Feeding animals with the lowest dose, 5 mg/kg, of pig spinal cord hydrolysate showed a tendency to decrease the area occupied by inflammatory infiltrations in comparison to non-fed EAE rats, whereas the highest dose, 100 mg/kg, had the opposite effect – we observed a tendency to increase the area occupied by inflammatory infiltrations. Feeding rats with a dose of 20 mg/kg shows a similar ratio of inflammatory infiltration areas in spinal cord sections as non-fed EAE rats.

Discussion

Multiple sclerosis is a disease known for almost two centuries, but still there is no proper and effective method of its treatment. Looking for new therapies is difficult because of not knowing the disease etiology. Each applied way of MS treatment is based on the disease mechanism, and since it is an autoimmune disorder, the most popular methods are based on suppression or modulation of immune system activity. Such a procedure is able to diminish the clinical symptoms of the disease, but at the same time it exposes the patient to infections [32]. That leads us to look for another MS therapy. In our opinion, reinstatement of immune tolerance for myelin autoantigens should be taken into account when looking for a new method of MS treatment. That can be provided by the oral tolerance phenomenon, as a mechanism that reduces the immune response to a previously fed antigen [39,41]. The first reports about involvement of oral tolerance in the treatment of the MS animal model, experimental allergic encephalomyelitis, came from 30 years ago. The best studied myelin protein is myelin basic protein, and its immunogenic properties are well known [37]. Most experiments were conducted using MBP as a source of myelin antigens in both the immunizing mixture and the orally given preparations. Orally given MBP protected rats from progression of subsequently induced MBP-EAE, reduced the anti-MBP antibody level in serum [22], and also inhibited clinical and histopathological symptoms of EAE [17].

In our experiments we induced EAE with a mixture containing whole guinea pig spinal cord homogenate as a source of myelin antigens. We found it more appropriate, since it is not known which particular antigen is immunogenic in MS pathogenesis, and antibodies against many myelin epitopes are found in CSF of the patients [14]. If as seems likely there are many immunogenic myelin antigens in the MS pathogenesis, it will also be more appropriate to restore immune tolerance for all those epitopes. In our experiments we used whole pig spinal cord hydrolysate as a source of all potential immunogenic myelin antigens in the orally given preparations. The approach where more than one myelin antigen was used was applied in studies in relapsing-remitting MS patients. Peptide fragments of three main myelin proteins, MBP, PLP and MOG, were given to patients transdermally, using patches stuck to the skin of the arm. There was a reduction in the number of lesions visible in MRI imaging and the annual relapse rate in patients treated transdermally with myelin antigens in comparison to the placebo group [15,38].

In our experiments we observed diminished clinical symptoms of induced EAE in rats previously fed with all three doses of pig spinal cord hydrolysate. The mean score was reduced by about 50% in comparison to the mean score in non-fed EAE rats. This result may indicate oral tolerance induction. We did not observe a reduction in body mass drop caused by EAE induction in rats fed with pig spinal cord hydrolysate. Nevertheless, this is a parameter reflecting the general condition of animals, and is not directly associated with induction of oral tolerance. No differences observed in body mass between non-treated rats and those that received pig spinal cord hydrolysate without EAE induction may indicate safety of using such preparations. Still, toxicology studies should be conducted to define the safeness of pig spinal cord hydrolysate. There are no known toxic prion proteins identified in swine which could exclude pig CNS tissue from usage in clinical trials [18].

Published data show that in rats immunized with a mixture containing syngeneic spinal cord as a source of myelin antigens in the acute phase of EAE (14 days after immunization) infiltration of immune cells into the lumbar spinal cord occurred [8]. In the spinal cord sections from animals used in our experiments, at the 14th day after immuni-

zation we observed infiltration of immune cells into the CNS.

Histopathological evaluations of spinal cord slices showed that lower doses of pig spinal cord hydrolysate given to rats intragastrically have no influence on the extent of the inflammatory process in the CNS of the EAE rats. A similar intensity in perivascular inflammatory infiltrations and astrocyte activity in fed and non-fed EAE rats was observed. Surprisingly, despite the decreased mean clinical score in rats fed with the highest hydrolysate dose, 100 mg/kg, the inflammatory process was intensified in comparison to non-fed EAE rats. It was pronounced as more numerous and abundant in immune cell infiltrations. Also higher astrocyte activity was observed. These evaluations were confirmed by the morphometric analysis. The results can be considered only as a tendency, because of strong diversity of the experimental groups, which causes the lack of significance of the results. Nonetheless, quite clear associations were seen in morphometric analysis, very similar in both cervical and lumbar segments of spinal cords. In rats fed with a higher dose of hydrolysate, 100 mg/kg, there was a tendency to increase the area of slice occupied by inflammatory infiltrations, which is in accordance with observations of intensity of infiltration in spinal cord slices. Interestingly, although microscopic observations did not allow one to notice the differences, morphometric study showed a tendency to decrease the area of the rat spinal cord cross-section occupied by inflammatory infiltrations in rats fed with a lower dose of pig spinal cord hydrolysate 5 mg/kg. Hydrolysate given in a dose of 20 mg/kg showed no effect.

Based on the obtained results, we can conclude that the lowest dose of given intragastrically pig spinal cord hydrolysate mitigates the clinical symptoms of induced EAE in rats, which may indicate oral tolerance to myelin antigen induction. Results obtained from animals fed with the medium dose of hydrolysate showed diminished clinical symptoms in animals, but no influence on intensity of the inflammatory process in the CNS. We know that regulatory T-cells induced by oral tolerance may infiltrate the CNS, where they suppresses inflammation [42]. Evaluation of the phenotype of infiltrated T-cells might show whether infiltration consists partly of regulatory cells, which would indicate oral tolerance induction. Our pilot trials examining the cytokine levels showed increased IL-10 levels in brain and spinal cord homogenates in rats fed with pig spinal cord hydrolysate in a dose of 20 mg/kg [20]. Peron *et al.* [29] observed that mice with MOG35-55-induced EAE, and the same antigen given orally to induce oral tolerance, had a reduced amount of both Th17 and Th1 cells infiltrating into the CNS. Diminished perivascular infiltrations in the CNS were also observed in rats fed with MBP conjugated with the cholera toxin B subunit [36].

The results of our investigations underline the importance of antigen doses. We found that the highest dose of the pig spinal cord hydrolysate caused intensification of inflammatory processes in the CNS, marked not only by greater immune cell infiltration, but also increased astrocyte activity, which indicates enhancement of the autoaggressive process.

Previously we also found that feeding animals with pig spinal cord hydrolysate influences the changes, such as opened tight junctions, in blood-brain barrier ultrastructure, after evoking EAE [19]. There was also a decreased concentration of metalloproteinases, which are responsible for rearrangements of extracellular matrix, which leads among other things to blood-brain barrier opening [21].

Clinical symptoms observed in animals reflect physical disability in patients suffering from MS, such as limb weakness and even paralysis, or incontinence [21,23]. Since we know that physical disability results from neurodegeneration, improvement in clinical symptoms should indicate a decrease in inflammatory process intensity. Also, oxidative stress plays a major role in tissue destruction. Reactive oxygen and nitrogen species (ROS, RNS) are excessively produced by activated immune cells. Myelin, being composed mainly of lipids and proteins, is very vulnerable to peroxidation, leading to function loss and damage [25]. It was shown that there is a temporal coincidence between myelin-specific T-cell CNS penetration and the first clinical symptoms of EAE occurrence [16]. This underlines the importance of sufficient infiltration prevention, or inactivation of already infiltrated immune cells in the CNS. In our experiments, administering hydrolysate in the dose of 5 mg/kg showed a tendency to diminish the area occupied by inflammatory infiltration.

The obtained results indicate that usage of preparations containing pig spinal cord hydrolysate, as a source of broad spectrum myelin antigens, is able to diminish clinical symptoms of ongoing EAE. The results also underline the very important aspect

of the dose of fed antigens. Decreased clinical symptoms may indicate oral tolerance induction, but further, antigen-specific analysis should be conducted. Nevertheless, preparations containing pig spinal cord hydrolysate may be in the future very promising as a new method for multiple sclerosis treatment.

Acknowledgements

The study was supported by grant MNI 017/PO5/2005/29.

Disclosure

Authors report no conflict of interest.

References

1. Axtell RC, de Jong BA, Boniface K, van der Voort LF, Bhat R, De Sarno P, Naves R, Han M, Zhong F, Castellanos JG, Mair R, Christakos A, Kolkowitz I, Katz L, Killestein J, Polman CH, de Waal Malefyt R, SteinmanL, Raman C. T helper type 1 and 17 cells determine efficacy of IFN-β in multiple sclerosis and experimental encephalomyelitis. Nat Med 2010; 16: 406-412.
2. Baker D, Jackson SJ. Models of multiple sclerosis. Adv Clin Neurosc Rehabil 2007; 6: 10-12.
3. Beeton C, Garcia A, Chandy KG. Induction and clinical scoring of chronic-relapsing experimental autoimmune encephalomyelitis. J Vis Exp 2007; 5: 1-2.
4. Benson JM, Campbell KA, Guan Z, Gienapp IE, Stuckman SS, Forsthuber T, Whitacre CC. T-cell activation and receptor downmodulation precede deletion induced by mucosally administered antigen. J Clin Invest 2000; 106: 1031-1038.
5. Castro-Borrero W, Graves D, Frohman TC, Bates Flores A, Hardeman P, Logan D, Orchard M, Greenberg B, Frohman EM. Current and emerging therapies in multiple sclerosis: a systematic review. Ther Adv Neurol Disord 2012; 5: 205-220.
6. Faria AMC, Maron R, Ficker SM, Slavin AJ, Spahn T, Weiner HL. Oral tolerance induced by continuous feeding: enhanced up-regulation of transforming growth factor-β/interleukin-10 and supression of experimental autoimmune encephalomyelitis. J Autoimmun 2003; 20: 135-145.
7. Faria AMC, Weiner HL. Oral tolerance: Therapeutic implications for autoimmune diseases. Clin Dev Immunol 2006; 13: 143-157.
8. Giatti S, Boraso M, Abbiati F, Ballarini E, Calabrese D, Santos-Galindo M, Rigolio R, Pesaresi M, Caruso D, Viviani B, Cavaletti G, Garcia-Segura LM, Melcangi RC. Multimodal analysis in acute and chronic experimental autoimmune encephalomyelitis. J Neuroimmune Pharmacol 2013; 8: 238-250.
9. Gravano DM, Vignali DAA. The battle against immunopathology: infectious tolerance mediated by regulatory T cells. Cell Mol Life Sci 2012; 69: 1997-2008.
10. Hellings N, Raus J, Stinissen P. Insights into the immunopathogenesis of multiple sclerosis. Immunol Res 2002; 25: 27-51.
11. Higgins PJ, Weiner HL. Supression of experimental autoimmune encephalomyelitis by oral administration of myelin basic protein and its fragments. J Immunol 1988; 140: 440-445.
12. Ichikawa M, Johns TG, Adelmass M, Bernard CCA. Antibody response in Lewis rats injected with myelin oligodendrocyte glycoprotein derived peptides. Int Immunol 1996; 8: 1667-1674.
13. Ichikawa M, Johns TG, Liu J, Bernard CCA. Analysis of the fine B cell specificity during the chronic/relapsing course of a multiple sclerosis-like disease in Lewis rats injected with the encephalitogenic myelin oligodendrocyte glycoprotein peptide 35-55. J Immunol 1996; 157: 919-926.
14. Jaśkiewicz E. Epitopy na białkach mieliny rozpoznawane przez autoprzeciwciała obecne u chorych na stwardnienie rozsiane. Postepy Hig Med Dosw 2004; 58: 472-482.
15. Juryńczyk M, Walczak A, Jurewicz A, Jesionek-Kupnicka D, Szczepanik M, Selmaj K. Immune Regulation of Multiple Sclerosis by Transdermally Applied Myelin Peptides. Ann Neurol 2010; 68: 593-601.
16. Kawakami N, Bartholomäus I, Pesic M, Mues M. An autoimmunity odyssey: how autoreactive T cells infiltrate into the CNS. Immunol Rev 2012; 248: 140-155.
17. Kelly KA, Whitacre CC. Oral tolerance in EAE: reversal of tolerance by T helper cell cytokines. J Neuroimmunol 1996; 66: 77-84.
18. Kurzepa K, Kasarełło K, Baranowska B, Grabowska A, Walisiewicz-Niedbalska W, Różycki K, Kwiatkowska-Patzer B, Lipkowski AW. Wykorzystanie odpadowego wieprzowego rdzenia kręgowego jako cennego źródła substancji aktywnych biologicznie. Polimery 2012; 57: 29-33.
19. Kwiatkowska-Patzer B, Baranowska B, Walski M, Lipkowski AW. Influence of spinal cord protein hydrolysate upon the blood brain barrier changes due to experimental allergic encephalomyelitis in Lewis rats. Ultrastructural study. Folia Neuropathol 2003; 41: 29-34.
20. Kwiatkowska-Patzer B, Michalkiewicz J, Kubiszewska I, Zielińska J, Kasarello K, Kurzepa K, Lipkowski AW. Spinal cord hydrolysate ameliorate immunological reaction in experimental allergic encephalomyelitis. Acta Neurobiol Exp (Warsz) 2009; 69: 73-78.
21. Kwiatkowska-Patzer B, Walski M, Frontczak-Baniewiecz M, Zalewska T, Baranowska B, Lipkowski AW. Matrix metalloproteinases activity and ultrastructural changes in the early phase of experimental allergic encephalomyelitis. The effect of oral treatment with spinal cord hydrolysate proteins in Lewis rat. The pilot study. Folia Neuropathol 2004; 42: 107-111.
22. Lider O, Santos LMB, Lee CSL, Higgins PJ, Weiner HL. Supression of Experimantal Autoimmune Encephalomyelitis by Oral Administration of Myelin Basic Protein. II. Suppression of Disease and in Vitro Immune Responses Is Mediated by Antigen Specific CD8+ T Lymphocytes. J Immunol 1989; 142: 748-752.
23. Link H., Xiao BG. Rat models as tool to develop new immunotherapies. Immunol Rev 2001; 184: 117-128.
24. Lipkowski AW, Baranowska B, Marczak E, Kwiatkowska-Patzer B, Gajkowska B, Walski M. Protein hydrolysates for oral tolerance. Biofactors 2000; 12: 147-150.
25. Ljubisavljevic S, Stojanovic I, Pavlovic D, Milojkovic M, Sokolovic D, Stevanovic I, Petrovic A. Suppression of the lipid peroxidation process in the CNS reduces neurological expression of experimentally induced autoimmune encephalomyelitis. Folia Neuropathol 2013; 51: 51-57.
26. Meyer AL, Benson JM, Giennap IE, Cox KL, Whitacre CC. Supression of murine chronic relapsing experimental autoimmune

encephalomyelitis by the oral administration of myelin basic protein. J Immunol 1996; 157: 4230-4238.
27. Milligan NM, Newcombe R, Compston DAS. A double-blind controlled trial of high dose methylprednisolone in patients with multiple sclerosis: 1. Clinical effects. J Neurol Neurosurg Psychiatry 1987; 50: 511-516.
28. O'Gorman C, Lucas R, Taylor B. Environmental risk factors for multiple sclerosis: a review with a focus on molecular mechanisms. Int J Mol Sci 2012; 13: 11718-11752.
29. Peron JPS, Yang K, Chen M, Brandao WN, Basso AS, Commodaro AG, Weiner HL, Rzzo LV. Oral tolerance reduces Th17 cells as well as the overall inflammation in the central nervous system of EAE mice. J Neuroimmunol 2010; 227: 10-17.
30. Pierson E, Simmons SB, Castelli L, Goverman JM. Mechanisms regulating regional localization of inflammation during CNS autoimmunity. Immunol Rev 2012; 248: 205-215.
31. Pré du MF, Samson JN. Adaptive T-cell responses regulating oral tolerance to protein antigen. Allergy 2011; 66: 478-490.
32. Sellebjerg F, Frederiksen JL, Nielsen PM, Olesen J. Double-blind, randomized, placebo-controlled study of oral, high-dose methylprednisolone in attacks of MS. Neurology 1998; 51: 529-534.
33. Selmaj K. Stwardnienie rozsiane – kryteria diagnostyczne i naturalny przebieg choroby. Polski Przegląd Neurologiczny 2005; 1: 99-105.
34. Seven A, Aslan M, Incir S, Altintas A. Evaluation of oxidative and nitrosative stress in relapsing remitting multiple sclerosis: effect of corticosteroid therapy. Folia Neuropathol 2013; 51: 58-64.
35. Sospedra M, Martin R. Immunology of multiple sclerosis. Annu Rev Immunol 2005; 23: 683-747.
36. Sun J, Rask C, Olsson T, Holmgren J, Czerkinsky C. Treatment of experimental autoimmune encephalomyelitis by feeding myelin basic protein conjugated to cholera toxin B subunit. Proceedings of the National Academy of Sciences 1996; 93: 7196-7201.
37. Vergelli M. Myelin Antigen autoreactivity in multiple sclerosis. Topics in Neuroscience 1999; 170-184.
38. Walczak A, Siger M, Ciach A, Szczepanik M, Selmaj K. Transdermal Application of Myelin Peptides in Multiple Sclerosis Treatment. JAMA Neurol 2013; 70: 1105-1109.
39. Wang X, Sherman A, Liao G, Leong KW, Daniell H, Terhorst C, Herzog RW. Mechanism of oral tolerance induction to therapeutic proteins. Adv Drug Deliv Rev 2013; 65: 759-773.
40. Wardrop RM, Whitacre CC. Oral tolerance in the treatment of inflammatory autoimmune diseases. Inflamm Res 1999; 48: 106-119.
41. Weiner HL. Oral tolerance: immune mechanisms and treatment of autoimmune diseases. Immunol Today 1997; 18: 335-343.
42. Weiner HL, Selkoe DJ. Inflammation and therapeutic vaccination in CNS diseases. Nature 2002; 420: 879-884.
43. Wekerle H, Kurschus FC. Animal models of multiple sclerosis. Drug Discovery Today: Disease Models 2006; 3: 359-367.
44. Wells JM, Rossi O, Meijerink M, Baarlen van P. Epithelial crosstalk at the microbiota-mucosal interface. Proc Natl Acad Sci U S A 2011; 108: 4607-4614.

Original article

Folia Neuropathologica

Increased nitric oxide levels in cerebellum of cachectic rats with Walker 256 solid tumor

Fabio Leandro Fenner[1], Flavia Alessandra Guarnier[2], Sara Santos Bernardes[1], Leandra Naira Zambelli Ramalho[3], Rubens Cecchini[2], Alessandra Lourenço Cecchini[1]

[1]Laboratório de Patologia Molecular, Universidade Estadual de Londrina (UEL), Londrina, [2]Laboratório de Fisiopatologia e Radicais Livres, Universidade Estadual de Londrina (UEL), Londrina, [3]Departamento de Patologia e Medicina Legal, Universidade de São Paulo, Ribeirão Preto, Brasil

Folia Neuropathol 2015; 53 (2): 139-146 DOI: 10.5114/fn.2015.52410

Abstract

In cancer cachexia, the role of nitric oxide (NO) in the central nervous system remains unclear. Cerebellar degeneration has been reported in cancer patients, but the participation of NO has not been studied. Thus, this study investigated the mechanism of oxidative cerebellar injury in a time-course cancer cachexia experimental model. The cachexia index is progressive and evident during the evolution of the tumor. Nitric oxide and lipid hydroperoxidation quantification was performed using a very sensitive and precise chemiluminescence method, which showed that both analyzed parameters were increased after tumor implantation. In the day 5 group, NO was significantly increased, and this experimental time was chosen to treat the rats with the NO inhibitors N-nitro-L-arginine methyl ester (L-NAME) and aminoguanidine (AG). When treated with NO inhibitors, a significant decrease in both NO and lipid hydroperoxide levels occurred in the cerebellum. 3-nitrotyrosine was also analyzed in cerebellar tissue by immunohistochemistry; it was increased at the three experimental time points studied, and decreased when treated with L-NAME and AG. Besides demonstrating that lipid hydroperoxidation in the cerebellum of rats with cachexia increases in a time-dependent manner, this study is the first to describe the participation of NO and its oxidized product 3-NT in the cerebellum of cachectic rats bearing the Walker 256 solid tumor.

Key words: *nitric oxide, oxidative stress, 3-nitrotyrosine, Walker 256 tumor, cerebellum.*

Introduction

Cachexia is characterized by marked metabolic alterations leading to massive weight loss, anorexia, asthenia and anemia [25]. Additionally, there is an inappropriate increase in energy expenditure, defects in protein, carbohydrate and lipid metabolism and muscle loss. The role of oxidative stress in the mechanism of muscle wasting was investigated in rats implanted with Walker 256 solid tumor [10], which leads to cachectic syndrome very quickly. Brain weight loss is also observed [6] and cerebellar degeneration with loss of Purkinje cells occurs in the course of neoplastic diseases [16]. Brain and nervous tissue are prone to oxidative damage for several reasons. The central nervous system (CNS) has a high rate of oxygen consumption, a high amount of poly-

Communicating author:
Alessandra L. Cecchini, Departamento de Patologia Geral – Centro de Ciencias Biologicas, Universidade Estadual de Londrina, Laboratorio de Patologia Molecular CEP 86051-990 Londrina, Brazil, phone: (+55-43) 3371-4529, fax: (+55-43) 3371-4267, e-mail: alcecchini@uel.br

unsaturated fatty acid and also many neurotransmitters which are autoxidizable molecules [11].

Nitric oxide (NO) is a highly reactive gas molecule that can either function as a beneficial physiological agent utilized for essential functions such as vasodilation, ischemia protection, and neurotransmission, or as a pathological agent that causes or exacerbates diseases, such as septic shock, cardiac hypertrophy and diseases of the central nervous system. Whether NO is helpful or harmful depends on a variety of factors, such as the cellular environment in which NO is released, and the dose released [4,8]. In the CNS, nitric oxide and its redox related forms have been reported to be both neuroprotective and neurodestructive [3]. However, several groups have been unable to demonstrate NO's direct toxicity or if it may contribute to oxidative stress and oxidative lesions of the CNS.

As a neuroprotector, NO is able to promptly react with free radicals in the medium, which allows it to act as a chain reaction terminator [7]. Cytotoxic NO may cause nitrosative and oxidative stress [2]. The death of cells or the ionic gradient collapse during energy depletion may cause a massive release of glutamate by neurons, causing a prolonged increase of intracellular Ca^{2+}, and overproduction of NO through nNOS [11]. According to Halliwell and Gutteridge [11], this excitotoxicity may become a vicious circle where more glutamate is released with concomitant generation of $O_2^{\bullet-}$ and NO. As a result, there is overproduction of peroxynitrite ($ONOO^{\bullet-}$), one of the most potent reactive species.

In this study we characterized the participation of nitrosative and oxidative stress in paraneoplastic cerebellar degeneration in a Walker 256 tumor progression experimental model in rats.

Material and methods

Animals

Adult male Wistar rats (250-350 g; *n* = 6/group) were obtained from the Animal House of the Biological Sciences Center at the Universidade Estadual de Londrina. The animals were given water and commercial food (Nuvilab CR1, Nuvital Nutrients Ltda., Curitiba, Brazil) *ad libitum*. The food intake was measured daily. The experimental protocol was approved by the Institutional Animal Care and Utilization Committee of our institution (protocol 7794/2011). In all respects, the protocols conformed to the Guide for the Care and Use of Laboratory Animals.

Reagents

All the chemicals were obtained from Merck (Darmstadt, Germany) or Sigma-Aldrich (St. Louis, USA) laboratories.

Tumor implantation

Rats were divided into six groups designated as controls and tumor hosts at three different days of tumor progression (5^{th}, 10^{th} and 14^{th}). The last time of sacrifice was determined based on the average time of survival, which was 15 days after tumor implantation. Tumor hosts at day 5 of tumor progression were treated with two different NOS inhibitors (aminoguanidine hydrochloride – AG [50 mg/kg] or N-nitro-L-arginine methyl ester – L-NAME [20 mg/kg daily, i.p.]. The control group received a 0.5 ml injection of PBS, and the tumor-bearing rats received a Walker 256 cell suspension (8.0×10^7 cells in 0.5 ml of PBS) injected subcutaneously on the right hind limb flank. The treated day 5 group received the same cell suspension as well as NOS inhibitors. Tumor cells were maintained in our laboratory as described by Guarnier *et al.* [10]. Three additional groups were included: a *pair-fed* group, where 6 animals inoculated with PBS were fed with the same amounts of food consumed by the tumor groups for 14 days, and a control group treated with NOS inhibitors for 5 days. On days 5, 10 and 14 after subcutaneous tumor implantation, the animals in both tumor groups were weighed and killed by decapitation. The tumor was carefully excised and weighed. The cachexia index was determined considering initial and final body weight, tumor weight and body weight gain in control groups, according to the formula: [(initial body mass – final body mass + body mass gain of control) / (initial body mass + body mass gain of control)] x 100% [10]. The cachexia index was calculated in order to determine the pattern of general wasting. The cerebellum was rapidly excised, weighed, and stored in liquid nitrogen until use (at most, 60 days of storage). Since the *pair-fed* group did not develop cachexia, all experimental results were compared to the control.

Tissue preparation

Cerebellum was placed on ice and gently homogenized manually for approximately 2 minutes in a Potter glass tube in Na_2CO_3 2 mM, pH 8.5, previously bubbled with N_2 to remove O_2. The samples

were centrifuged at 1,500 x g for 10 min at 4°C in a Jouan BR4i Multifunction centrifuge (Thermo Electron Corporation, USA). The supernatants were distributed in 4 Eppendorf tubes and kept in ice away from light until the moment of analysis. For the NO and lipid hydroperoxide quantification, samples were prepared in the concentration of 1.25 and 15 mg/ml, respectively.

Quantification of nitric oxide

The production of nitric oxide (NO) was quantified in the cerebellum in the experimental animals through the technique based on the reaction of chemiluminescence initiated in the presence of H_2O_2 and luminol. The chemiluminescence was detected at 302 nm as described by Kikuchi *et al*. [14], modified by Terra *et al*. [22]. Briefly, a solution composed by 360 µM Luminol/3 mM DFX was added to an equal volume of solution of 200 mM H_2O_2 and 1400 µl of buffer (2 mM Na_2CO_3). Both solutions were prepared with the same buffer, 2 mM Na_2CO_3, pH 8.5, previously bubbled with N_2. The mixture was incubated at approximately 25°C under mild agitation for 5 min. After this period, this solution (180 µM Luminol/1.5 mM DFX/200 mM H_2O_2) was added to the sample (1.25 mg/ml) through a precision syringe (SGE, Australia). The chemiluminescence spectrum was monitored for 5 minutes using a luminometer model TD 20/20 (Turner Designs, USA) with detection capacity in wavelengths from 300 to 650 nm and 68.5% sensitivity. The luminometer was connected to a microcomputer through the program Spreadsheet Interface v1.0, making possible the registration of the emitted chemiluminescence. The program Origin v.7.5 was used for construction of the chemiluminescense curves. Samples were analyzed in quadruplicate.

Cerebellum 3-nitrotyrosine immunohistochemistry

The cerebellum preparations were also submitted to immunohistochemical analysis of 3-nitrotyrosine (3-NT), a protein nitrosative/oxidative stress biomarker. Briefly, 3-µm-thick sections mounted on poly-l-lysine-coated slides were deparaffinized, rehydrated, immersed in 10 mmol/l citrate buffer, pH 6.0, and submitted to heat-induced epitope retrieval using a vapor lock for 45 min. The slides were rinsed with phosphate-buffered saline (PBS) and immersed in 3% hydrogen peroxide for 20 min to block endogenous peroxidase. Non-specific protein binding was blocked with normal serum (Vectastain Elite ABC Kit, Universal, Vector Laboratories Inc., Burlingame, CA, USA) for 30 min. The sections were then incubated with monoclonal primary antibodies specific for nitrotyrosine (clone HM11; Santa Cruz Biotechnology, Santa Cruz, USA) for 2 h at room temperature (25ºC) in a humid chamber. Following washes in PBS, biotinylated pan-specific universal secondary antibody (Vectastain Elite ABC Kit, Universal, Vector Laboratories Inc.) was applied for 30 min. Next, the slides were incubated with the avidin-biotin-peroxidase complex (Vectastain Elite ABC Kit, Universal, Vector Laboratories Inc.) for 30 min and developed with a NovaRed kit (Vector Laboratories Inc.) for 5 min. The slides were counterstained with hematoxylin, dehydrated and mounted with Permount (Biomeda, Foster City, CA, USA). As negative controls, all specimens were incubated with an isotope-matched control antibody under identical conditions. The immunolabeling was considered to be positive when distinct red nuclear or cytoplasmic staining was present homogeneously. The percentage of nitrotyrosine-positive cells was obtained by Image J software developed at the U.S. National Institute of Health and available on the internet at *http://rsb.info.nih.gov/nih image*. Results are presented as % mean ± SEM.

Determination of oxidative stress by highly sensitive chemiluminescence induced by tert-butyl hydroperoxide

Reaction mixtures were placed in 2-ml luminescence tubes containing the following: cerebellum homogenate of control or experimental groups (15 mg/ml), 30 mM KH_2PO_4/K_2HPO_4 buffer (with 120 mM KCl, pH 7.4), and 3 mM *tert*-butyl hydroperoxide, in a final volume of 1 ml. The tert-butyl hydroperoxide-initiated chemiluminescence (CL) reaction was assessed in a TD/20 20 luminometer (Turner Designs), with a response range of 300-650 nm. The tubes were kept in the dark until the moment of assay, which was carried out in a room at 30ºC [9,17]. For each animal, a 60-min curve, where each point represented the differential smoothing of 600 readings, was obtained by interpolation. The results were expressed in relative light units/g tissue (RLU/g tissue).

Statistical analysis

The results are shown as means ± SEM. Two-way ANOVA with the Bonferroni post-hoc test was used to analyze the lipid peroxidation, NO and the entire chemiluminescence curve. Quantitative results were analyzed by one-way ANOVA with the Bonferroni post-hoc test. Statistical analysis was performed using GraphPad Prism 4.0 and 5.0 (GraphPad, San Diego, CA).

Results

Characterization of cachexia

Table I shows the cachexia index, mass of the tumor and the cerebellum absolute weight variation with or without AG and LNAME treatment on day 5. Animals with a cachexia index equal to or greater than 10% were considered as suffering from cachexia. The cachexia index is progressive and evident during evolution of the tumor. The animals did not present cachexia on D5, and when the animals were treated with aminoguanidine (D5AG) or L-NAME (D5LN) there was no difference when compared to D5. The same result could be seen in tumor weight, as the variation between D5, D5AG and D5LN was not significant. The cerebellum absolute weight did not change, although it showed an increase in weight variation in relation to the control group on day 5 and day 10. When the day 5 group was treated with L-NAME (day 5LN) and aminoguanidine (day 5AG) the percentage of weight variation was negative compared to the control, or the weight gain variation of the cerebellum was reverted by these treatments.

Nitric oxide quantification by chemiluminescence and 3-nitrotyrosine by immunohistochemistry

Figure 1 illustrates the chemiluminescence induced by H_2O_2-luminol for the quantification of NO in the cerebellum of control and tumor-bearing rats on day 5, day 10, day 14 (Fig. 1A) and day 5 treated with aminoguanidine (AG) and L-NAME (LN) (Fig. 1B). As observed in Figure 1A, the NO levels in cerebellum of the day 5 group was significantly increased compared to the control ($p < 0.0001$), so this experimental day was chosen to evaluate the effect of NO inhibitor treatment. The groups of animals pair-fed D5, D10 and D14 did not show levels of NO significantly higher compared to control PBS. Thus, it was demonstrated that the decrease in food intake does not interfere with increased levels of NO, and it was not subjected to further investigation. Figure 1B shows the NO quantification in the cerebellum of 5-day tumor-bearing rats treated with inhibitors of cNOS (LNAME) and iNOS (aminoguanidine), D5AG and D5LN, respectively. The NO levels of D5AG and D5LN were significantly decreased compared to group D5 ($p < 0.0001$). The inhibition with LNAME is 1300 times greater than with AG. Figure 2 shows the increase of labeled area for 3-nitrotyrosine (3-NT) of the day 5 (6.40 ± 0.15%), day 10 (10.99 ± 0.098%) and day 14 (14.12 ± 0.14%) groups when compared to the control (2.14 ± 0.07%). When

Table I. Cachexia index, tumor and cerebellum weights in tumor-bearing rats in NO inhibitor treated and non-treated animals

	Tumor weight (g)	Cachexia index (%)	Cerebellum	
			Weight (mg)	Percent variation
Control	–	–	0.287 ± 0.007[a]	–
D5	6.192 ± 1.11[a]	7.88 ± 0.01[a]	0.290 ± 0.006[a]	+1.04
D10	22.057 ± 2.55[b]	14.02 ± 1.05[b]	0.306 ± 0.01[a]	+6.60
D14	38.84 ± 5.89[c]	17.91 ± 2.25[b]	0.287 ± 0.01[a]	0.00
D5AG	4.73 ± 0.33[a]	6.23 ± 0.65[a]	0.283 ± 0.01[a]	–1.39
D5LN	4.32 ± 0.49[a]	8.07 ± 1.08[a]	0.280 ± 0.01[a]	–2.43

Groups represent number of days after subcutaneous injection of 8.0 x 10^7 tumor cells with or without treatment with aminoguanidine (AG – 50 mg/kg daily, i.p.) or L-NAME (LN – 20 mg/kg daily, i.p.). Each group consisted of 6 animals. Control received an injection of 0.5 ml of PBS. Cachexia index = [(initial body mass – final body mass + tumor weight + body mass gain of control)/(initial body mass + body mass gain of control)] x 100%. Values are expressed as mean ± SE. Positive values represent gain, and negative values decrease when compared with the control group. (–) in spaces means no comparison. In statistical evaluation, in the same column, different letters indicate statistical differences (p < 0.05 evaluated by one-way ANOVA, followed by Bonferroni's multiple comparison test), while the same letters indicate no statistical differences (n = 6 for all groups).

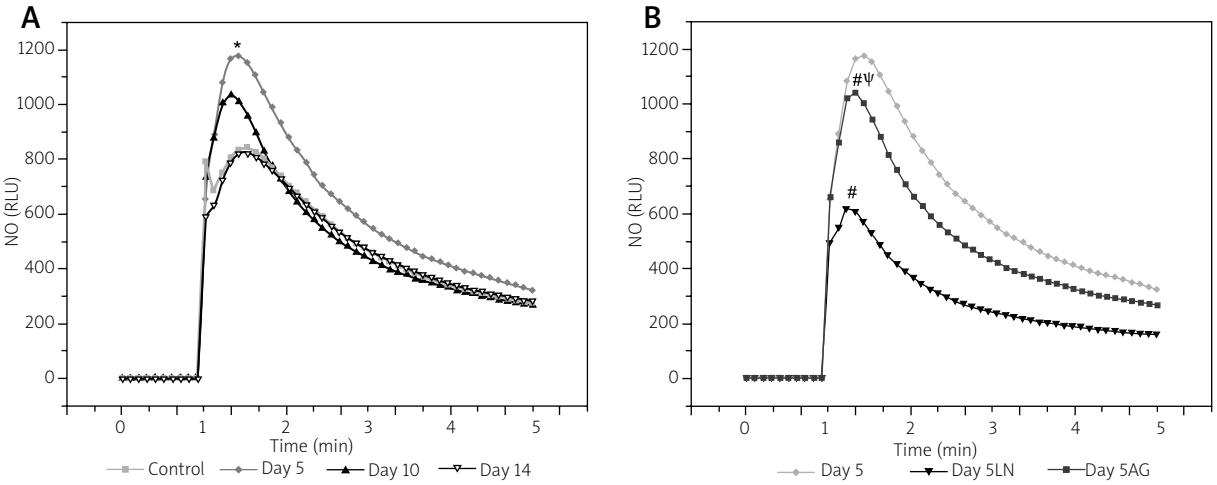

Fig. 1. Nitric oxide quantification by chemiluminescence. **(A)** Nitric oxide quantification of tumor-bearing rats on day 5, day 10, day 14. *$p < 0.0001$ compared to control. **(B)** Effect of NOS inhibitors on the level of NO measured by chemiluminescence initiated by H_2O_2-luminol in cerebellum of tumor-bearing rats on day 5, #$p < 0.0001$ compared to D5. Ψ$p < 0.0001$ compared to day 5LN ($n = 6$ for all groups).

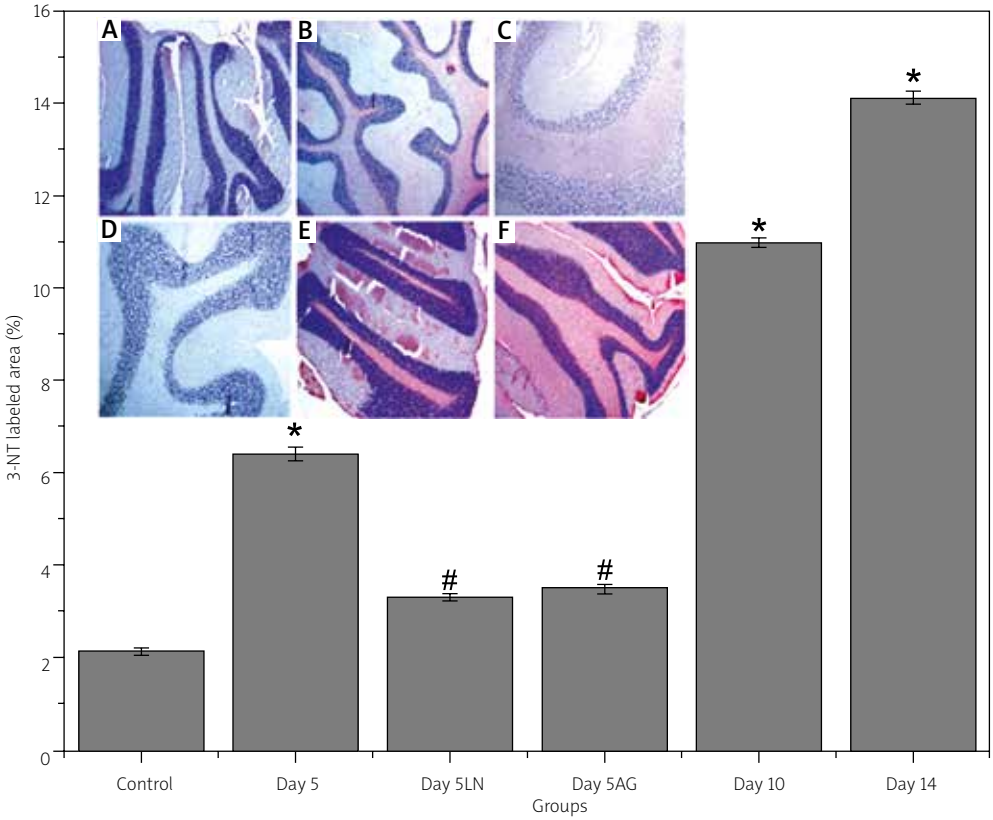

Fig. 2. 3-Nitrotyrosine (3-NT) immunohistochemistry in cerebellum. Groups were compared using one-way ANOVA with Bonferroni's post hoc test and $p < 0.05$ was considered significant. *$p < 0.05$ in relation to control group; #$p < 0.05$ in relation to day 5 group. AG – aminoguanidine, L-NAME – N-nitro-L-arginine methyl ester. Above, representative photomicrographs (20x) of immunohistochemistry of 3-NT labeled area: **A)** control group; **B)** day 5; **C)** day 5LN; **D)** day 5AG; **E)** day 10; **F)** day 14 ($n = 6$ for all groups).

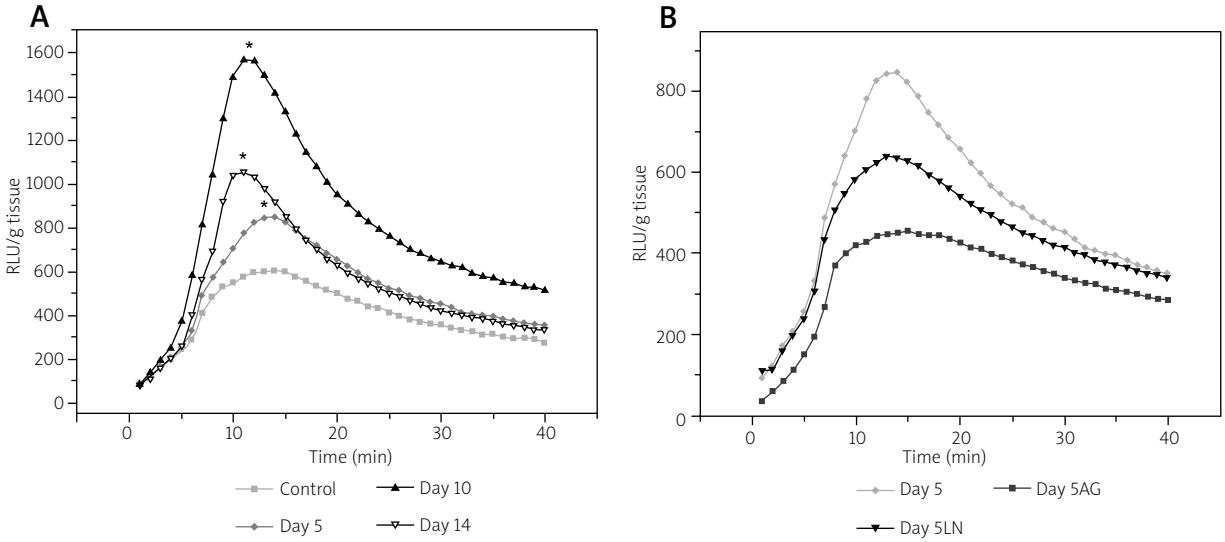

Fig. 3. Lipid hydroperoxide quantification of cerebellum determined by highly sensitive chemiluminescence induced by tert-butyl hydroperoxide. **(A)** Lipid hydroperoxide formation on day 5, day 10 and day 14 of cerebellum of tumor-bearing rats, $^{*}p < 0.0001$ compared to control. **(B)** Effect of NOS inhibitors on the levels of lipid hydroperoxides in the cerebellum of tumor-bearing rats on day 5. $^{\#}p < 0.0001$ compared to D5 ($n = 6$ for all groups).

D5 was treated with L-NAME (3.61 ± 0.11%) and AG (3.30 ± 0.08%) 3-NT levels decreased significantly.

Quantification of lipid hydroperoxides by tert-butyl hydroperoxide initiated chemiluminescence

Figure 3A shows the levels of lipid hydroperoxides formed in tumor-bearing rats during cachexia progression. The curves of the day 5, day 10 and day 14 groups were significantly higher ($p < 0.0001$) compared to the control group. Figure 3B shows the levels of lipid hydroperoxides in cerebellum of tumor-bearing rats on D5 days treated with inhibitors of cNOS (LNAME) and iNOS (aminoguanidine), respectively day 5LN and day 5AG. The groups and day 5LN and day 5AG curves were significantly lower than group D5.

Discussion

Tumor growth induces marked changes in the oxidative metabolism of distant tumor-free tissues and organs of the host [24], and these tumor effects on the brain are poorly understood. Cerebellar degeneration is observed in the course of neoplastic diseases (paraneoplastic neurological syndrome), defined as non-metastatic neurological complications [5]. The release of neurotoxic factors by microglia has a triggering role in the development of neurological disorders. After microglia and astrocyte activation, there is a massive release of TNF-α, ROS and RNS, especially NO, which contributes to the establishment of neurodegeneration [18]. In low concentrations, NO acts as a powerful lipid peroxidation chain reaction terminator, but its pro-oxidant activity is evidenced when NO is generated in high concentrations [21].

It has been shown that Walker 256 tumor growth causes oxidative stress in the brain [6]. However, the participation of NO in the cellular damage in the establishment of cerebellar degeneration in the cachectic state has not been demonstrated. Oxidative stress was demonstrated in the hippocampus, cortex and cerebellum of Walker 256 tumor-bearing rats by the determination of thiobarbituric acid reactive substances (TBARS) and enzymatic activities (superoxide dismutase and catalase) [6]. The TBARS technique was used as a marker of oxidative stress evaluation. In this study, a very sensitive tert-butyl hydroperoxide-initiated chemiluminescence assay (CL) was used to analyze the levels of lipid peroxides in the cerebellum of cachectic tumor-bearing rats. This assay indicates that

the increase in CL is closely related to the oxidative stress previously suffered by the tissue [10,19].

From D5 to D14 there was a progressive body weight loss, compatible to the cachectic syndrome, and it remained even when NOS inhibitors were administered. The same happened for the tumor weight and the progression of the cachexia index, which did not change with the use of inhibitors. The cerebellum weight showed a different behavior. Although there is no statistical difference, day 5 and day 10 showed an increase of weight variation compatible with the establishment of a systemic inflammatory state in cancer disease [20]. This evidence was better observed when AG and LN were administered on day 5 and the cerebellum weight variation decreased.

Although oxidative stress was evidenced, the participation of NO in cachexia-induced cerebellar degeneration remained unclear. In the present study, cachectic state establishment, NO production, 3-NT quantification and lipid peroxidation of the cerebellum were analyzed during progression of the cachectic state in Walker 256 tumor-bearing rats. The cancer-cachectic state of the present model showed that there was significant NO production on D5 in the cerebellum of tumor-bearing rats that decreased when AG and LNAME were used, indicating that both NO production pathways (iNOS and cNOS) are induced. The inhibition by LNAME reduced NO production 1,300 fold compared to AG inhibition. This fact suggests that the NO production through constitutive NOS, mainly nNOS, plays a crucial role in the cerebellum of cachectic rats just before macro alterations start to happen. In chemically controlled NO production by the reaction with potassium iodate [14], NO reacts with H_2O_2 in an aqueous phase, giving a stronger oxidizing species, peroxynitrite ($ONOO^-$), under basic conditions. cPTIO, a specific NO scavenger [22], was used to provide additional evidence that the object of analysis was in fact NO. The scavenger decreased in a dose-dependent manner the light emission in both biological and chemical systems [23].

Nitrotyrosine (3-NT) is a product of tyrosine oxidation mediated mainly by endogenous peroxynitrite ($ONOO^-$). This molecule is a powerful oxidant that interacts with many proteins, which can lead to the formation of nitrotyrosine, the oxidation of thiol groups, lipid peroxidation induction and even DNA damage, as well as the depletion of stored antioxidants [11]. The occurrence of 3-NT in tissues is a marker of $ONOO^-$ formation and, therefore, the presence of NO and $O_2^{\bullet-}$ [12]. Nitrotyrosine was measured in the cerebellum and was coordinated with the increase in NO chemiluminescence on day 5. Increased levels of 3-NT in the day 10 and day 14 groups can be explained by the capacity of deposits of this oxidized protein on the tissue to induce proteotoxicity. When AG or L-NAME was used in the day 5 group, this protein aggregate decreased, as verified by NO chemiluminescence, which also decreased.

The increase of NO on day 5 is followed by an increase in lipid peroxidation in the cerebellum. The lipid peroxidation evidenced at the beginning of the cachectic state (day 5) may be dependent on the production of NO, and probably its reaction products with oxygen reactive substances [11]. This was confirmed by the use of the inhibitors L-NAME and AG, which reduced the NO production and also membrane lipid hydroperoxide formation. Tert-butyl hydroperoxide-initiated CL was used to evaluate the integral level of nonenzymatic antioxidant defense. A lower level of antioxidant as a consequence of previous oxidative stress corresponds to an accentuated peak and a shift to the left in CL curves, giving a positive correlation between CL and lipid peroxidation [15,17]. In this study, we demonstrated a qualitative difference in all CL curves, indicating alterations in cell membrane properties, such as antioxidant composition, which modifies the kinetics pattern by exhausting the oxidizable species [1].

Michalak *et al*. [16] demonstrated that circulating TNF-α and MCP-1 (macrophage chemoattractant protein-1), together with decreased levels of insulin and thyroxine, may produce a milieu of factors involved in the mechanism of the development of cerebellar degeneration in cachectic hepatoma-bearing rats, but the overproduction of NO in the cerebellum was not mentioned. The lipid peroxidation profile shows that on all days of tumor progression there was a significant increase in cell membrane lesions. The same pattern of oxidative injury was also observed in muscle of tumor-bearing rats in the same period of cachexia progression [10], and more, that muscular waste is evident, and that oxidative stress is part of the modulation process of ubiquitin-proteasome-induced proteolysis.

According to Keynes *et al*. [13], the concentration of NO in the cerebellum is dependent on its generation and degradation rate. The consumption of NO by these cells decreases by 50% when lipid

peroxidation inhibitors are used. Changes in the activity of the total antioxidants impair the antioxidant defense capacity of the brain and may lead to oxidative stress. Walker 256 tumor growth caused a consistent increase of chemiluminescence in the cerebellum that probably resulted from the changes observed in NO content.

This is the first time that nitric oxide has been related to induced nitrosative and oxidative cerebellar injury in an experimental cancer model that leads to cachexia. It is still unclear whether the role of NO is one of protection or harmful action in cachexia. Nevertheless, this study reveals that in cachexia-induced cerebellar degeneration, nitrosative stress and lipid hydroperoxidation occur in a time-dependent manner, probably induced by the high concentration of NO produced by the cerebellum at the onset of the cachectic state.

Acknowledgments

Grant support was provided by Coordenação de Aperfeiçoamento de Pessoal de Nível Superior – CAPES. We are very grateful to J. A. Vargas for excellent technical assistance.

Disclosure

Authors report no conflict of interest.

References

1. Azorin I, Bella MC, Iborra FJ, Fornas E, Renau-Piqueras J. Effect of tert-butyl hydroperoxide addition on spontaneous chemiluminescence in brain. Free Rad Biol Med 1995; 19: 795-803.
2. Brown GC, Bal-Price A. Inflammatory neurodegeneration mediated by nitric oxide, glutamate, and mitochondria. Mol Neurobiol 2003; 27: 325-355.
3. Calabrese V, Mancuso C, Calvani M, Rizzarelli E, Butterfield DA, Stella AM. Nitric oxide in the central nervous system: neuroprotection versus neurotoxicity. Nat Rev Neurosci 2007; 8: 766-775.
4. Culotta E, Koshland DE Jr. NO news is good-news. Science 1992; 258: 1862-1865.
5. Darnell RB, Posner JB. Paraneoplastic syndromes involving the nervous system. N Engl J Med 2003; 349: 1543-1554.
6. Freitas JJS, Pompéia C, Miyasaka CK, Curi R. Walker-256 tumor growth causes oxidative stress in rat brain. J Neurochem 2001; 77: 655-663.
7. Fukuto, JM, Cho JY, Switzer CH. The chemical properties of nitric oxide and related nitrogen oxides. In: Nitric Oxide – Biology and Pathobiology. Ignarro LJ (ed). Academic Press, San Diego 2000; pp. 23-40.
8. Galla HJ. Nitric oxide, NO, an intercellular messenger. Angew Chem Int Ed Engl 1993; 32: 378-380.
9. Gonzalez-Flecha B, Llesuy S, Boveris A. Hidroperoxide-initiated chemiluminescence: an assay for oxidative stress in biopsies of heart, liver, and muscle. Free Radic Biol Med 1991; 10: 93-100.
10. Guarnier FA, Cecchini AL, Suzukawa AA, Maragno ALGC, Simão ANC, Gomes MD, Cecchini R. Time course of skeletal muscle loss and oxidative stress in rats with Walker 256 solid tumor. Muscle Nerve 2010; 42: 950-958.
11. Halliwell B, Gutteridge JMC. Free Radicals in Biology and Medicine. Oxford University Press, Oxford 2007.
12. Ischiropoulos H, Zhu L, Chen J, Tsai M, Martin JC, Smith CD, Beckman JS. Peroxynitrite-mediated tyrosine nitration catalyzed by superoxide dismutase. Arch Biochem Biophys 1992; 298: 431-437.
13. Keynes RG, Griffiths CH, Hall C, Garthwaite, J. Nitric oxide consumption through lipid peroxidation in brain cell suspensions and homogenates. Biochem J 2005; 387: 685-694.
14. Kikuchi K, Nagano T, Hayakawa H, Hirata Y, Hirobe M. Detection of nitric oxide production from a perfused organ by a luminol-H_2O_2 system. Anal Chem 1993; 65: 1794-1799.
15. Llesuy SF, Milei J, Gonzalez-Flecha B, Boveris A. Myocardial damage induced by doxorubicins: hydroperoxide-initiated chemiluminescence and morphology. Free Rad Biol Med 1990; 8: 259-264.
16. Michalak S, Wender M, Michalowska-Wender G. Cachexia-induced cerebellar degeneration: involvement of serum TNF and MCP-1 in the course of experimental neoplastic disease. Acta Neurobiol Exp 2006; 66: 113-122.
17. Oliveira FJA, Cecchini R. Oxidative stress of liver in hamsters infected with Leishmania (L.) chagasi. J Parasitol 2000; 86: 1067-1072.
18. Pannu R, Singh I. Pharmacological strategies for the regulation of inducible nitric oxide synthase: neurodegenerative versus neuroprotective mechanisms. Neurochem Int 2006; 49: 170-182.
19. Peres PS, Terra VA, Guarnier FA, Cecchini R, Cecchini AL. Photoaging and chronological aging profile: understanding oxidation of the skin. J Photochem Photob B 2001; 103: 93-97.
20. Roxburgh CS, McMillan DC. Role of systemic inflammatory response in predicting survival in patients with primary operable cancer. Future Oncol 2000; 6: 149-163.
21. Rubbo H, Radi R, Trujillo M, Telleri R, Kalyanaraman B, Barnes S, Kirk M, Freeman BA. Nitric oxide regulation of superoxide and peroxynitrite-dependent lipid peroxidation. J Biol Chem 1994; 269: 26066-26075.
22. Terra VA, Souza-Neto F, Pereira RC, Silva TNX, Costa ACC, Luiz RC, Cecchini R, Cecchini AL. Time-dependent reactive species formation and oxidative stress damage in the skin after UVB irradiation. Photochem Photobiol B 2012; 109: 34-41.
23. Terra VA, Souza-Neto FP, Pereira RC, Xavier Da Silva TN, Ramalho LN, Luiz RC, Cecchini R, Cecchini AL. Nitric oxide is responsible for oxidative skin injury and modulation of cell proliferation after 24 hours of UVB exposures. Free Radic Res 2012; 46: 872-882.
24. Ushmorov A, Hack V, Dröge W. Differential reconstitution of mitochondrial respiratory chain activity and plasma redox state by cysteine and ornithine in a model of cancer cachexia. Cancer Res 1999; 59: 3527-3534.
25. Ventrucci G, Mello MAR, Gomes-Marcondes MCC. Proteasome activity is altered in skeletal muscle tissue of tumour-bearing rats fed a leucine-rich diet. Endocr Relat Cancer 2004; 11: 887-895.

Original paper

Folia Neuropathologica

Administration of leukemia inhibitory factor increases Opalin and myelin oligodendrocyte glycoprotein expression in the cerebral cortex in a cuprizone-induced model of demyelination

Farhad Mashayekhi, Sara Pishgah Hadiyan, Zivar Salehi

Department of Biology, Faculty of Sciences, University of Guilan, Rasht, Iran

Folia Neuropathol 2015; 53 (2): 147-152 DOI: 10.5114/fn.2015.52411

Abstract

Multiple sclerosis (MS) lesions are characterized by inflammatory demyelination and reactive gliosis, and although remyelination occurs in some lesions it is limited and incomplete. Leukemia inhibitory factor (LIF) is an important cytokine that stimulates oligodendrocyte proliferation and survival in vitro. Opalin is a unique molecular marker for mature oligodendrocytes. The aim of this study was to demonstrate the role of LIF on Opalin and myelin oligodendrocyte glycoprotein (MOG) expression in the cerebral cortex of cuprizone-induced MS mice. The mice were treated with cuprizone for five weeks in order to induce MS. The mice were then divided into 3 groups. The first group was injected intraperitoneally (IP) with LIF for six weeks in the amount of 30 µg/kg bw per day. The second group (SHAM) was injected IP with normal saline and the third group was left without injection as a control. After six weeks the mice were killed, the cerebral cortex was harvested, and the expression of MOG and Opalin was studied. Using western blotting we found that LIF increases Opalin and MOG expression in the cerebral cortex extracts as compared to SHAM and control groups. However, no significant difference in the Opalin and MOG expression was seen between SHAM and control groups. It is concluded that LIF may have an important role in the process of remyelination by increasing Opalin expression and MOG expression.

Key words: *leukemia inhibitory factor, Opalin, myelin oligodendrocyte glycoprotein, cuprizone, remyelination.*

Introduction

Multiple sclerosis (MS) is a chronic demyelinating disease of the central nervous system (CNS). Approximately 2.5 million people currently live with MS globally. Susceptibility to MS varies in different ethnic groups, with people of Scottish origin being more likely to develop the disease [5]. Family members of MS patients have a higher risk of developing the disease than individuals without a family history [1].

Multiple sclerosis lesions are characterized by inflammatory demyelination and reactive gliosis, and although remyelination occurs in some lesions it is limited and incomplete. Possible reasons for this abortive remyelination include astrogliosis and accumulation of extracellular matrix, lack of myelinating

Communicating author:

Professor Farhad Mashayekhi, Department of Biology, Faculty of Sciences, University of Guilan, Rasht, Iran, phone: 0098-9113330017, fax: 0098-131-3233647, e-mail: umistbiology@yahoo.co.uk

cells or an unfavorable combination of growth factors. Growth factor expression could participate in the repair process of this demyelinating disease by modulating the activity of microglia/macrophages in an autocrine fashion, by inducing the expression of other factors that can affect myelin regeneration or degeneration, and also by directly stimulating the localized proliferation and/or regeneration of oligodendrocytes within lesion areas [21]. It has been shown that one of the identified proteins, transmembrane protein 10 (Tmem10; also known as Opalin or oligodendrocyte paranodal loop protein), whose expression is specific to the brain, predominantly localized in many white matter regions and was upregulated during the postnatal developmental stages [2]. It was shown that Opalin protein is specifically expressed by myelinating oligodendrocytes, suggesting that it plays a unique role in mammalian myelin [11]. In the CNS the main proteins of myelin are proteolipid protein (PLP), myelin basic protein (MBP) and myelin oligodendrocyte glycoprotein (MOG). Myelin oligodendrocyte glycoprotein is a minor component of the myelin sheath, but it is an important autoantigen linked to the pathogenesis of MS. It has been shown that MOG is a potent encephalitogen that triggers strong T cell and B cell responses. It has been recently shown that MOG antibodies could be associated with a broad spectrum of acquired human CNS demyelinating diseases [20].

Cytokines and growth factor play important roles in brain development and function [14,15]. Growth factor expression could participate in the repair process of demyelinating disease by modulating the activity of microglia/macrophages, inducing the expression of other factors that can affect myelin regeneration or degeneration, and also by directly stimulating the localized proliferation and/or regeneration of oligodendrocytes within lesion areas [21]. Among growth factors, leukemia inhibitory factor (LIF) is a cytokine that has been demonstrated to play an important role in neural cell survival, including cholinergic neurons. It has been demonstrated that LIF limits autoimmune demyelination and oligodendrocyte loss in a murine model of MS [7]. Leukemia inhibitory factor promotes the differentiation of either neurons or astrocytes depending on the culture conditions [19]. Increased LIF concentration in the cerebrospinal fluid (CSF) of patients with MS has been demonstrated [16]. It has been suggested that LIF is a potential therapeutic candidate for MS [23].

Leukemia inhibitory factor binds to a heterodimeric membrane receptor complex consisting of LIF receptor (LIFR) and glycoprotein 130 (gp120) [25]. Leukemia inhibitory factor receptor has been shown to be expressed in the dorsal ventricular zone and subventricular zone of the cerebral cortex [4]. Co-operative expression of LIF and LIFR in the brain of patients with neurodegenerative disease including Parkinson's disease (PD) and Alzheimer's disease (AD) may indicate a role for LIF in neuronal damage or repair in these diseases [24]. It was shown that LIF delivery to oligodendrocyte progenitor cells (OPCs) stimulates their proliferation through the activation of gp130 receptor signaling within these cells, and it has been suggested that LIF has both reparative and protective activities that make it a promising potential therapy for CNS demyelinating disorders and injuries [9]. It has been shown that LIF is a neurotrophic cytokine and plays an important role in neural cell survival and myelin formation *in vitro* [13]. It has been shown that suppressing expression of CNTF, which is an LIF family, plays a key role in the remyelination process in cuprizone-induced demyelinated mouse [26]. Addition of LIF neutralizing antibodies inhibited oligodendrocyte differentiation, indicating a crucial role of TNFR2-induced astrocyte derived LIF for oligodendrocyte maturation [10].

As Opalin is a unique molecular marker for mature oligodendrocytes and MOG is a component of the myelin sheath which is an important autoantigen linked to the pathogenesis of MS [11,20], we aimed to examine the *in vivo* effects of LIF on the remyelination process in the cerebral cortex of the cuprizone-induced MS mouse.

Material and methods

Animals

Balb/c mice were purchased from Pasteur Institute, Tehran, Iran and maintained on a 12-12 light: dark cycle beginning at 8.00 am. They were kept at a constant temperature in mouse boxes with unrestricted access to laboratory food and water. The colony was maintained through random pair mating. Timed mating was ca rried out by placing a male and female together and checking for the presence of a vaginal plug. The presence of a vaginal plug was taken as gestational day zero (E0) and the day of birth was designated postnatal day 0 (P0).

Induction of demyelination and treatment with leukemia inhibitory factor

Demyelination was induced by feeding 8-10-week-old mice a diet containing 0.2% cuprizone (bis-cyclohexanone oxaldihydrazone, Sigma-Aldrich Inc.) mixed into ground standard rodent chow.

The cuprizone diet was administered for 5 weeks for demyelination. The control group received breeder chow without the cuprizone admixture. Animals were then put on standard rodent chow without cuprizone to induce remyelination. The mice were then divided into three groups. The first group was injected intraperitoneally (IP) with LIF for 6 weeks in the amount of 30 µg/kg bw per day. The second group (SHAM) was injected with normal saline and the third group was left without injection as the control group. After four weeks the cerebral cortex was harvested after euthanasia by intraperitoneal injection of an overdose of anesthetic (sodium pentobarbitone) and the cerebral cortex was removed and processed as described. In total, 42 animals were used in this study (n = 14 for each group).

Cell extract

Fresh tissue samples (10 mg each) were chopped into tiny pieces and suspended in 0.5 ml of protein lysis buffer [150 mM NaCl, 1.0% NP40, 20 mM Tris (pH 7.5), 5 mM EDTA, and Complete Mini protease inhibitor cocktail (Roche Diagnostics Ltd., West Sussex, UK)] and then mechanically homogenized by sonication. After centrifugation, the protein extracts were recovered and stored at –70°C until they were used.

Total protein concentration and western blotting

The total protein concentration in the cerebral cortex extracts was determined by the Bio-Rad protein assay based on the Bradford dye procedure. For western blot, protein extracts (50 µg/lane) were separated on 10% SDS-polyacrylamide gel and transferred to a polyvinylidene difluoride membrane (Bio-Rad Laboratories Ltd. Hertfordshire, UK). The membranes were blocked with phosphate-buffered saline (PBS) containing 0.05% Tween 20 and 5% dry milk and probed either with polyclonal anti-Opalin antibody (Santa Cruz Biotechnology; sc-135362) (1 : 1000 dilution), polyclonal anti-MOG antibody or a mouse monoclonal anti-β-tubulin antibody (as a loading control) (Abcam plc, Cambridge, UK) (1 : 10,000 dilution) and then treated with the appropriate horseradish peroxidase-conjugated secondary antibodies. Immunoreactive protein was visualized using the Enhanced Chemiluminescence western blotting detection system (Amersham Pharmacia Biotech, Piscataway, NJ). Densitometric analysis was performed by scanning immunoblots and quantitating protein bands using an image analyzer (Metaview Software).

Statistical analysis

All data presented are expressed as mean ± standard error of the mean (SEM). Statistical analysis was performed using the one-way ANOVA to test for differences among the groups, and only values with $p \leq 0.05$ were considered significant.

Results

Total protein concentration

The total protein concentration in the cerebral cortex extracts from LIF injected, SHAM and control groups was determined by the Bio-Rad protein assay based on the Bradford dye mixture. The total protein contents of LIF injected, SHAM and control were 1.11 ± 0.12, 1.07 ± 0.18 and 1.05 ± 0.18 (g/l), respectively. No significant increase in the total protein concentration was seen in the LIF-injected brain samples compared with those from the SHAM and control groups ($p > 0.05$).

Analysis of Opalin and myelin oligodendrocyte glycoprotein expression by western blotting

Western blot analysis was performed to quantitatively evaluate Opalin and MOG expression in the cerebral cortical extracts. A western blot analysis using anti-Opalin and MOG antibodies as a probe confirmed the presence of Opalin and MOG in all the extracts (Fig. 1A and Fig. 2A). An image analyzer was used to determine the intensities of the band in the respective lanes. Quantification of the western blot bands from repeated experiments (n = 14) showed that the amount of Opalin and MOG was significantly increased in the LIF-injected cerebral cortical extracts when compared with SHAM and control groups ($p < 0.0001$) (Fig. 1B and Fig. 2B).

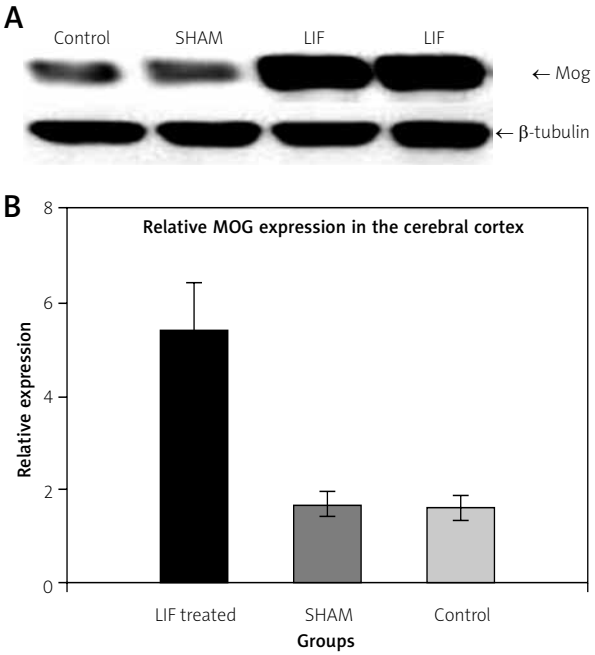

Fig. 1. (A) Myelin oligodendrocyte glycoprotein (MOG) expression in the cerebral cortex extracts from leukemia inhibitory factor (LIF) treated, SHAM and control groups. β-tubulin (50 kDa) expression was determined as a protein loading control. **(B)** Signal intensities from MOG expression in the LIF treated, SHAM and control cerebral cortex immunoblotting experiments were determined by densitometric analysis. In each of the experimental groups the number of animals investigated was 14. A significant increase in MOG expression was seen in the LIF-injected group when compared with SHAM and control groups ($p < 0.001$). No significant differences were seen between the SHAM and control group ($p = 0.42$).

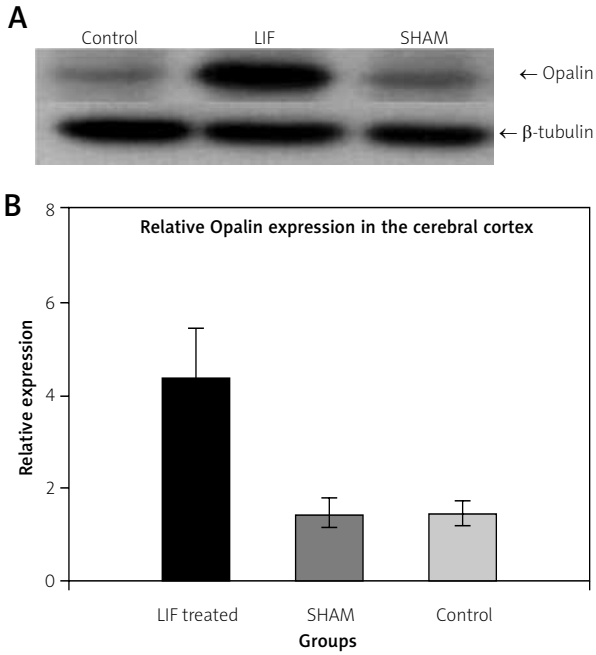

Fig. 2. (A) Opalin expression in the cerebral cortex extracts from leukemia inhibitory factor (LIF) treated, SHAM and control groups. β-tubulin (50 kDa) expression was determined as a protein loading control. **(B)** Signal intensities from Opalin expression in the LIF treated, SHAM and control cerebral cortex immunoblotting experiments was determined by densitometric analysis. In each of the experimental groups the number of animals investigated was 14. A significant increase in Opalin expression was seen in the LIF-injected group when compared with SHAM and control groups ($p < 0.001$). No significant difference was seen between SHAM and control groups ($p = 0.82$).

Discussion

Acute demyelination of the CNS in MS is initially followed by a process of remyelination [3]. This repair process is guaranteed by the extensive proliferation of oligodendrocyte progenitor cells (OPCs) in response to demyelination. It has been demonstrated that growth factor expression could be important in the repair process of this demyelinating disease by modulating the activity of microglia/macrophages by inducing the expression of other factors that can affect myelin regeneration and also by directly stimulating the localized proliferation and/or regeneration of oligodendrocytes within lesion areas.

Among growth factors, LIF has been shown to play an important role in neural cell survival [8]. Leukemia inhibitory factor has been demonstrated to limit autoimmune demyelination and oligodendrocyte loss in a murine model of MS [6]. Spinal cord precursors also synthesize LIF, and anti-LIFRβ antibodies completely blocked the generation of neurons. Leukemia inhibitory factor plays an important role in generation, maturation and survival of oligodendrocytes [17]. Data supporting a neuroprotective role of LIF have been obtained in MS, where LIF has been demonstrated to be produced by myelin-reactive T cells isolated from MS patients and protect

against tumor necrosis factor-α-induced oligodendrocyte apoptosis [27].

We investigated LIF as it is one of the most important growth factors involved in the survival of oligodendrocytes [12]. Leukemia inhibitory factor contributes to differentiation of the glial cell lineage [18].

The role of ciliary neurotrophic factor (CNTF) in the process of remyelination has been demonstrated [22]. Here we show that daily administration of LIF significantly increases MOG and Opalin expression in the cuprizone-induced mouse cerebral cortex. As Opalin is a unique molecular marker for mature oligodendrocytes, the increased Opalin expression in the cerebral cortex of LIF injected mouse may be due to increased differentiation of oligodendrocyte progenitor cells into mature oligodendrocytes. We have also shown that LIF increases MOG expression in the cerebral cortex, which indicates the role of LIF in myelin formation. The results of this study could have been anticipated with some certainty given the findings of other studies that have investigated the role of LIF in MS.

It is thus concluded that LIF may have an important role in the process of remyelination by increasing either Opalin expression and oligodendrocyte differentiation or MOG expression. It is also suggested that LIF may have an important role in the process of remyelination by increasing MOG expression in the cerebral cortex.

Acknowledgements

This study was supported by the University of Guilan.

Disclosure

Authors report no conflict of interest.

References

1. Al Jumah M, Kojan S, Al Khathaami A, Al Abdulkaream I, Al Blawi M, Jawhary A. Familial multiple sclerosis: does consanguinity have a role? Mult Scler 2011; 17: 487-489.
2. Aruga J, Yoshikawa F, Nozaki Y, Sakaki Y, Toyoda A, Furuichi T. An oligodendrocyte enhancer in a phylogenetically conserved intron region of the mammalian myelin gene Opalin. J Neurochem 2007; 102: 1533-1547.
3. Barnett MH, Sutton I. The pathology of multiple sclerosis: a paradigm shift. Curr Opin Neurol 2006; 9: 242-247.
4. Bauer S, Rasika S, Han J, Mauduit C, Raccurt M, Morel G, Jourdan F, Benahmed M, Moyse E, Patterson PH. Leukemia inhibitory factor is a key signal for injury-induced neurogenesis in the adult mouse olfactory epithelium. J Neurosci 2003; 23: 1792-1803.
5. Bayes HK, Weir CJ, O'Leary C. Timing of birth and risk of multiple sclerosis in the Scottish population. Eur Neurol 2010; 63: 36-40.
6. Butzkueven H, Emery B, Cipriani T, Marriott MP, Kilpatrick TJ. Endogenous leukemia inhibitory factor production limits autoimmune demyelination and oligodendrocyte loss. Glia 2006; 53: 696-703.
7. Butzkueven H, Zhang JG, Soilu-Hanninen M, Hochrein H, Chionh F, Shipham KA, Emery B, Turnley AM, Petratos S, Ernst M, Bartlett PF, Kilpatrick TJ. LIF receptor signaling limits immune-mediated demyelination by enhancing oligodendrocyte survival. Nat Med 2002; 8: 613-619.
8. Cheema SS, Arumugam D, Murray SS, Bartlett PF. Leukemia inhibitory factor maintains choline acetyltransferase expression in vivo. Neuroreport 1998; 9: 363-366.
9. Deverman BE, Patterson PH. Exogenous leukemia inhibitory factor stimulates oligodendrocyte progenitor cell proliferation and enhances hippocampal remyelination. J Neurosci 2012; 32: 2100-2109.
10. Fischer R, Wajant H, Kontermann R, Pfizenmaier K, Maier O. Astrocyte-specific activation of TNFR2 promotes oligodendrocyte maturation by secretion of leukemia inhibitory factor. Glia 2014; 62: 272-283.
11. Golan N, Adamsky K, Kartvelishvily E, Brockschnieder D, Möbius W, Spiegel I, Roth AD, Thomson CE, Rechavi G, Peles E. Identification of Tmem10/Opalin as an oligodendrocyte enriched gene using expression profiling combined with genetic cell ablation. Glia 2008; 56: 1176-1186.
12. Ishibashi T, Lee PR, Baba H, Fields RD. Leukemia inhibitory factor regulates the timing of oligodendrocyte development and myelination in the postnatal optic nerve. J Neurosci Res 2009; 87: 3343-3355.
13. Marriott MP, Emery B, Cate HS, Binder MD, Kemper D, Wu Q, Kolbe S, Gordon IR, Wang H, Egan G, Murray S, Butzkueven H, Kilpatrick TJ. Leukemia inhibitory factor signaling modulates both central nervous system demyelination and myelin repair. Glia 2008; 56: 686-698.
14. Mashayekhi F, Gholizadeh L. Administration of anti-c-kit antibody into the cerebrospinal fluid leads to increased cell death in the developing cerebral cortex. Saudi J Biol Sci 2011; 18: 261-266.
15. Mashayekhi F, Sadeghi M, Rajaei F. Induction of perlecan expression and neural cell proliferation by FGF-2 in the developing cerebral cortex: an in vivo study. J Mol Neurosci 2011; 45: 87-93.
16. Mashayekhi F, Salehi Z. Expression of leukemia inhibitory factor in the cerebrospinal fluid of patients with multiple sclerosis. J Clin Neurosci 2011; 18: 951-954.
17. Mayer M, Bhakoo K, Noble M. Ciliary neurotrophic factor and leukemia inhibitory factor promote the generation, maturation and survival of oligodendrocytes in vitro. Development 1994; 120: 143-153.
18. Nakagaito Y, Yoshida T, Satoh M, Takeuchi M. Effects of leukemia inhibitory factor on the differentiation of astrocyte progenitor cells from embryonic mouse cerebral hemispheres. Brain Res Dev Brain Res 1995; 87: 220-223.

19. Nakanishi M, Niidome T, Matsuda S, Akaike A, Kihara T, Sugimoto H. Microglia-derived interleukin-6 and leukaemia inhibitory factor promote astrocytic differentiation of neural stem/progenitor cells. Eur J Neurosci 2007; 25: 649-658.
20. Reindl M, Di Pauli F, Rostásy K, Berger T. The spectrum of MOG autoantibody-associated demyelinating diseases. Nat Rev Neurol 2013; 9: 455-461.
21. Rosenberg SS, Ng BK, Chan JR. The quest for remyelination: a new role for neurotrophins and their receptors. Brain Pathol 2006; 16: 288-294.
22. Salehi Z, Hadiyan SP, Navidi R. Ciliary neurotrophic factor role in myelin oligodendrocyte glycoprotein expression in Cuprizone-induced multiple sclerosis mice. Cell Mol Neurobiol 2013; 33: 531-535.
23. Slaets H, Hendriks JJ, Stinissen P, Kilpatrick TJ, Hellings N. Therapeutic potential of LIF in multiple sclerosis. Trends Mol Med 2010; 16: 493-500.
24. Soilu-Hänninen M, Broberg E, Röyttä M, Mattila P, Rinne J, Hukkanen V. Expression of LIF and LIF receptor beta in Alzheimer's and Parkinson's diseases. Acta Neurol Scand 2010; 121: 44-50.
25. Takahashi Y, Carpino N, Cross JC, Torres M, Parganas E, Ihle JN. SOCS3: an essential regulator of LIF receptor signaling in trophoblast giant cell differentiation. EMBO J 2003; 22: 372-384.
26. Tanaka T, Murakami K, Bando Y, Yoshida S. Minocycline reduces remyelination by suppressing ciliary neurotrophic factor expression after cuprizone-induced demyelination. J Neurochem 2013; 127: 259-270.
27. Vanderlocht J, Hellings N, Hendriks JJ, Vandenabeele F, Moreels M, Buntinx M, Hoekstra D, Antel JP, Stinissen P. Leukemia inhibitory factor is produced by myelin-reactive T cells from multiple sclerosis patients and protects against tumor necrosis factor-alpha-induced oligodendrocyte apoptosis. J Neurosci Res 2006; 83: 763-774.

Folia Neuropathologica

Adult, isolated respiratory chain complex IV deficiency with minimal manifestations

Josef Finsterer[1], Gabor G. Kovacs[2], Helmut Rauschka[3], Uwe Ahting[4]

[1]Krankenanstalt Rudolfstiftung, Vienna, Austria, [2]Institute of Neurology, Medical University of Vienna, Vienna, Austria, [3]Neurological Department, SMZO, Vienna, Austria, [4]Institute of Clinical Chemistry, Munich, Germany

Folia Neuropathol 2015; 53 (2): 153-157 DOI: 10.5114/fn.2015.52412

Abstract

Objectives: *Isolated complex IV (cytochrome c oxidase) deficiency is one of the most frequent respiratory chain defects in mitochondrial disorders (MIDs) and usually occurs together with severe pediatric or rarely adult multisystem disease. Here we report an adult with isolated complex IV deficiency with unusually mild clinical manifestations.*
Case report: *A 50-year-old man had developed generalized muscle aches and occasional twitching and stiffness of the musculature since age 48 years. He had a previous history of diabetes, acute hearing loss, hyperlipidemia, hyperuricemia, arterial hypertension, polyarthrosis, hypogonadism, and hypothyroidism. The family history was positive for diabetes (mother), CK elevation (brother), myalgias (brother), and proximal weakness of the upper limbs (mother). Work-up revealed hypoacusis, postural tremor and reduced tendon reflexes, recurrent mild hyper-CK-emia, neurogenic needle electromyography, and a muscle biopsy with mild non-specific changes. Biochemical investigations of the muscle homogenate revealed an isolated complex IV defect and reduced amounts of coenzyme Q (CoQ). He profited from CoQ supplementation, low-carbohydrate diet, and gluten-free diet.*
Conclusions: *Isolated complex IV deficiency may present with only mild muscular, endocrine, or cardiac manifestations in adults. Coenzyme Q supplementation, low-carbohydrate diet, and gluten-free diet may have a beneficial effect at least on some of the manifestations.*

Key words: *mitochondrial, myopathy, metabolic, multisystem, complex IV, cytochrome c oxidase, muscle biopsy, creatine kinase.*

Introduction

Primary mitochondrial disorders (MIDs) are due to mutations in mitochondrial DNA (mtDNA) or nuclear DNA (nDNA)-located genes that encode subunits of respiratory chain complexes, assembly factors (ancillary proteins), proteins involved in mtDNA maintenance (intergenomic signaling), in the mitochondrial protein synthesis machinery, in coenzyme Q generation, in the mitochondrial transport machinery, or in apoptosis [7,8]. These mutations may occur together with reduced activity of single or multiple respiratory chain complexes in biochemical investigations [7,8]. Isolated complex IV (cytochrome c oxidase) deficiency is one of the most frequent respiratory chain defects in MIDs and usually occurs together with severe pediatric or rarely adult multisystem disease [20]. Here we report an adult with

Communicating author:
Josef Finsterer, MD, PhD, Postfach 20, 1180 Vienna, Austria, phone: +43-1-71165-92085, fax: +43-1-4781711, e-mail: fifigs1@yahoo.de

isolated complex IV deficiency with unusually mild clinical manifestations.

Case report

The patient is a 50-year-old Caucasian man, height 172 cm, weight 84 kg, with a history of spontaneous, permanent aching predominantly of the thighs and less intense aching of the lower legs, the neck, and the shoulder girdle muscles since the age of 48 years. Muscle aching could be slightly reduced by initiation of exercise but was markedly intensified after exercise during several days. He reported "heavy legs" after running and occasional twitching and stiffness of the musculature. His previous history was noteworthy for diabetes, acute hearing loss, hyperlipidemia, hyperuricemia, arterial hypertension, which had been well controlled with appropriate medication for 3 years, polyarthrosis, hypogonadism, and hypothyroidism since age 38 years. He also reported a mushy stool for years with slight improvement after changing to a gluten-free diet. The family history was positive for diabetes (mother), CK elevation (brother), myalgias (brother), and proximal weakness of the upper limbs (mother). Clinical neurologic examination at age 50 years revealed slight hypoacusis, mild postural tremor and markedly reduced tendon reflexes. His muscles were generally sore.

Work-up revealed recurrently elevated creatine kinase (CK) values with a maximum value of 1200 U/l (*n*, < 190 U/l) but normal values during several months prior to the last visit in 2/2014. Serum lactate and the forearm ischemic test were normal. Nerve conduction studies of the right femoral nerve, the median and peroneal nerves bilaterally, the left sural nerve and the sensory fibers of the median nerves bilaterally, were all normal. Needle electromyography of two muscles in 6/2011 was normal. Needle electromyography of the right quadriceps femoris muscle in 10/2013 was, in contrast, neurogenic, revealing extensive fibrillations and fasciculations at all recording points, enlarged motor units, and a clear interference pattern. Muscle biopsy from the left lateral vastus muscle in 4/2012 showed two "Ringbinden" (Fig. 1A), one COX-negative fiber (Fig. 1B), and slight type 2 fiber predominance. Ultrastructural examination revealed fibers with subsarcolemmal accumulation of mitochondria and lipid droplets (Fig. 1C), but there was a lack of paracrystalline inclusions or other structural alterations. Biochemical investigations of the muscle homogenate revealed an isolated complex IV defect and reduced amounts of CoQ (Table I). HbA_{1c} was 6.5 (*n*, < 6.0). Echocardiography revealed only mild concentric hypertrophy. Ultrasound of the upper abdomen revealed steatosis hepatis exclusively. Magnetic resonance imagine of the cervical spine was normal. His last medication comprised amlodipine (10 mg/d), L-thyroxine (50 μg/d), CoQ (300 mg/d), and metformin (1000 mg/d). He could accomplish his daily job as an engineer with only progressively stiff neck muscles with increasing duration of his working hours.

Discussion

Isolated complex IV deficiency is one of the most common biochemical abnormalities in MIDs [4,19]. Isolated complex IV deficiency is clinically and genetically extremely heterogeneous (Table II). Clinical manifestations may range from fatal encephalopathy [19], Leigh syndrome (a severe neurodegenerative disorder with characteristic bilateral lesions in the basal ganglia and the brainstem [20]), or epilepsy to myopathy, rhabdomyolysis, or hypertrophic cardiomyopathy (Table II). Genetically, isolated complex IV deficiency may be due to mtDNA mutations or nDNA mutations. mtDNA-located genes associated with isolated complex IV deficiency include genes encoding tRNAs or subunits of complex IV (COX-I, COX-II, COX-III) (Table II). nDNA-located genes associated with isolated complex IV deficiency include an even larger number of genes (Table II). Genes most commonly mutated in isolated complex IV deficiency include SURF1 [20] and SCO2 [3,31].

The reason why such a heterogeneous genetic background leads to the same biochemical defect remains elusive, but it can be speculated that the so far reported genes involved in isolated complex IV deficiency contribute to the composition, assembly, or maintenance of complex IV. Why tRNA mutations cause complex IV deficiency also remains elusive, but these mutations may specifically impair the translation of components of complex IV. Whether hypoacusis, diabetes, arterial hypertension, hyperlipidemia, polyarthralgia, hyperuricemia, hypothyroidism, and hypogonadism have to be regarded as manifestations of the mitochondrial defect remains speculative but previous reports suggest that these manifestations can be occasionally found in patients with MIDs [9]. Since serum CoQ levels were markedly

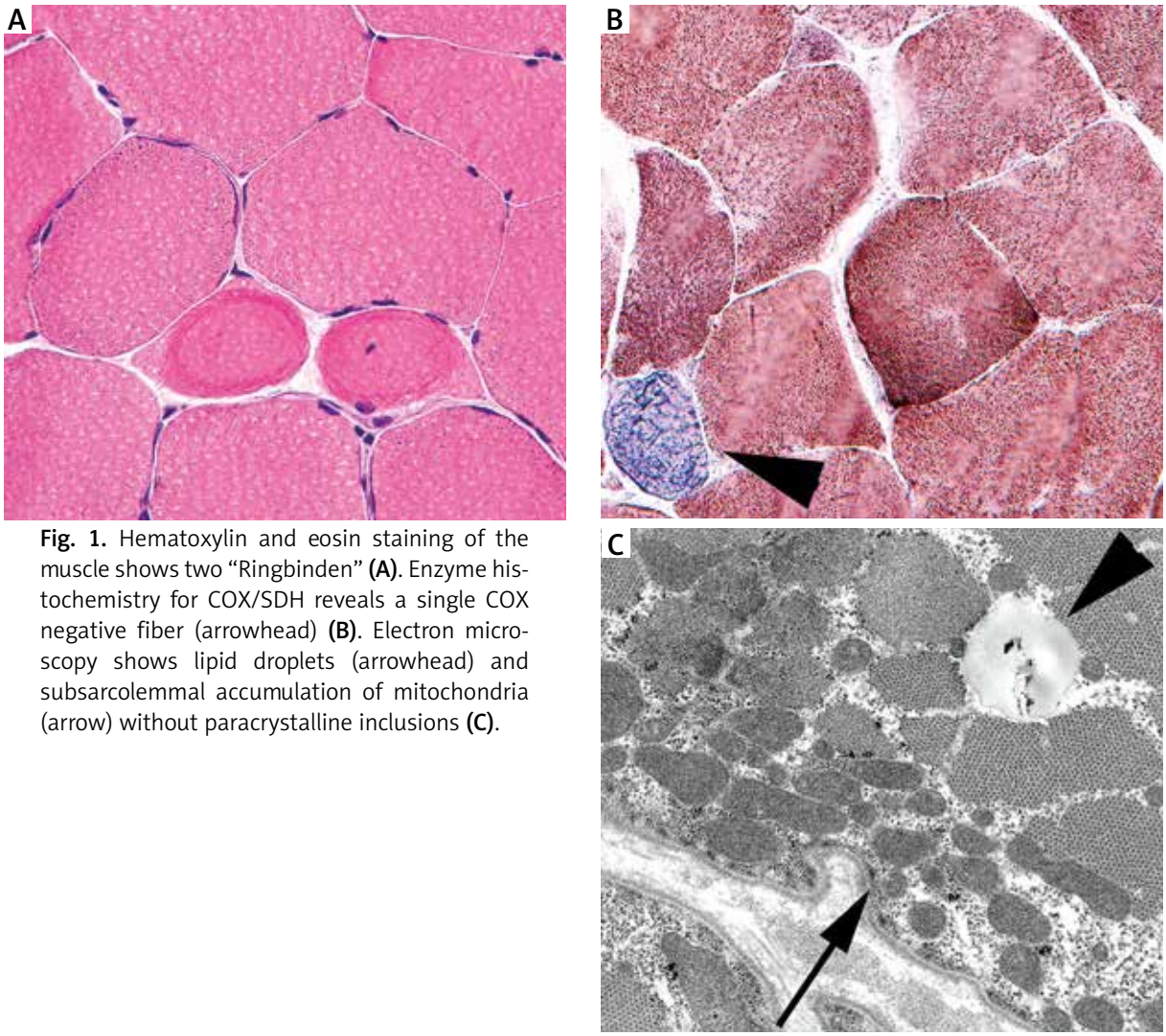

Fig. 1. Hematoxylin and eosin staining of the muscle shows two "Ringbinden" **(A)**. Enzyme histochemistry for COX/SDH reveals a single COX negative fiber (arrowhead) **(B)**. Electron microscopy shows lipid droplets (arrowhead) and subsarcolemmal accumulation of mitochondria (arrow) without paracrystalline inclusions **(C)**.

Table I. Results of biochemical investigations of muscle homogenate in the presented patient

Enzyme activity	Reference limit	Result
Related to non-collagen protein		
Complex I (NADH-CoQ oxidoreductase)	15.8-42.8 U/gNCP	15.6
Complex II/III (succinate cytochrome c oxidoreductase)	6.0-25.0 U/gNCP	9.1
Complex IV (cytochrome c oxidase)	112-351 U/gNCP	46.4
Coenzyme Q	160-1200 mmol/gNCP	111.6
Related to citrate synthetase		
Complex I (NADH-CoQ oxidoreductase)	0.17-0.56 U/U CS	0.26
Complex II/III (succinate cytochrome c oxidoreductase)	0.08-0.45 U/U CS	0.15
Complex IV (cytochrome c oxidase)	1.1-5.0 U/U CS	0.76
Coenzyme Q	2.7-7.0 mmol/U CS	1.8

NCP – non-collagen protein

Table II. Clinical manifestations of and mutated genes in isolated complex IV deficiency

	Mutated gene	Reference
Clinical presentation mtDNA		
Encephalomyopathy	tRNA(Arg)	[24]
Leigh syndrome	tRNA(Leu)	[3]
Leigh syndrome (8344, 8363)	tRNA(Lys)	[3]
Deafness, epilepsy, ataxia	tRNA(Ser)	[29]
Stroke, epilepsy, lactic acidosis	COX-I	[16]
MELAS, encephalomyopathy	COX-II	[15,25]
Myopathy	COX-III	[15]
Myoglobinuria	COX-III	[14]
Encephalomyopathy	COX-III	[13,18]
nDNA		
Leigh syndrome	SURF1	[3,6,20]
Fatal encephalopathy	SCO1	[19]
Cardioencephalomyopathy	SCO2	[3,10,31]
Werdnig-Hoffmann disease	SCO2	[27]
Leigh syndrome, anemia, deafness	COX10	[1,6]
Leigh syndrome	COX15	[5]
Hypertrophic cardiomyopathy	COX15	[2]
Epilepsy	C19orf79	[20]
COX-deficiency	NDUFA4	[23]
Megaconial myopathy	CHKB	[12]
Cognition ↓, dystonia, vision ↓	TACO1	[28]
Encephalomyopathy	FASTKD2	[11]
No mutations described		
Isolated myopathy	n.s.	[17]
Adult Leigh syndrome	n.s.	[22]
Hypertrophic cardiomyopathy	n.s.	[30]
Encephalo-hepatopathy	n.s.	[19,26]
Hypertrophic cardiomyopathy	n.s.	[19,26]
MERRF	n.s.	[21]
Myalgia, diabetes, hypoacusis	n.s.	[Current case]

n.s. – not specified

reduced, a substitution therapy with CoQ 300 mg/d was begun, with some beneficial effect. Low carbohydrate diet enhanced this effect.

This case shows that isolated complex IV deficiency may present with only mild muscular, endocrine, or cardiac manifestations. Coenzyme Q supplementation, low-carbohydrate diet, and gluten-free diet may have a beneficial effect at least on some of the manifestations.

Disclosure

The authors report no conflict of interest.

References

1. Antonicka H, Leary SC, Guercin GH, Agar JN, Horvath R, Kennaway NG, Harding CO, Jaksch M, Shoubridge EA. Mutations in COX10 result in a defect in mitochondrial heme A biosynthesis and account for multiple, early-onset clinical phenotypes associated with isolated COX deficiency. Hum Mol Genet 2003; 12: 2693-2702.
2. Antonicka H, Mattman A, Carlson CG, Glerum DM, Hoffbuhr KC, Leary SC, Kennaway NG, Shoubridge EA. Mutations in COX15 produce a defect in the mitochondrial heme biosynthetic pathway, causing early-onset fatal hypertrophic cardiomyopathy. Am J Hum Genet 2003; 72: 101-114.
3. Böhm M, Pronicka E, Karczmarewicz E, Pronicki M, Piekutowska-Abramczuk D, Sykut-Cegielska J, Mierzewska H, Hansikova H, Vesela K, Tesarova M, Houstkova H, Houstek J, Zeman J. Retrospective, multicentric study of 180 children with cytochrome C oxidase deficiency. Pediatr Res 2006; 59: 21-26.
4. Bourens M, Boulet A, Leary SC, Barrientos A. Human COX20 cooperates with SCO1 and SCO2 to mature COX2 and promote the assembly of cytochrome c oxidase. Hum Mol Genet 2014; 23: 2901-2913.
5. Bugiani M, Tiranti V, Farina L, Uziel G, Zeviani M. Novel mutations in COX15 in a long surviving Leigh syndrome patient with cytochrome c oxidase deficiency. J Med Genet 2005; 42: e28.
6. Coenen MJ, Smeitink JA, Pots JM, van Kaauwen E, Trijbels FJ, Hol FA, van den Heuvel LP. Sequence analysis of the structural nuclear encoded subunits and assembly genes of cytochrome c oxidase in a cohort of 10 isolated complex IV-deficient patients revealed five mutations. J Child Neurol 2006; 21: 508-511.
7. DiMauro S, Schon EA, Carelli V, Hirano M. The clinical maze of mitochondrial neurology. Nat Rev Neurol 2013; 9: 429-444.
8. Finsterer J. Inherited mitochondrial disorders. Adv Exp Med Biol 2012; 942: 187-213.
9. Finsterer J, Jarius C, Eichberger H. Phenotype variability in 130 adult patients with respiratory chain disorders. J Inherit Metab Dis 2001; 24: 560-576.
10. Foltopoulou PF, Tsiftsoglou AS, Bonovolias ID, Ingendoh AT, Papadopoulou LC. Intracellular delivery of full length recombinant human mitochondrial L-Sco2 protein into the mitochondria of permanent cell lines and SCO2 deficient patient's primary cells. Biochim Biophys Acta 2010; 1802: 497-508.

11. Ghezzi D, Saada A, D'Adamo P, Fernandez-Vizarra E, Gasparini P, Tiranti V, Elpeleg O, Zeviani M. FASTKD2 nonsense mutation in an infantile mitochondrial encephalomyopathy associated with cytochrome c oxidase deficiency. Am J Hum Genet 2008; 83: 415-423.
12. Gutiérrez Ríos P, Kalra AA, Wilson JD, Tanji K, Akman HO, Area Gómez E, Schon EA, DiMauro S. Congenital megaconial myopathy due to a novel defect in the choline kinase Beta gene. Arch Neurol 2012; 69: 657-661.
13. Hanna MG, Nelson IP, Rahman S, Lane RJ, Land J, Heales S, Cooper MJ, Schapira AH, Morgan-Hughes JA, Wood NW. Cytochrome c oxidase deficiency associated with the first stop-codon point mutation in human mtDNA. Am J Hum Genet 1998; 63: 29-36.
14. Hoffbuhr KC, Davidson E, Filiano BA, Davidson M, Kennaway NG, King MP. A pathogenic 15-base pair deletion in mitochondrial DNA-encoded cytochrome c oxidase subunit III results in the absence of functional cytochrome c oxidase. J Biol Chem 2000; 275: 13994-14003.
15. Horváth R, Schoser BG, Müller-Höcker J, Völpel M, Jaksch M, Lochmüller H. Mutations in mtDNA-encoded cytochrome c oxidase subunit genes causing isolated myopathy or severe encephalomyopathy. Neuromuscul Disord 2005; 15: 851-857.
16. Jaksch M, Hofmann S, Kleinle S, Liechti-Gallati S, Pongratz DE, Müller-Höcker J, Jedele KB, Meitinger T, Gerbitz KD. A systematic mutation screen of 10 nuclear and 25 mitochondrial candidate genes in 21 patients with cytochrome c oxidase (COX) deficiency shows tRNA(Ser)(UCN) mutations in a subgroup with syndromal encephalopathy. J Med Genet 1998; 35: 895-900.
17. Karadag A, Avci Z, Catal F, Odemis E. Cytochrome c oxidase deficiency in a child with isolated myopathy. Fetal Pediatr Pathol 2005; 24: 149-153.
18. Keightley JA, Hoffbuhr KC, Burton MD, Salas VM, Johnston WS, Penn AM, Buist NR, Kennaway NG. A microdeletion in cytochrome c oxidase (COX) subunit III associated with COX deficiency and recurrent myoglobinuria. Nat Genet 1996; 12: 410-416.
19. Leary SC, Antonicka H, Sasarman F, Weraarpachai W, Cobine PA, Pan M, Brown GK, Brown R, Majewski J, Ha KC, Rahman S, Shoubridge EA. Novel mutations in SCO1 as a cause of fatal infantile encephalopathy and lactic acidosis. Hum Mutat 2013; 34: 1366-1370.
20. Lim SC, Smith KR, Stroud DA, Compton AG, Tucker EJ, Dasvarma A, Gandolfo LC, Marum JE, McKenzie M, Peters HL, Mowat D, Procopis PG, Wilcken B, Christodoulou J, Brown GK, Ryan MT, Bahlo M, Thorburn DR. A founder mutation in PET100 causes isolated complex iv deficiency in Lebanese individuals with Leigh syndrome. Am J Hum Genet 2014; 94: 209-222.
21. Lombes A, Mendell JR, Nakase H, Barohn RJ, Bonilla E, Zeviani M, Yates AJ, Omerza J, Gales TL, Nakahara K, et al. Myoclonic epilepsy and ragged-red fibers with cytochrome oxidase deficiency: neuropathology, biochemistry, and molecular genetics. Ann Neurol 1989; 26: 20-33.
22. Marsac C, Degoul F, Bonne G, Romero N, Nelson I, Fardeau M, François D, Ponsot G, Harpey JP, Eymard B, et al. Mitochondrial function and mitochondrial DNA in a series of 64 patients suspected of having mitochondrial myopathy. Rev Neurol (Paris) 1991; 147: 462-466.
23. Pitceathly RD, Rahman S, Wedatilake Y, Polke JM, Cirak S, Foley AR, Sailer A, Hurles ME, Stalker J, Hargreaves I, Woodward CE, Sweeney MG, Muntoni F, Houlden H, Taanman JW, Hanna MG; UK10K Consortium. NDUFA4 mutations underlie dysfunction of a cytochrome c oxidase subunit linked to human neurological disease. Cell Rep 2013; 3: 1795-1805.
24. Roos S, Darin N, Kollberg G, Andersson Grönlund M, Tulinius M, Holme E, Moslemi AR, Oldfors A. A novel mitochondrial tRNA Arg mutation resulting in an anticodon swap in a patient with mitochondrial encephalomyopathy. Eur J Hum Genet 2013; 21: 571-573.
25. Rossmanith W, Freilinger M, Roka J, Raffelsberger T, Moser-Their K, Prayer D, Bernert G, Bittner R. Isolated cytochrome c oxidase deficiency as a cause of MELAS. BMJ Case Rep 2009; 2009.
26. Sacconi S, Salviati L, Sue CM, Shanske S, Davidson MM, Bonilla E, Naini AB, De Vivo DC, DiMauro S. Mutation screening in patients with isolated cytochrome c oxidase deficiency. Pediatr Res 2003; 53: 224-230.
27. Salviati L, Sacconi S, Rasalan MM, Kronn DF, Braun A, Canoll P, Davidson M, Shanske S, Bonilla E, Hays AP, Schon EA, DiMauro S. Cytochrome c oxidase deficiency due to a novel SCO2 mutation mimics Werdnig-Hoffmann disease. Arch Neurol 2002; 59: 862-865.
28. Seeger J, Schrank B, Pyle A, Stucka R, Lörcher U, Müller-Ziermann S, Abicht A, Czermin B, Holinski-Feder E, Lochmüller H, Horvath R. Clinical and neuropathological findings in patients with TACO1 mutations. Neuromuscul Disord 2010; 20: 720-724.
29. Tam EW, Feigenbaum A, Addis JB, Blaser S, Mackay N, Al-Dosary M, Taylor RW, Ackerley C, Cameron JM, Robinson BH. A novel mitochondrial DNA mutation in COX1 leads to strokes, seizures, and lactic acidosis. Neuropediatrics 2008; 39: 328-334.
30. Venditti CP, Harris MC, Huff D, Peterside I, Munson D, Weber HS, Rome J, Kaye EM, Shanske S, Sacconi S, Tay S, DiMauro S, Berry GT. Congenital cardiomyopathy and pulmonary hypertension: another fatal variant of cytochrome-c oxidase deficiency. J Inherit Metab Dis 2004; 27: 735-739.
31. Vesela K, Hansikova H, Tesarova M, Martasek P, Elleder M, Houstek J, Zeman J. Clinical, biochemical and molecular analyses of six patients with isolated cytochrome c oxidase deficiency due to mutations in the SCO2 gene. Acta Paediatr 2004; 93: 1312-1317.

Folia Neuropathologica

Multiple schwannomas of the digital nerves and superficial radial nerve: two unusual cases of segmental schwannomatosis

Jerzy Gosk[1], Olga Gutkowska[1], Sebastian Kuliński[1], Maciej Urban[1], Agnieszka Hałoń[2]

[1]Department of Traumatology, Clinic of Traumatology and Hand Surgery, Wroclaw Medical University, Wroclaw, [2]Division of Pathomorphology and Oncological Cytology, Wroclaw Medical University, Wroclaw, Poland

Folia Neuropathol 2015; 53 (2): 158-167 DOI: 10.5114/fn.2015.52413

Abstract

Two cases of segmental sporadic schwannomatosis characterized by unusual location of multiple schwannomas in digital nerves (case 1) and the superficial radial nerve (case 2) are described in this paper. In the first of the described cases, 6 tumours located at the base of the middle finger and in its distal portion were excised from both digital nerves. In the second case, 3 tumours located in the proximal 1/3 and halfway down the forearm were removed from the superficial radial nerve. In both cases, symptoms such as palpable tumour mass, pain, paraesthesias, and positive Tinel-Hoffman sign resolved after operative treatment. Final diagnoses were made based on histopathological examination results. In the second of the described cases, the largest of the excised lesions had features enabling diagnosis of a rare tumour type – ancient schwannoma.

Key words: *schwannomatosis, multiple neurilemmomas, ancient schwannoma, superficial radial nerve, digital nerve.*

Introduction

Schwannomas are benign neoplasms derived from Schwann cells. They mostly occur as solitary tumours [6,7,25]. Multiple schwannomas developing in individual nerves are very rare [14,24,29,33,35]. Their presence may be one of the symptoms indicative of neurofibromatosis type 2 or schwannomatosis [5,13,25]. In material presented by Ogose *et al*. multiple schwannomas were found in 4.6% of all patients treated for schwannoma [25]. Qualification for surgical treatment of multiple schwannomas is controversial. Some authors highlight elevated risk of iatrogenic damage to the nerve during tumour excision [24]. Advocates of surgical treatment raise the possibility of development of multilevel compression neuropathy as a result of the growth of tumours [5]. It is obvious that only symptomatic tumours are qualified for excision [5].

Case report

Case 1

A 26-year-old woman was admitted to our ward for surgical treatment of multiple nodules located in the middle finger of her left hand. The nodules began to be palpable 6 years earlier. There was no history of significant trauma or inflammation of the left hand. The patient reported pain that increased when pressure was applied on the nodules and with finger movements. Paraesthesias were present in the fingerpad of the patient's third finger.

On ultrasound examination performed on 1.04.2011 a polycyclic lesion consisting of 3 nodules was seen

Communicating author:
Jerzy Gosk, Department of Traumatology, Clinic of Traumatology and Hand Surgery, Wroclaw Medical University, 213 Borowska St., 50-556 Wrocław, Poland, phone: +48 71 734 38 00, fax: +48 71 734 38 09, e-mail: chiruraz@umed.wroc.pl

along the proper digital nerve on the radial side of the third finger. The lesion originated at the level of the metacarpophalangeal joint and continued for about 33 mm. Consecutive individual nodules were 7.5, 11 and 9 mm in diameter, going proximally. In the same nerve, presence of another solitary nodule with a diameter of 3.6 mm located 3 mm distally from the proximal interphalangeal joint was detected. Presence of another nodule measuring 4.5 mm in diameter was revealed in the proper digital nerve on the ulnar side near the distal interphalangeal joint. Magnetic resonance imaging (MRI) examination (Siemes Essenza 1.5T) performed on 25.03.2013 showed a polycyclic lesion about 36 mm long derived from the proper digital nerve on the radial side of the third finger. Presence of another tumour measuring 5 mm in diameter and located in the proper digital nerve on the ulnar side of the distal portion of the middle phalanx was also revealed. The tumours showed significant enhancement after administration of contrast agent – Figure 1.

On clinical examination presence of palpable nodules both on the radial and the ulnar side of the third finger was detected. Local pain was triggered by applying pressure on the nodules. The metacarpophalangeal as well as proximal and distal interphalangeal flexion range was also limited by pain. On percussion of the nodules, positive Tinel-Hoffman sign was observed together with paraesthesias in the fingerpad of the third finger. Superficial sensation in the fingerpad of the third finger was unaltered, with static and dynamic sensory discrimination comparable to the opposite side. Neither muscle atrophy nor impaired digital blood flow in the patient's hand was observed. It was decided that the patient qualified for operative treatment. During the first operation performed on 7.05.2013, four nodules located in the proper digital nerve on the radial side were removed. The nodules were 12, 10, 8 and 3 mm in diameter – Figure 2. The smallest of the removed nodules was not visualized on imaging tests. During the second opera-

Fig. 1. Magnetic resonance imaging examination results. **A)** Visualization of tumours located in both digital nerves of the third finger. **B)** Contrast enhancement of the tumours.

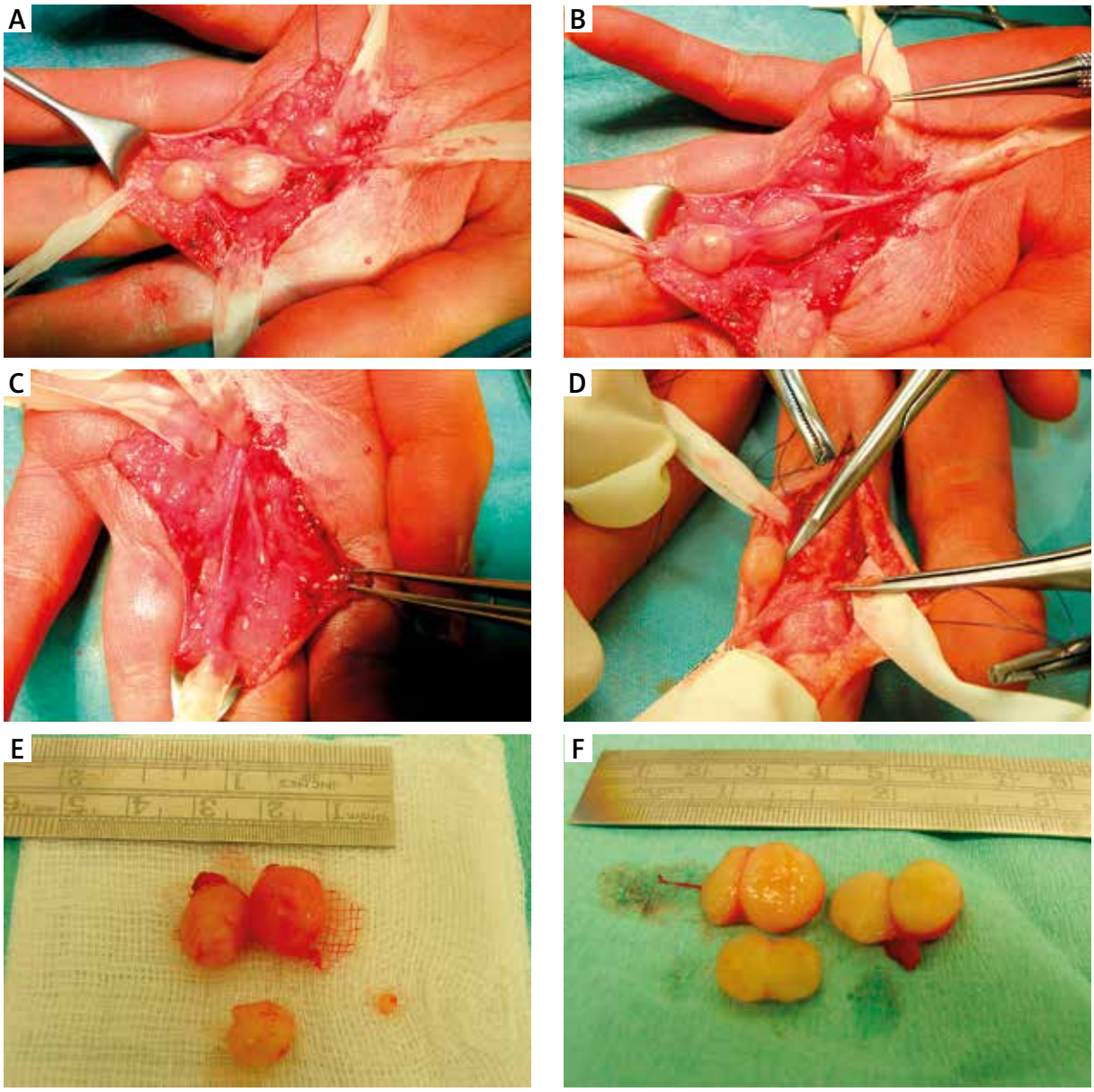

Fig. 2. Intraoperative view: **A)** tumours in the course of radial digital nerve, **B)** view of operative field after removal of one of the tumours, **C)** radial digital nerve after resection of the tumours, **D)** tumour of ulnar digital nerve, **E)** appearance of the tumours after removal from radial digital nerve, **F)** cross-section of the tumours.

tion performed on 30.09.2013 a nodule located in the proper digital nerve on the ulnar side at the level of the distal interphalangeal joint and another nodule located on the opposite side at the level of the base of the middle phalanx were removed. The nodules were 5 and 3 mm in diameter – Figure 2. Surgical treatment was divided into two stages in order to avoid vast dissection of tissues of the third finger. Both operations were performed using tourniquet ischemia, microsurgical tools and an operating microscope. All nodules were excised without damage to the fascicular structure of nerves.

On postoperative histopathological examination all tumours had the same histopathological pattern – neurilemmoma Antoni A (sample numbers: 26895 from 17.05.2013 and 31909 from 18.10.2013). Im-

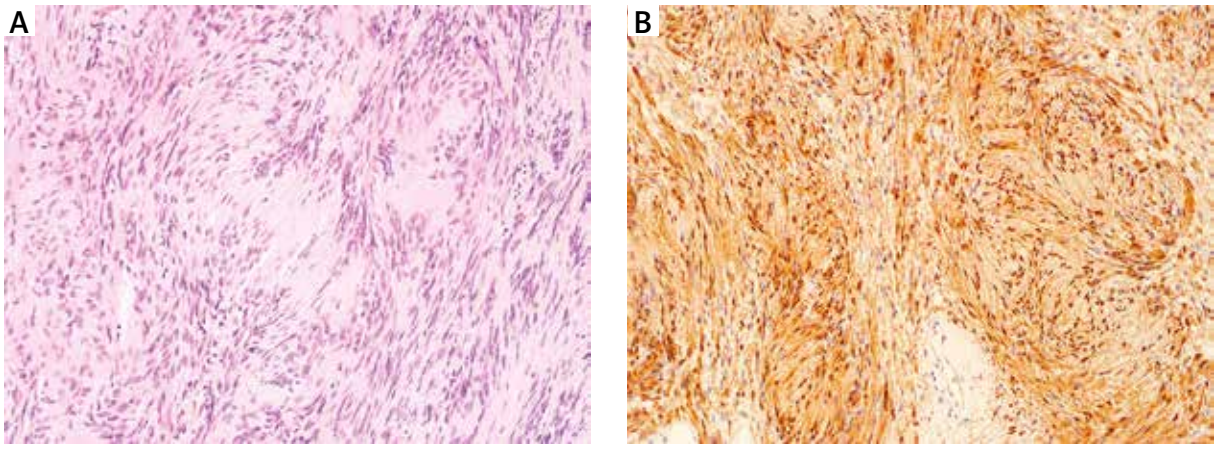

Fig. 3. Histopathological examination results: **A)** neurilemmoma Antoni A, H&E stain, ×100 magnification; **B)** immunohistochemical expression of S-100 protein in Schwann cell.

munohistochemical analysis showed positive reaction against S-100 protein – Figure 3.

In the early postoperative stage no worsening of function of digital nerves was observed. The patient is under ambulatory surveillance. In the long-term postoperative course no signs of recurrence of nodules were observed. Pain and paraesthesias in the fingerpad of the third finger resolved. Tinel-Hoffman sign is currently negative. The postoperative scar formed at the base of the third finger slightly limits full extension of the finger.

Case 2

A 22-year-old woman was admitted to our ward for operative treatment of tumours located on her left forearm. The tumours first appeared about two years earlier. The patient had no history of trauma to the affected area. In anamnesis, the patient reported pain elicited by applying pressure to the tumour mass and after overstraining the limb as well as presence of paraesthesias in the dorsum of the 1st and 2nd fingers of her left hand. On ultrasound examination performed on 19.07.2013 presence of 2 tumours in the course of the superficial branch of the radial nerve was detected. The proximal lesion measuring 23 × 16 × 36 mm was located about 2 cm from the site of division of the major trunk of the radial nerve. This tumour was well encapsulated, located under the epineurium and caused displacement of nerve fascicles. Matrix of the tumour was heterogeneous with numerous fluid collections. The peripheral lesion had the dimensions 17 × 7 × × 5 mm and its matrix was homogeneous. On MRI examination performed on 11.04.2013, presence of two nodules differing in size located in the superficial radial nerve was detected. The larger of them, measuring 37 × 20 × 18 mm, was located about 3 cm from the cubital joint. The other one was located peripherally, about 9 cm from the cubital joint, and measured 7 × 6 × 16 mm. The tumours showed heterogeneous contrast enhancement – Figure 4.

Presence of a palpable mass of two tumours located in the proximal 1/3 and halfway down the forearm was confirmed on clinical examination. Pain was triggered by applying pressure to the tumours. On percussion of the tumours Hoffman-Tinel sign was elicited, and the patient reported paraesthesias of the dorsal side of the 1st and 2nd finger as well as radial aspect of the dorsum of the hand. Examination of superficial sensory function in this region did not reveal significant impairment compared to the opposite side. No muscle atrophy in the hand and forearm was observed. The patient was scheduled for surgical removal of the tumours. The procedure was performed on 15.10.2013 from a single incision in the proximal 1/3 and halfway down the forearm. The operation was performed using tourniquet ischemia and an operating microscope. Two tumours measuring 32 × 20 × 15 mm and 12 × 8 × × 5 mm were excised with transection of one fascicle – Figures 5 and 6. In the peripheral portion of the superficial radial nerve, presence of a third nodule, previously not visible on imaging scans, was detected. This small nodule, measuring 3 mm in diameter, was removed without damage to the fascicular structure. The cross-section of the largest of the excised

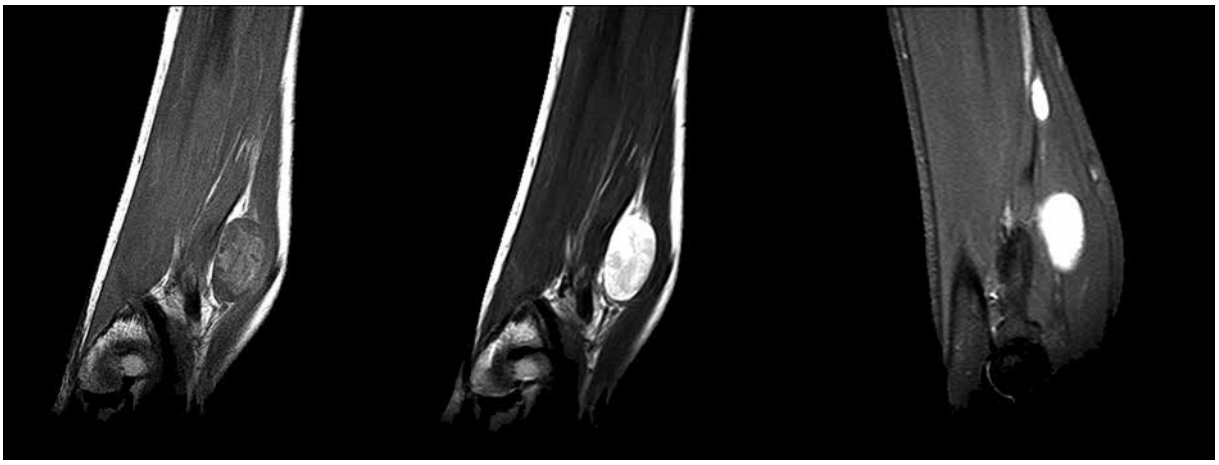

Fig. 4. Magnetic resonance imaging examination results: visualization of tumours in the course of the superficial radial nerve.

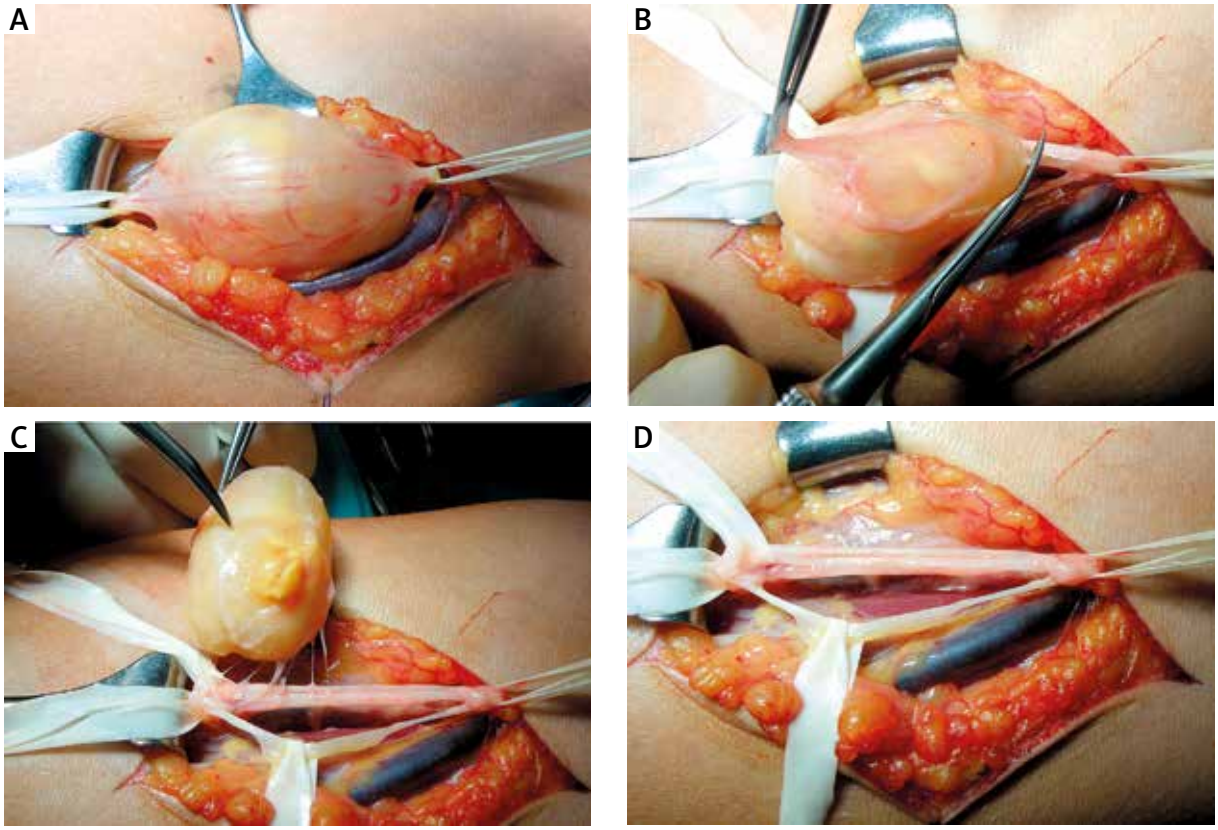

Fig. 5. Intraoperative view: **A)** larger tumour of superficial radial nerve in proximal third of the forearm, **B)** transection of the single fascicle entering the tumour, **C)** removal of the tumour from the superficial radial nerve, **D)** appearance of the superficial radial nerve after tumour resection.

tumours (located in the proximal forearm) revealed macroscopic features of cystic degeneration with a leak of gelatinous, yellowish liquid and presence of tiny beige nodules – Figure 7. On histopathological examination this tumour had characteristics enabling diagnosis of ancient schwannoma: microcyst and cyst formation, perivascular hyalinisation, nuclear atypia without mitotic figures (sample number – 32456

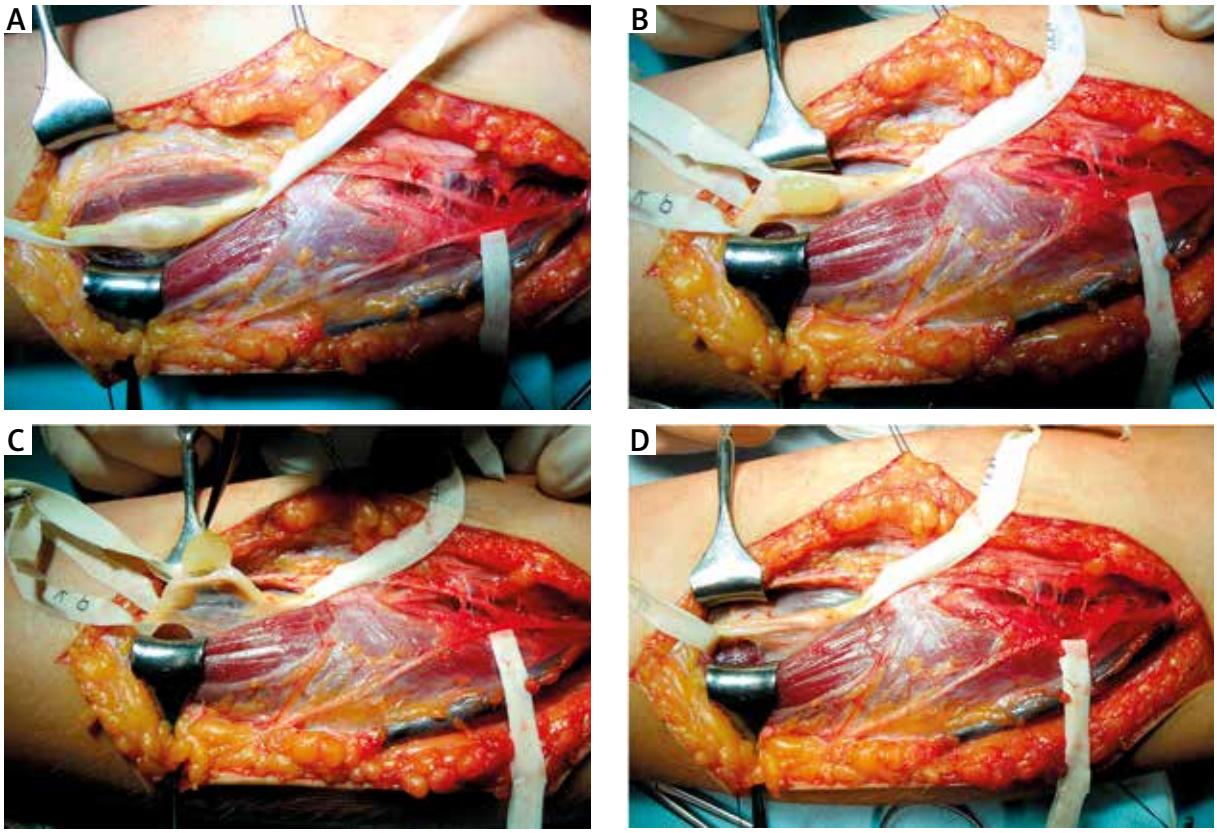

Fig. 6. Intraoperative view: **A)** smaller tumour of the superficial radial nerve located halfway down the forearm, **B)** dissection of the tumour, **C)** removal of the tumour, **D)** appearance of the superficial radial nerve after resection of the tumour.

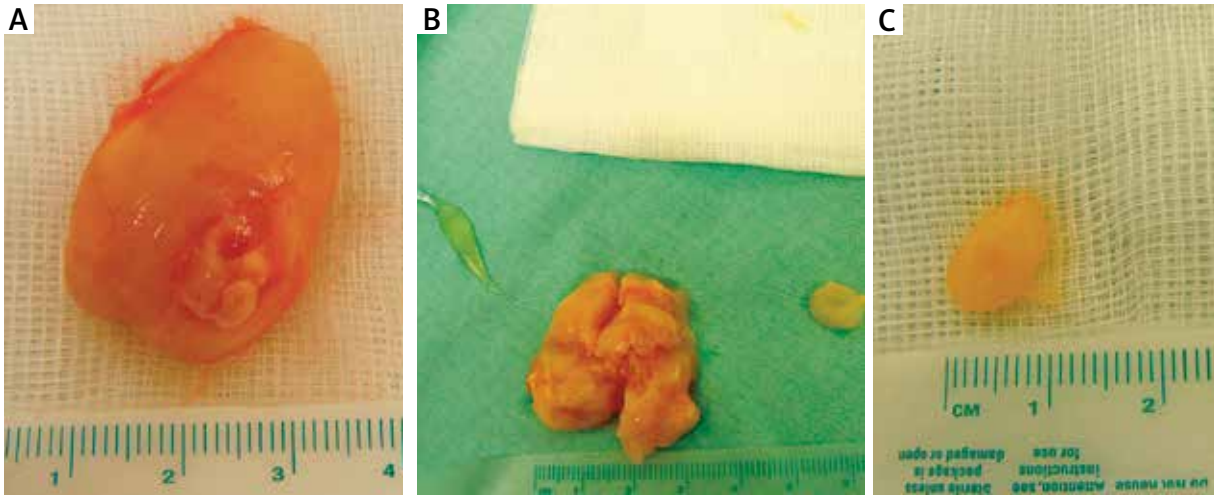

Fig. 7. Postoperative view: **A)** larger tumour after removal, **B)** both tumours after removal (cross-section of the larger tumour with leak of gelatinous substance), **C)** smaller tumour after removal.

from 24.10.2013) – Figure 8. The other two tumours had a histological pattern of classical schwannoma. The postoperative course was uncomplicated. No symptoms of recurrence of tumours were detected at follow-up examinations, and pain and paraesthesias resolved. Tinel-Hoffman sign is negative.

Discussion

Location of solitary schwannomas in the hand and fingers is rare [8,27]. Cases of multiple schwannomas in this region are of great rarity [41]. In material presented by Rockwell *et al*. schwannomas located in the hand and wrist constituted 7.5% of all schwannomas. The most frequent site of origin in material presented by authors mentioned above were proper digital nerves (52%) and common digital nerves (19%). Multiple tumours were detected in two female patients described by these authors; they derived, however, from separate nerves. Rockwell *et al*. did not describe any tumours located peripherally to the proximal interphalangeal joint [27]. Peripheral location of schwannomas in fingers is a subject of casuistic reports [15,32]. Kilic *et al*. presented a case of a painful solitary schwannoma located in middle and distal phalanges of the 3rd finger of the left hand [15]. Takeuchi *et al*. described a solitary schwannoma located in the distal phalanx of the 4th finger of the right hand [32]. The case presented in this work is unique due to the fact that schwannomas developed in both digital nerves and occurred simultaneously proximally and distally to the proximal interphalangeal joint.

In the second of the described cases the tumours were located in the superficial radial nerve. The superficial radial nerve is a sensory branch of the radial nerve that provides cutaneous innervation to the dorsal aspect of the hand, including the thumb, index finger and the radial aspect of the long finger [23]. The superficial radial nerve might be compressed or injured at various anatomical sites along its course in the forearm [26]. Cases of external compression by an osteochondroma, lipoma or ganglion cyst [19,26,36,40] as well as development of tumours such as nerve sheath ganglion, lipofibroma and plasmocytoma intraneurally [4,11,30] have been described. The first case of schwannoma located in the superficial radial nerve was described by Visser in 2009 [37]. The tumour was located 7 cm above the styloid process of the radius [37]. Other cases of solitary schwannoma were presented by Kim *et al*. and Tang *et al*. and were located halfway down the forearm and in the wrist, respectively [16,34]. Compression of the superficial radial nerve occurring at the proximal third of the forearm is unusual [26,36]. In our material the largest tumour was located in the proximal third of the forearm and 2 smaller ones halfway down its length. Tanabe *et al*. presented a case of a 38-year-old woman with multiple schwannomas (5 tumours) in the radial nerve (arm) and posterior interosseous nerve (forearm) [33]. According to the authors it was the first documented description of multiple schwannomas in the radial nerve and its motor branch [33]. To the best of our knowledge, multiple schwannomas of the superficial radial nerve have not previously been described.

Cystic degeneration of the largest tumour located in the superficial radial nerve (case 2), which was detected both on imaging scans and intraoperatively,

Table I. Criteria for diagnosis of schwannomatosis

Schwannomatosis*		Diagnostic criteria
Definite		Age > 30 years and two or more non-intradermal schwannomas (at least one with histological confirmation)
	or	One schwannoma confirmed with histology and a first-degree relative who meets the above criteria
Possible		Age < 30 years and two or more non-intradermal schwannomas (at least one with histological confirmation)
	or	Age > 45 years and no symptoms of eighth cranial nerve dysfunction and two or more non-intradermal schwannomas (at least one with histological confirmation)
	or	Radiographic evidence of a schwannoma and a first-degree relative who meets the criteria for definite schwannomatosis
Segmental		Meets criteria for definite or possible schwannomatosis but limited to one limb or five or fewer contiguous segments of the spine

**Individuals must not fulfil the criteria for NF2 or have any of the following: Vestibular schwannoma on MRI, constitutional NF2 mutation, or a first degree relative with NF2.*

prompted us to perform detailed histopathological examination. Ancient schwannoma was diagnosed on the basis of the following features: microcyst and cyst formation, perivascular hyalinisation and nuclear atypia. In our histopathological samples no calcification or hemorrhagic areas were detected. However, these features are not always present. Isobe *et al*. observed calcification only in two out of

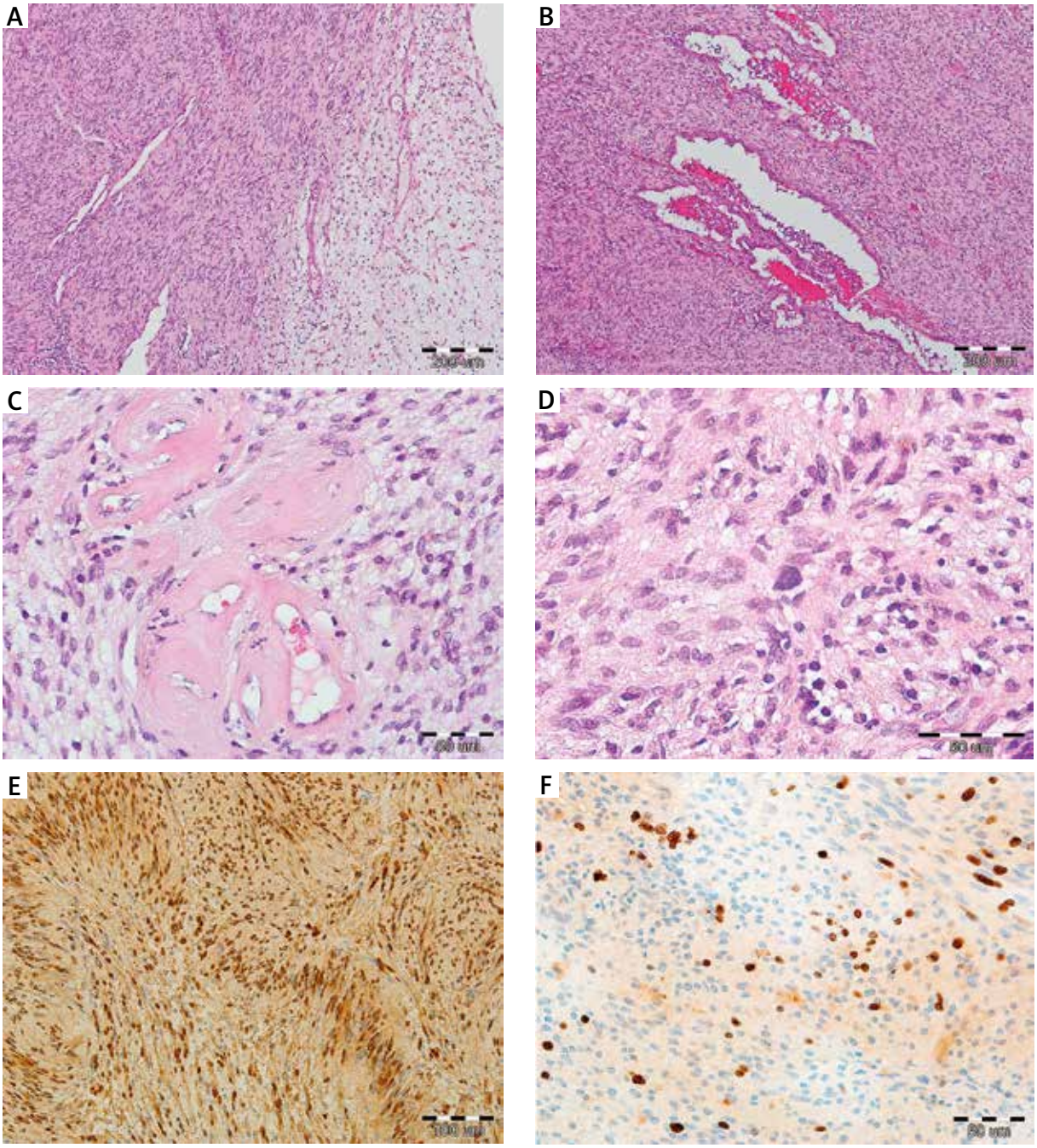

Fig. 8. Histopathological examination results: **A)** focally palisading nuclei of spindle cells represented by a Verocay body ("Antoni A") (left side of the image) and marked myxoid degeneration area (right side of the image), **B)** multiple microcyst formation, **C)** irregular vessels with hyalinized walls, **D)** marked cellular and nuclear atypia but no mitotic figures, **E)** immunohistochemical expression of S-100 protein in differentiated Schwann cells, **F)** proliferative index Ki-67 positive, low (4%).

seven patients diagnosed with ancient schwannoma [10]. Ancient schwannoma is a rare degenerative type of schwannoma described for the first time in 1951 by Ackerman and Taylor [1] and accounts for 0.8% of soft tissue tumours [4,22]. This type of neoplasm occurs predominantly in the form of large, slow-growing tumours located in deep tissue layers of the head, neck, chest, retroperitoneum, pelvis and limbs [10,18,31,38]. Ancient schwannoma develops mainly in elderly people [38]. Presence of degenerative changes in this type of tumour is associated with a prolonged period of its growth [10,38]. Very rare cases of ancient schwannoma characterised by rapid growth have been described. Isobe *et al*. in their material comprising 7 patients diagnosed with ancient schwannoma in 2 cases observed a short period of tumour growth lasting one and two years [10]. Lee *et al*. described a case of ancient schwannoma development in a thigh with very fast increase in tumour size within one year [18]. Likewise, in our 22-year-old female patient development of ancient schwannoma in the superficial radial nerve lasted only 2 years. Lee *et al*. concluded that long-term clinical history is not essential for ancient schwannoma diagnosis [18]. Ancient schwannoma with degenerative changes including nuclear atypia, hyperchromasia and pleomorphism can be misdiagnosed as sarcoma [17]. According to Klijanienko *et al*., the principal discriminative morphological differences between well-differentiated malignant peripheral nerve sheath tumour (MPNST) and schwannoma rely on the presence of mitotic figures and the absence of Verocay bodies [17].

In both of the described cases, diagnosis of neurofibromatosis type 1 and 2 was excluded based on clinical examination and additional examinations' results. The patients' families had no history of neurofibromatosis type 1 and 2 or schwannomatosis. Both described cases can be classified as segmental schwannomatosis. Schwannomatosis is a genetic disorder described for the first time in the 1970s and for more than 20 years considered a form of neurofibromatosis [13]. In the late 1990s the suggestion was made that schwannomatosis should be classified as a separate condition [21]. The first clinical diagnostic criteria were formulated in 1997 by Jacoby *et al*. [12]. Contemporary diagnostic clinical criteria for schwannomatosis were established in 2005 during a meeting under the patronage of the National Neurofibromatosis Foundation [20]. One year later they were made even more precise, and in this form they are valid until today [2,3] – Table I.

Schwannomatosis occurs with an annual incidence estimated at 0.58 cases/1 000 000 persons [5,20]. There are two types of schwannomatosis: sporadic and familial [5]. Patients diagnosed with schwannomatosis constitute a small fraction of all patients treated surgically for schwannomas. In material presented by Seppälä *et al*. patients with schwannomatosis accounted for 3.7% and in material by Huang for 4.6% of all patients who underwent operative treatment [9,28]. In material presented by Wang *et al*. 5 cases of segmental schwannomatosis constituted 1.4% of all treated patients [39]. It is estimated that segmental schwannomatosis constitutes about 30% of all cases of schwannomatosis [20]. Gonzalvo *et al*. described 4 cases of the segmental form among 14 patients diagnosed with schwannomatosis. The segmental form was found only in patients with sporadic schwannomatosis [5]. It was similar in our two patients. Medical history and clinical manifestations enabled diagnosis of segmental sporadic schwannomatosis.

Conclusions

To conclude, we have presented two cases of a rare disorder (segmental schwannomatosis) of an extremely rare location (digital nerves, superficial radial nerve) and histopathological pattern – ancient schwannoma (case 2).

Acknowledgements

We thank Bartosz Witkowski, who provided medical writing service on behalf of Wroclaw Medical University.

Disclosure

The authors report no conflict of interest.

References

1. Ackerman LV, Taylor FH. Neurogenous tumors within the thorax; a clinicopathological evaluation of forty-eight cases. Cancer 1951; 4: 669-691.
2. Baser ME, Friedman JM, Evans DG. Increasing the specificity of diagnostic criteria for schwannomatosis. Neurology 2006; 66: 730-732.
3. Ferner RE. Neurofibromatosis 1 and neurofibromatosis 2: a twenty first century perspective. Lancet Neurol 2007; 6: 340-351.
4. Gillies RM, Burrows C. Nerve sheath ganglion of the superficial radial nerve. J Hand Surg [Br] 1991; 16: 94-95.

5. Gonzalvo A, Fowler A, Cook RJ, Little NS, Wheeler H, McDonald KL, Biggs MT. Schwannomatosis, sporadic schwannomatosis, and familial schwannomatosis: a surgical series with long-term follow-up. J Neurosurg 2011; 114: 756-762.
6. Gosk J, Rutowski R, Rabczyński J. Peripheral nerve tumours in own material. Folia Neuropathol 2004; 42: 203-207.
7. Gosk J, Zimmer K, Rutowski R. Peripheral nerve tumours – diagnostic and therapeutical basics. Folia Neuropathol 2004; 42: 31-35.
8. Han K-J, Lee YS, Park M. Digital nerve schwannoma of the hand. J Hand Surg [Eur] 2012; 37: 361-362.
9. Huang JH, Simon SL, Nagpal S, Nelson PT, Zager EL. Management of patients with schwannomatosis: report of six cases and review of the literature. Surg Neurol 2004; 62: 353-361.
10. Isobe K, Shimizu T, Akahane T, Kato H. Imaging of ancient schwannoma. AJR Am J Roentgenol 2004; 183: 331-336.
11. Jacob RA, Buchino JJ. Lipofibroma of the superficial branch of the radial nerve. J Hand Surg [Am] 1989; 14: 704-706.
12. Jacoby LB, Jones D, Davis K, Kronn D, Short MP, Gusella J, MacCollin M. Molecular analysis of the NF2 tumor-suppressor gene in schwannomatosis. Am J Hum Genet 1997; 61: 1293-1302.
13. Javalkar VK, Pigott T, Pal P, Findlay G. Multiple schwannomas: report of two cases. Eur Spine J 2007; 16: s287-s292.
14. Joyce M, Laing AJ, Mullet H, Mofidi A, Tansey D, Connolly CE, Mccabe JP. Multiple schwannomas of the posterior tibial nerve. Foot Ankle Surg 2002; 8: 101-103.
15. Kilic A, Cinar C, Arslan H, Pilanci O, Altindas M. Re: A benign schwannoma of the digital nerve distal to the proximal interphalangeal joint. J Hand Surg Eur Vol 2008; 33: 212-213.
16. Kim HS, Kim CH, Kang SG, Tark MS. Compression of the Superficial Radial Nerve by Schwannoma: A Case Report. J Korean Soc Plast Reconstr Surg 2011; 38: 494-497.
17. Klijanienko J, Caillaud JM, Lagacé R. Cytohistologic correlations in schwannomas (neurilemmomas), including "ancient", cellular, and epithelioid variants. Diagn Cytopathol 2006; 34: 517-522.
18. Lee YS, Kim JO, Park SE. Ancient schwannoma of the thigh mimicking a malignant tumour: a report of two cases, with emphasis on MRI findings. Br J Radiol 2010; 83: e154-e157.
19. Lewkonia P, Medlicott SAC, Hildebrand KA. Intramuscular myxoid lipoma in the proximal forearm presenting as an olecranon mass with superficial radial nerve palsy: a case report. J Med Case Reports 2011; 5: 321-324.
20. MacCollin M, Chiocca EA, Evans DG, Friedman JM, Horvitz R, Jaramillo D, Lev M, Mautner VF, Niimura M, Plotkin SR, Sang CN, Stemmer-Rachamimov A, Roach ES. Diagnostic criteria for schwannomatosis. Neurology 2005; 64: 1838-1845.
21. MacCollin M, Woodfin W, Kronn D, Short MP. Schwannomatosis: a clinical and pathologic study. Neurology 1996; 46: 1072-1079.
22. Malizos K, Ioannou M, Kontogeorgakos V. Ancient schwannoma involving the median nerve: a case report and review of the literature. Strategies Trauma Limb Reconstr 2013; 8: 63-66.
23. Marchant MH Jr, Gambardella RA, Podesta L. Superficial radial nerve injury after avulsion fracture of the brachioradialis muscle origin in a professional lacrosse player: a case report. J Shoulder Elbow Surg 2009; 18: e9-e12.
24. Molina AR, Chatterton BD, Kalson NS, Fallowfield ME, Khandwala AR. Multiple schwannomas of the upper limb related exclusively to the ulnar nerve in a patient with segmental schwannomatosis. J Plast Reconstr Aesthet Surg 2013; 66: e376-e379.
25. Ogose A, Hotta T, Morita T, Otsuka H, Hirata Y. Multiple schwannomas in the peripheral nerves. J Bone Joint Surg Br 1998; 80: 657-661.
26. Öz O, Yücel M, Ulaş U, Eroğlu E, Odabaşi Z. Superficial radial neuropathy and brachioradial motor nerve palsy associated with proximal radius osteochondroma. Neurol Neurochir Pol 2010; 44: 208-210.
27. Rockwell GM, Thoma A, Salama S. Schwannoma of the hand and wrist. Plast Reconstr Surg 2003; 111: 1227-1232.
28. Seppälä MT, Sainio MA, Haltia MJ, Kinnunen JJ, Setälä KH, Jääskeläinen JE. Multiple schwannomas: schwannomatosis or neurofibromatosis type 2? J Neurosurg 1998; 89: 36-41.
29. Shao X, Zhang X, Su X. Multiple schwannomas of the ulnar nerve. J Plast Surg Hand Surg 2014; 48: 281-282.
30. Stuart JE, Smith AC. Plasmocytoma of the superficial radial nerve. J Hand Surg Am 2001; 26: 776-780.
31. Tadvi JS, Anand A, Humphrey A. Ancient schwannoma of the middle finger. J Hand Surg Eur 2007; 32: 722.
32. Takeuchi A, Yoshida T, Mori H, Tateno M, Satoh H. A case of neurilemmoma on the distal phalanx of the hand. Jap J Plast Reconstr Surg 1999; 52: 145-148.
33. Tanabe K, Tada K, Ninomiya H. Multiple schwannomas in the radial nerve. J Hand Surg Br 1997; 22: 664-666.
34. Tang CY, Fung B, Fok M, Zhu J. Schwannoma in the upper limbs. Biomed Res Int 2013; 2013: 167196.
35. Trăistaru R, Enăchescu V, Manuc D, Gruia C, Ghiluşi M. Multiple right schwannoma. Rom J Morphol Embryol 2008; 49: 235-239.
36. Tzeng CY, Lee TS, Chen IC. Superficial radial nerve compression caused by a parosteal lipoma of proximal radius: a case report. Hand Surg 2005; 10: 293-296.
37. Visser LH. High-resolution sonography of the superficial radial nerve with two case reports. Muscle Nerve 2009; 39: 392-395.
38. Vlychou M, Dailiana ZH. Ancient schwannoma of the hand. J Hand Surg Am 2011; 36: 2030-2033.
39. Wang ZX, Chen SL, Yi CJ, Li C, Rong YB, Tian GL. Segmental schwannomatosis in upper-extremity: 5 cases report and literature review. J Peking University Health Sciences 2013; 45: 698-703.
40. Yoshii S, Ikeda K, Murakami H. Compression neuropathy of the superficial branch of the radial nerve. Scand J Plast Reconstr Surg Hand Surg 2000; 34: 93-95.
41. Zhou J, Man X-Y, Zheng M, Cai S-Q. Multiple plexiform schwannoma of a finger. Eur J Dermatol 2012; 22: 149-150.

Folia Neuropathologica

Are granular osmiophilic material deposits an epiphenomenon in CADASIL?

Roberto Erro[1,2], Marcello Moccia[3], Mariarosaria Cervasio[4], Silvana Penco[5], Marialaura Del Basso De Caro[4], Paolo Barone[6]

[1]Sobell Department of Motor Neuroscience and Movement Disorders, University College London, London, UK, [2]Department of Neurological and Movement Sciences, University of Verona, Verona, Italy, [3]Department of Neuroscience, University Federico II, Naples, Italy, [4]Department of Biomorphological and Functional Sciences, Section of Pathology, University "Federico II", Naples, Italy, [5]Medical Genetics Unit, Department of Laboratory Medicine, Niguarda Ca'Granda Hospital, Milan, Italy, [6]University of Salerno, Center for Neurodegenerative Diseases – CEMAND, Salerno, Italy

Folia Neuropathol 2015; 53 (2): 168-171 DOI: 10.5114/fn.2015.52414

Abstract

Cerebral autosomal dominant arteriopathy with subcortical infarcts and leukoencephalopathy (CADASIL) is caused by mutations in the NOTCH3 gene. Pathophysiologically, there seems to be multimerization of the extracellular domain of the protein with a possible gain of function on vascular smooth muscular cells. However, the mechanisms and determinants of NOTCH3 multimerization are not completely understood, and it is not completely elucidated whether NOTCH3 multimerization contributes to the appearance of granular osmiophilic material (GOM) deposits, which are the pathological hallmark of CADASIL.

We recently reported a patient with parkinsonism and cognitive impairment and with evidence of diffuse white matter changes on imaging, carrying a NOTCH3 nonsense mutation in exon 3 (c.307C>T), and suggested that such a hypomorphic NOTCH3 mutation was likely to be pathogenic.

We further pursued ultrastructural examination of skin vessels in our case, and here we report the results, wishing to make a comment on whether GOM deposits should be considered the pathological hallmark for a definitive diagnosis of CADASIL in those patients whose mutations are predicted in the production of hypomorphic protein products.

Key words: *CADASIL, NOTCH3, granular osmiophilic material, GOM deposits.*

Cerebral autosomal dominant arteriopathy with subcortical infarcts and leukoencephalopathy (CADASIL) is the most common heritable cerebral small vessel disease, caused by mutations in the *NOTCH3* gene [2]. The gene encodes a single pass transmembrane protein, which is predominantly expressed in vascular smooth muscle cells (VSMC) [2]. *NOTCH3* mutations typically affect the extracellular domain ($N3^{ECD}$) within one of the 34 epidermal growth factor (EGF)-like repeat domains [2]. Each EGF-like repeat domain contains a highly conserved number of cysteine residues which seem to stabilize the $N3^{ECD}$ by the formation of disulfide bonds. Virtually, all CADASIL mutations hitherto described result

Communicating author:

Prof. Paolo Barone, University of Salerno, Center for Neurodegenerative Disease – CEMAND, Via S. Allende. 84081 Baronissi (SA), phone: (+39)089-969119, fax: (+39)089-672328, e-mail: pbarone@unisa.it

in an uneven number of cysteine residues, leading to a multimerization of the $N3^{ECD}$ with a possible gain of function effect on VSMC [2,3]. However, mechanisms and determinants of *NOTCH3* multimerization are not completely understood.

We recently described a subject carrying a *NOTCH3* nonsense mutation in exon 3 (c.307C>T), who presented parkinsonism, cognitive impairment, and psychiatric features in his seventies. Despite the late onset, he had typical CADASIL imaging features and a positive family history for cerebral ischemic events in at least two different generations [4,13]. The variant is located in the EGF-like 2 region of exon 3 and causes the substitution of arginine with a stop codon at position 103 of the protein (p.R103X). The formation of such a premature stop codon results in the production of a truncated protein product lacking part of exon 3 and all the subsequent exons (4/33) and therefore characterized by the absence of all EGF-like repeat domains with the exception of EGF-like 1. A number of pieces of evidence (i.e., family history, MRI findings and the segregation of the mutation with the disease) led us to suggest that such a variant was likely to be pathogenic [4,13]. Concomitantly, Rutten *et al*. described another patient carrying the same variant [16]. They argued that it was a neutral polymorphism, based on immunohistochemical analysis and ultra-structural examination of skin vessels, which were found negative for $N3^{ECD}$ and granular osmiophilic material (GOM) deposits [16]. GOM deposits have been in fact described only in CADASIL patients and constitute a pathognomonic feature for the disease [1,10,15]. Prompted by their report, we further pursued ultrastructural examination of skin vessels in our case. Here, we report such results, aiming to make a comment on whether GOM deposits should be considered the pathological hallmark for a definitive diagnosis of CADASIL in those patients whose mutations are predicted in the production of hypomorphic protein products.

Skin biopsy samples were fixed in 2.5% glutaraldehyde/0.1 M cacodylate buffer, rinsed in cacodylate buffer and post-fixed in 1% osmium tetroxide/0.1 M cacodylate buffer, then rinsed again in buffer. Tissue samples were gradually dehydrated in a series of ascending concentrations of ethanol and, then, were immersed in propylene oxide before infiltration with the epoxy resin Epon 812. Ultrathin sections double stained with uranyl acetate and lead citrate were examined with a transmission electron microscope (Zeiss 900).

At the ultrastructural level, analysis of two skin biopsies performed in two different body sites (right and left arm) showed endothelial cells and smooth muscle cells with electron-lucent vacuoles and nuclear chromatin condensation (Figs. 1 and 2). Furthermore, smooth muscle cells presented irregular shape and electron-lucent vacuoles within the cytoplasm, as for degeneration or absence of cytoplasmic organelles (Fig. 3). Notably, such abnormalities were only observed in cells of the blood vessel walls and not in other regions of examined samples, arguing against fixation or orientation artefacts. Ultrastructural analysis of at least 20 vessels per skin biopsy did not show presence of GOM deposits (Figs. 1-3).

Presence of multiple deposits of GOM at ultrastructural examination of brain or skin vessels is the pathognomonic hallmark of CADASIL [1,8,11], with 100% specificity and 96% sensitivity [7]. Nevertheless, the origin, chemical nature and function of GOM deposits are still not clear. There is a suggestion that $N3^{ECD}$ constitutes a component of GOM deposits [5]. If the latter hypothesis is true, then it is not surprising that our patient did not show GOM deposits. His genetic variant is indeed characterized by a premature stop codon, which results in a truncated protein product lacking almost all the $N3^{ECD}$. On the other hand, it is still unknown whether GOM accumulation is necessary for development of the disease. In fact, analysis of vessels from transgenic

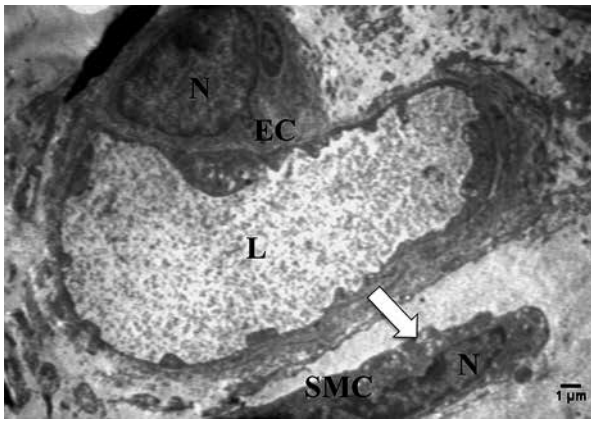

Fig. 1. Endothelial cell (EC) and smooth muscle cell (SMC) with electron-lucent vacuoles (arrow) and nuclear chromatin condensation. L – lumen, N – nucleus.

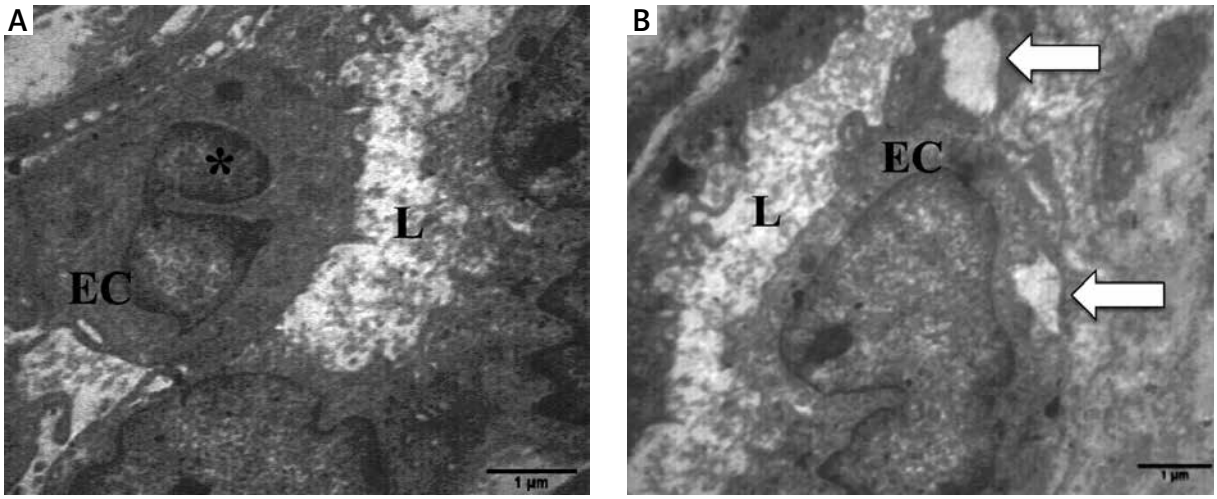

Fig. 2. Endothelial cells (EC) with irregularly shaped nuclei (asterisk) and clear areas located in the cytoplasm (arrows). L – lumen.

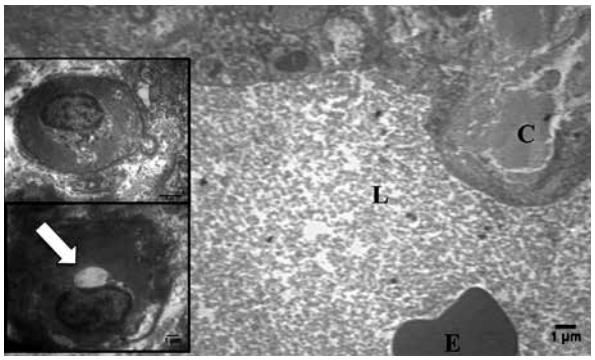

Fig. 3. A blood vessel. Insets showing smooth muscle cells irregular in shape and size, with a few degenerated cytoplasmic organelles and clear variable areas (arrows). L – lumen, C – collagen fibrils, E – erythrocyte.

mice expressing mutant *NOTCH3* shows that VSMC damage precedes $N3^{ECD}$ and GOM accumulation [6,12]. Moreover, there is no apparent correlation between the presence and number of GOM deposits and severity of VSMC damage [9,15]. In addition, it is interesting that even though GOM deposits are detected along the vasculature throughout the body, the symptoms of CADASIL are almost exclusively restricted to the central nervous system [12]. Although a gain of function effect on VSMC triggered by multimerization of the mutated protein (and possibly by presence of GOM deposits) is the most supported pathophysiological mechanism in CADASIL, certain naturally occurring mutations unambiguously result in abolished *NOTCH3* signaling and function [14]. In addition, several studies have revealed that mutations leading to *NOTCH3* over-expression dominantly suppress Notch signaling rather than increase it [12]. However, it has also been argued that the archetypal Arg169Cys mutation in *NOTCH3* does not drive the pathogenesis through a loss-of-function mechanism [16]. Overall, it is conceivable that different mechanisms can contribute to the pathophysiology of CADASIL, among which one holds that accumulation of $N3^{ECD}$/GOM in the brain vessels would promote the abnormal recruitment of functionally important extracellular matrix proteins that may eventually cause multifactorial toxicity. Unfortunately, the lack of appropriate instruments to directly assess, *in vivo*, the consequence of mutations on *NOTCH3* transcriptional activity in the brain arteries leaves opens the question of whether hypomorphic *NOTCH3* can drive CADASIL-like symptoms, regardless of the presence of the GOM.

More consistent data on the role of *NOTCH3* in VSMC have been obtained from animal models, even though both knock-out and knock-in mice are not entirely considered robust models of CADASIL [6]. On the one hand, Notch3–/– mice exhibit abnormalities in the cerebrovascular patterning [6] and show marked defects in distal muscular arteries, particularly in the cerebral ones, in the absence of $N3^{ECD}$ and GOM accumulation, even if they do not develop the disease [6]. On the other hand, in some of the knock-in models overexpression of *NOTCH3* up to

4-fold does not lead to CADASIL features or to GOM accumulation (for an extensive review, see [6]).

Such a pattern (i.e., vascular abnormalities in the absence of GOM accumulation) might resemble what we observed in our patient (Figs. 1-3), and we would argue that another mechanism, which is not mediated by $N3^{ECD}$ and GOM accumulation, might underlie such vascular abnormalities, at least for hypomorphic *NOTCH3* mutations. We acknowledge that a higher vascular abnormality burden may have been expected in our case. However, it is conceivable that a brain vessel biopsy would have shown more extensive damage. Moreover, we acknowledge that we did not use another technique (e.g. immunogold staining), but, as stated above, we only found abnormalities in the VSMC and consistently within different samples, rendering the chance of artefacts unlikely.

In summary, there seems to be a spectrum of disorders associated with different *NOTCH3* mutations, with hypomorphic *NOTCH3* presumably causing CADASIL-like symptoms via loss-of-function mechanisms, in line with other studies showing that common *NOTCH3* variants may increase the cerebrovascular risk in the elderly [13,17].

A number of lines of evidence support the hypothesis that *NOTCH3* haploinsufficiency can be clinically relevant, and further neuropathological data will be crucial to define the spectrum of CADASIL-like disorders and to definitively elucidate the role of GOM deposits.

Disclosure

Authors report no conflict of interest.

References

1. Baudrimont M, Dubas F, Joutel A, Tournier-Lasserve E, Bousser MG. Autosomal dominant leukoencephalopathy and subcortical ischemic stroke. A clinicopathological study. Stroke 1993; 24: 122-125.
2. Chabriat H, Joutel A, Dichgans M, Tournier-Lasserve E, Bousser MG. CADASIL. Lancet Neurol 2009; 8: 643-653.
3. Cognat E, Baron-Menguy C, Domenga-Denier V, Cleophax S, Fouillade C, Monet-Leprêtre M, Dewerchin M, Joutel A. Archetypal Arg169Cys mutation in NOTCH3 does not drive the pathogenesis in cerebral autosomal dominant arteriopathy with subcortical infarcts and leucoencephalopathy via a loss-of-function mechanism. Stroke 2014; 45: 842-849.
4. Erro R, Lees AJ, Moccia M, Picillo M, Penco S, Mosca L, Vitale C, Barone P. Progressive parkinsonism, balance difficulties, and supranuclear gaze palsy. JAMA Neurol 2014; 71: 104-107.
5. Ishiko A, Shimizu A, Nagata E, Takahashi K, Tabira T, Suzuki N. Notch3 ectodomain is a major component of granular osmiophilic material (GOM) in CADASIL. Acta Neuropathol 2006; 112: 333-339.
6. Joutel A. Pathogenesis of CADASIL: transgenic and knock-out mice to probe function and dysfunction of the mutated gene, Notch3, in the cerebrovasculature. BioEssays 2011; 33: 73-80.
7. Kalaria RN, Viitanen M, Kalimo H, Dichgans M, Tabira T; CADASIL Group of Vas-Cog. The pathogenesis of CADASIL: an update. J Neurol Sci 2004; 226: 35-39.
8. Lewandowska E, Felczak P, Buczek J, Gramza K, Rafałowska J. Blood vessel ultrastructural picture in a CADASIL patient diagnosed at an advanced age. Folia Neuropathol 2014; 52: 443-451.
9. Lewandowska E, Leszczynska A, Wierzba-Bobrowicz T, Pasennik E. Ultrastructural picture of blood vessels in muscle and skin biopsy in CADASIL. Folia Neuropathol 2006; 44: 265-273.
10. Lewandowska E, Wierzba-Bobrowicz J, Gromadzka G, Dziewulska D. CADASIL patient with extracellular calcium deposits. Folia Neuropathol 2013; 51: 302-311.
11. Malandrini A, Gaudiano C, Gambelli S, Berti G, Serni G, Bianchi S, Federico A, Dotti MT. Diagnostic value of ultrastructural skin biopsy studies in CADASIL. Neurology 2007; 68: 1430-1432.
12. Meng H, Zhang X, Yu G, Lee SJ, Chen YE, Prudovsky I, Wang MM. Biochemical characterization and cellular effects of CADASIL mutants of NOTCH3. PLoS One 2012; 7: e44964.
13. Moccia M, Mosca L, Erro R, Cervasio M, Allocca R, Vitale C, Leonardi A, Caranci F, Del Basso-De Caro ML, Barone P, Penco S. Hypomorphic NOTCH3 mutation in an Italian family with CADASIL features. Neurobiol Aging 2015; 36: 547.e5-547.e11.
14. Monet-Leprêtre M, Bardot B, Lemaire B, Domenga V, Godin O, Dichgans M, Tournier-Lasserve E, Cohen-Tannoudji M, Chabriat H, Joutel A. Distinct phenotypic and functional features of CADASIL mutations in the Notch3 ligand binding domain. Brain 2009; 132: 1601-1612.
15. Ruchoux MM, Domenga V, Brulin P, Maciazek J, Limol S, Tournier-Lasserve E, Joutel A. Transgenic mice expressing mutant Notch3 develop vascular alterations characteristic of cerebral autosomal dominant arteriopathy with subcortical infarcts and leukoencephalopathy. Am J Pathol 2003; 162: 329-342.
16. Rutten JW, Boon EMJ, Liem MK, Dauwerse JG, Pont MJ, Vollebregt E, Maat-Klevit AJ, Ginjaar HB, Lakeman P, van Duinen SG, Terwindt GM, Lesnik Oberstein SA. Hypomorphic NOTCH3 alleles do not cause CADASIL in humans. Hum Mutat 2013; 34: 1486-1489.
17. Schmidt H, Zeginigg M, Wiltgen M, Freudenberger P, Petrovic K, Cavalieri M, Gider P, Enzinger C, Fornage M, Debette S, Rotter JI, Ikram MA, Launer LJ, Schmidt R; CHARGE consortium Neurology working group. Genetic variants of the NOTCH3 gene in the elderly and magnetic resonance imaging correlates of age-related cerebral small vessel disease. Brain 2011; 134: 3384-3397.

Instructions to Authors

This instruction is based upon *Uniform Requirements for Manuscripts Submitted to Biomedical Reviews* (the complete document appears in N Engl J Med 1997; 336, 309-315).

Aims and scope

Folia Neuropathologica is an official journal of the Mossakowski Medical Research Centre Polish Academy of Sciences and the Polish Association of Neuropathologists. The journal publishes original articles and reviews that deal with all aspects of clinical and experimental neuropathology and related fields of neuroscience research. The scope of journal includes surgical and experimental pathomorphology, ultrastructure, immunohistochemistry, biochemistry and molecular biology of the nervous tissue. Papers on surgical neuropathology and neuroimaging are also welcome. The reports in other fields relevant to the understanding of human neuropathology might be considered.

Ethical consideration

Papers describing animal experiments can be accepted for publication only if the experiment conforms to the legal requirements in Poland as well as with the European Communities Council Directive of November 24, 1986 or the National Institute of Health Guide (National Institute of Health Publications No. 80-23, Revised 1978) for the care and use of Laboratory Animals for experimental procedure. Authors must provide a full description of their anesthetics and surgical procedures. Papers describing experiments on human subjects must include a statement that experiments were performed with the understanding and consent of each subject, with the approval of the appropriate local ethics committee.

Submission of manuscripts

Articles should be written in English. All new manuscripts should be submitted through the online submission at http://panel2.termedia.pl/fn
For authors unable to submit their manuscript online, please contact with Prof. E. Matyja, Editor-in-Chief of *Folia Neuropathologica*, ematyja@imdik.pan.pl
The Editorial Board reserves the right to reject a paper without reviewers' opinion if the content or the form of the paper does not meet minimum acceptance criteria or if the subject of the paper is beyond the aims and scope of the journal.

Legal aspects

In sending the manuscript the author(s) confirm(s) that (s)he has (they have) not previously submitted it to another journal (except for abstracts of no more than 400 words) or published it elsewhere. The author(s) also agree(s), if and when the manuscript is accepted for publication, to automatic and free transfer of copyright to the Publisher allowing for the publication and distribution of the material submitted in all available forms and fields of exploitation. The author(s) accept(s) that the manuscript will not be published elsewhere in any language without the written consent of the copyright holder, i.e. the Publisher.
All manuscripts submitted should be accompanied by an authors' statement including signed confirmation of the above and confirming that this publication has been approved by all co-authors (if any), as well as by the responsible authorities at the institution where the work has been carried out. The authors' statement should be signed by ALL co-authors. Additionally, the author(s) confirm(s) that (s)he is (they are) familiar with and will observe the "Instruction to Authors" included in *Folia Neuropathologica* and also that all sources of financial support have been fully disclosed. Materials previously published should be accompanied by written consent for reprinting from the relevant Publishers. In the case of photographs of identifiable persons, their written consent should also be provided. Any potential conflict of interest will be dealt with by the local court specific to the Publisher. Legal relations between the Publisher and the author(s) are in accordance with Polish law and with international conventions binding on Poland.
Authors agree to waive their royalties.

Anonymous review

All manuscripts will be subject to a process of anonymous editorial review.

Preparation of manuscripts

Articles must be written in English, with British spelling used consistently throughout. Authors not entirely familiar with English are advised to correct the style by professional language editors or native English speakers.

- The length of original article should not exceed 20 printed pages including text, illustrations, tables, and references.
- Manuscripts should be typed using 12pts.font, double-spaced, and fully corrected. Allow a margin at least 2.5 cm at the top, bottom and left side of the page. Text should not be justified.

- The title page should contain: the author's full names, title of the paper, all authors' affiliations, full name and address of the communicating author (including e-mail address and fax number), running title (not exceed 40 characters including spaces).
- The abstract should not exceed 350 words. A list of 3–10 key words is recommended below the abstract.
- The manuscript body should be organized in a standard form with separate sections: Introduction, Material and Methods, Results, Discussion, and References. Review articles should be divided into sections and subsections as appropriate without numbering.
- Do not underline in the text. Avoid footnotes.
- All dimensions and measurements must be specified in the metric system.
- The source of any drug and special reagent should be identified.
- Particular attention needs to be paid to the selection of appropriate analysis of data and the results of statistical test should be incorporated in the results section.
- The nomenclature used should conform to the current edition of the Nomina Anatomica or Nomina Anatomica Veterinaria.
- Acknowledgements should be made in a separate sheet following Discussion and before References. These should contain a list of dedications, acknowledgements, and funding sources.
- Legends of figures and tables should be typed on separate pages.
- The editor reserves the right to make corrections.

Tables

- Tables numbered in Roman numerals require a brief but descriptive heading.
- The major divisions of the table should be indicated by horizontal rules.
- Explanatory matter should be included in footnotes, indicated in the body of the table in order of their appearance.
- Tables must not duplicate material in the text or in illustration.

Illustrations

All figures should be supplied electronically at resolution 300dpi in all standard formats (tiff, jpg, Adobe Photoshop, Corel Draw, and EPS). Name your figure files with "Fig" and the figure number, e.g., Fig1.tif

- The maximum figure size is 84 mm or 174 mm for use in a single or double column width, respectively.
- When possible, group several illustrations on one block for reproduction. Like all other figures, block should be prepared within a rectangular frame to fit within a single or double column width of 84 and 174 mm, respectively, and a maximum page height of 226 mm.
- Each figure should include scale magnification bar; do not use magnification factors in the figure legends.
- All figures, whether photographs, graphs or diagrams, should be numbered using Arabic numerals and cited in the text in consecutive numerical order
- **Immunohistochemical study requires color illustrations of very good quality. The papers with white and black immunohistochemistry will not be accepted.**
- **The expense of color illustrations must be borne by the authors.** The cost of color print for every successive 8 pages is 200 euro irrespective of the number of color pages, i.e., the price remains the same whether there is one or eight pages.

The Publisher makes out the bill to the communicating Author.

References

The list of references (written on a separate page) should include only those publications that are cited in the text. Avoid citation of academic books, manuals and atlases. References may be arranged alphabetically and numbered consecutively. References should be given in square brackets with no space between the comma and the consecutive number, e.g. [3,4,6-12].

References should be written as follows:

Journal papers: initials and names of all authors, full title of paper, journal abbreviation (according to Index Medicus), year of publication, volume (in Arabic numerals), first and last page (example below):

1. Valverde F. The organization of area 18 in the monkey. Anat Embryol 1978; 154: 305-334.
2. Uray NJ, Gona AG. Calbindin immunoreactivity in the auricular lobe and interauricular granular band of the cerebellum in bullfrogs. Brain Behav Evol 1999; 53: 10-19.

Book and monographs: initials and names of all authors, full title, edition, publisher, place, year (examples below):

1. Pollack RS. Tumor surgery of the head and neck. Karger, Basel 1975.
2. Amaral DG, Price JL, Pitkanen A, Carmichael ST. Anatomical organization of the primate amygdaloid complex. In: Aggleton JP (ed.). The amygdala. Wiley-Liss, New York 1992; pp. 1-66.

Reference to articles that are accepted for publication may be cited as „in press" or Epub.

Proofs

Corrections to the proofs should be restricted to printer's errors only; other alterations will be charged to the authors. In order to maintain rapid publication, proofs should be returned within 48 hours, preferably by e-mail, fax or courier mail. If the Publisher receives no response from the authors after 10 days, it will be assumed that there are no errors to correct and the article will be published.

Subscription information

The journal is published in one volume per year consisting of four numbers. The annual subscription price is 160 PLN for Institutions from Poland and 80 PLN for individual subscribers from Poland and 140 Euro for foreign Institutions and 70 Euro for foreign individual subscribers.
Payment should be made to:
Termedia sp. z o.o., ul. Kleeberga 8, 61-615 Poznan
BZ WBK III O/Poznan PL 61 1090 1359 0000 0000 3505 2645
SWIFT: WBKPPLPP

The publisher must be notified of a cancellation of a subscription not later than two months before the end of the calendar year. After that date the subscription is automatically prolonged for another year.
Publishing, Subscription and Advertising Office:
TERMEDIA Publishing House
ul. Kleeberga 2
61-615 Poznan, Poland
phone/fax +48 61 822 77 81
e-mail: termedia@termedia.pl
http://www.folianeuro.termedia.pl

Folia Neuropathologica

AUTHOR'S STATEMENT

Title of the article

.....

.....

.....

The author(s) hereby confirm(s) that:

☐ The above-mentioned work has not previously been published and that it has not been submitted to the Publishers of any other journal (with the exception of abstracts not exceeding 400 words).

☐ All co-authors named and the relevant authorities of the scientific institutions at which the work has been carried out are familiar with the contents of this work and have agreed to its publication.

☐ In sending the manuscript together with illustrations and tables agree(s) to automatic and free transfer of copyright to the Publisher allowing for the publication and distribution of the material submitted in all available forms and fields of exploitation, without limits of territory or language, provided that the material is accepted for publication. At the same time the author(s) accept(s) that the submitted work will not be published elsewhere and in whatever language without the earlier written permission of the copyright holder, i.e. the Publisher.

☐ (S)he (they) agree to waive his(her)(their) royalties (fees).

☐ (S)he (they) empower(s) the Publisher to make any necessary editorial changes to the submitted manuscript.

☐ All sources of funding of the work have been fully disclosed.

☐ The manuscript has been prepared in accordance with the Publisher's requirements.

☐ (S)he (they) is (are) familiar with the regulations governing the acceptance of works as published in *Folia Neuropathologica* and agree(s) to follow them.

☐ (S)he (they) agree to accept appropriate invoice from the Publisher in case colour illustrations are implemented.

Date *Signatures of* ***all authors***

The covering letter formula can be found at: www.folianeuro.termedia.pl
-The covering letter should be sent to Associate Editor:

Milena Laure-Kamionowska
-Editorial Office of Folia Neuropathologica
Mossakowski Medical Research Centre, Polish Academy of Sciences
Poland Medical Research Centre
ul. Pawinskiego 5
02-106 Warszawa, Poland

CONTENTS